

https://dspace.org/

Radioactivity assessment of radium and radon concentrations in water sources at and near selected former uranium mines in the West-Rand area of Johannesburg

Tsewu, Ayabulela

2021
https://hdl.handle.net/10539/32473

Downloaded from a DSpace repository. https://dspace.org/

Radioactivity assessment of radium and radon concentrations in water sources at and near selected former uranium mines in the West-Rand area of Johannesburg

Ayabulela Tsewu

Dissertation presented in the Science Faculty, University of the Witwatersrand, Johannesburg,
in fulfillment of the requirements for the degree
Master of Science.

April 21, 2021

Supervisor: Prof. Iyabo Usman (University of the Witwatersrand)
Co-supervisor: Prof. Ivo Petr (University of the Witwatersrand)

Declaration

I hereby declare that this dissertation is my own, unaided original work and that all sources have been accurately reported and acknowledged. It is being submitted for fulfillment of the Degree of Master of Science at the University of the Witwatersrand, Johannesburg. It has not been submitted before for any degree or examination at any other University.



21/04/21

Abstract

The present work aimed at establishing the extent and distribution of the activity concentration levels of ^{238}U daughter-nuclides; ^{226}Ra and ^{222}Rn in the West Rand-area of Johannesburg. The main motive was to ascertain whether the exposure of the nearby residents to ionising radiation due to former mining activities was within the maximum acceptable limit of 1.0 mSv/y for the public. Measurements include the use of Alpha Spectroscopy system (Canberra) with Passivated Implanted Planar Silicon (PIPS) and Solid-state Alpha Detectors for Radon measurements (RAD-7) to identify radionuclides, quantify and analyze isotopes of interest.

A seasonal collection of 32 water samples from the mining areas was carried out and analysed for ^{226}Ra and ^{222}Rn. The higher and lower radium (^{226}Ra) concentration values in water samples recorded at Ezulwini inlet in winter (June 2019) and Kloof down in Summer (December 2019) found to be (164.42±18.47) mBq/l and (-3.38±-2.39) mBq/l, respectively. The average radium concentration for the water samples survey in the West-Rand area was 73,4±10,0 mBq/l, 74,6±9,6 mBq/l, 71,6±10,5 mBq/l, and 60,9±5,8 mBq/l for June 2019, September 2019, December 2019 and March 2020, respectively. The ^{226}Ra activity concentration (mBq/l) of analysed samples mean values are not significantly different ($p>0.05$) from June 2019 to March 2020 consecutive seasons. The comparison of the mean values within pair of groups shows no statistical significance. The radium values were lower than the suggested maximum contamination levels by US-EPA of 555 mBq/l [1].

The measurements show that the radon (^{222}Rn) concentration higher and lower values were recorded at (Bly6) Blyvooruitzicht shaft 6 discharge in Autumn (March 2020) and (Ezul) Ezulwini Outlet discharge in Winter (June 2019) and found to be 289±272 mBq/l, and 37.1±74.1 mBq/l, respectively. The average radon concentration for the water samples survey was 142,1±79,8

mBq/l, 126.2±95.1 mBq/l, 134.2±108.9 mBq/l, and 140.6±123 mBq/l for June 2019, September 2019, December 2019 and March 2020, respectively. The obtained ^{222}Rn concentration results in drinking water samples in the current study are low than the approved maximum contamination level (MCL) 11.1 Bq/l as approved by US-EPA [1].

The obtained average values for radium annual effective dose (AED_{Ra}) were found to be 1,06E-02 mSv/y, 1,46E-02 mSv/y, 1,47E-02 mSv/y, and 1,07E+02 mSv/y from June 2019 to March 2020, respectively, while the radon annual effective dose (AED_{Rn}) averages were 8.53E-05 mSv/y, 7.57E-05 mSv/y, 8.05E-05 mSv/y, and 8.44E-05 mSv/y June 2019 to March 2020, respectively. The maximum AED_{Ra} value found at Bly4 in December 2019 (Summer) was 3.19E-02 mSv/y. Meanwhile, the maximum AED_{Rn} effective dose value was found in drinking water sample (Drink) in March 2020 (Autumn) as 3.38E-04 mSv/y.

The radon annual ingestion dose from the current study is lower than the European Commission and the World Health Organization proposed concentration of ^{222}Rn in drinking water of 100 Bq/l [2]. The results of this study indicate that the total annual effective doses from possible intake of ^{226}Ra and ^{222}Rn radionuclides in sampled water in West-Rand area are found below the World Health Organisation (WHO) recommended limit of 0.1 mSv/y as well as the average radiation dose of 0.29 mSv/y received per head worldwide due to ingestion of natural radionuclides assessed by UNSCEAR (2000) [3].

Finally, the physico-chemical properties of water samples such as pH and electrical conductivity (EC) are studied for all the surveyed seasons. The pH averaged 1.18, 0.94, 1.13 and 1.20 for Winter (June 2019), Spring (September 2019), Summer (December 2019) and Autumn (March 2020) seasons, respectively. Also, the EC averaged 3134, 5566, 2872, and 3086 mS/m for Winter (June 2019), Spring (September 2019), Summer (December 2019) and Autumn (March 2020) seasons, respectively. Above all, no significant health risk may be posed on the population surrounding the West-Rand area from ^{226}Ra and ^{222}Rn radionuclides present in the water samples as indicated in obtained results.

Dedication

To my mother and my late father, who always supported and encouraged to go on every adventure, especially this one

Acknowledgements

I give all the glory and the honour to God, the Creator of Knowledge in the name of my Saviour Jesus Christ, who gave me strength and courage behind scenes to complete this study.

I am expressing my deep gratitude to my supervisor council that includes Prof. Iyabo Usman, Dr. Risimati Mavunda and Prof. Ivo Petr, who have provided, without hesitation, guidance in giving constructive comments, suggestions and criticism, all of which produced a strong backing for this Masters research study. I credit my developed interest in this field of environmental radiations studies to your stimulating guidance and encouragements at all stages of the work. i'd like to also thank my Wits colleague Armand Bahini for always encouraging me to work hard.

I am highly beholden to Centre of Nuclear Safety and Security (CNSS), for the funding opportunity and giving the environment that enabled the development and completion of this study through the National Nuclear Regulator (NNR) Laboratory. The financial aid and project study field you supplied is well treasured. A shout out to the NNR Lab staff distinctly the Lab manager N. Mohlala, and the lab analysts L. Mkhize, O. Moya, Q. Mahlangu, M. Segaole. Similarly, I am grateful to the staff of the Radio-Analysis Laboratory at NECSA.

I give many thanks to my partner (Lukhanyo Mabongo) and all my friends specifically; Nolitha Mabutya and Sibabale Pongoma, your constant check ups and support provided me with the enthusiasm to continue during challenging moments in the course of this study.
Finally, my most sincere gratitude to my late father Mendo Nkonki who left while completing this work. Also my mother Funeka Tsewu who continued to offer love, sacrifice in abundance and moral support.

Contents

Declaration ii

Abstract iv

Dedication v

Acknowledgements vi

List of Figures xiii

List of Tables xv

1 Introduction 1

1.1 Background 1

1.2 Studies of Radium and Radon around mining sites 4

1.3 Problem statement 6

1.4 Scope of the dissertation 8

2 Theoretical Considerations 9

2.1 Radioactive decay 9

2.1.1 Alpha Decay 10

2.2 Radioactivity Kinetics 11

2.2.1 Decay Equations 12

2.2.2 Two-Stage Radioactive Decay 13

2.2.3 Secular Equilibrium 15

2.3 Occurrence of Radium and Radon 17

2.4 Radium and Radon Properties 20

2.4.1 Radium, Radon and their Progeny Decay Series 23

2.5 Radiation interaction with matter 25

2.5.1 photoelectric effect 25

2.5.2 Compton Scattering 26

2.5.3 Pair Production 27
2.5.4 Alpha radiation on Materials of the Detector 27
2.6 Radiation Health effects 30
2.7 Radiation Exposure effects 32
2.7.1 Acute effects 33
2.7.2 Chronic effects 34
2.8 Radiation Dosimetry 34
2.8.1 Exposure 34
2.8.2 Absorbed Dose 35
2.8.3 Dose Equivalent 35
2.8.4 Effective Dose 36
2.9 Radiological Hazard Indices 37
2.9.1 Excess Life Time Cancer Risk (ELCR) 38
2.10 Radiation Protection and Exposure Limits 38
2.10.1 The radiological protection principles 39

3 Experimental Methods **40**
3.1 Study Area 40
3.1.1 Demography 42
3.1.2 Climate 43
3.2 Sample collection 43
3.2.1 Sample receipt and storage 44
3.2.2 Sample Preparation for alpha and gamma spectroscopy . 46
3.3 Detection System 48
3.3.1 Semiconductor Silicon Detectors 49
3.3.2 Scintillation Detectors 49
3.4 Applied Measurement Techniques for this study 51
3.4.1 Alpha Spectrometry for analysis of Radium 51
3.4.2 Alpha Spectroscopy Experimental Set-up 53
3.4.3 Calibration of Alpha Spectrometry 54
3.4.4 System background check 58
3.5 Gamma Spectrometry 59
3.5.1 Hyper-pure Germanium Detector 59
3.5.2 Operational Principles of Gamma- ray Spectroscopy . . . 61
3.6 Solid-state Alpha Detectors for Radon measurements 63
3.6.1 RAD-7 unit 64
3.6.2 An Infrared (IR) printer 66
3.6.3 RAD-7 Spectrum Analysis 67

3.6.4 Measurement procedure for the study 68
3.7 Quality Control of RAD-7 alpha-Spectrometer 69
3.7.1 Preparation of standards 69
3.7.2 RAD-7 Calibration 70
3.7.3 Effects of measuring time on Radon Concentration . . . 72
3.7.4 Decay correction 74
3.8 Statistical Analysis of result 74

4 Results, Analysis and Discussions 76
4.1 Activity of Radium in water 77
4.1.1 Overview of the Ra-226 data collected over four seasons . 77
4.1.2 Interpretation and discussion of radium results 78
4.2 Activity of Radon in water 85
4.2.1 Overview of radon data collected over four seasons . . . 85
4.2.2 Discussion of radon results 88
4.3 Statistical analysis of results 95
4.3.1 Overall Average Activity Concentrations 95
4.4 Estimations of Radiation Protection quantities due to Radium and Radon in water sources 98

5 Conclusion and Recommendations 109
5.1 Recommendations for future studies 111

Bibliography 120

A Anova Analysis 121

List of Figures

1.1 Decay chain of uranium series (taken from Ref. [4]) 2

2.1 Growth of activity and secular equilibrium of ^{222}Rn produced by the decay of ^{226}Ra (taken from Ref. [25]) 16
2.2 Decay series of uranium-238 (^{238}U), uranium-235 (^{235}U), and thorium-232 (^{232}Th). Time shown are half-lives inside the squares and mode of decay indicated (taken from Ref. [29]) 18
2.3 Decay scheme of ^{226}Ra into ^{222}Rn with corresponding alpha and gamma decay energies (taken from Ref. [33]) 19
2.4 Plot of the coefficient for radon as a function of water temperature. The solubility coefficient in water is defined as the ratio C_w/C_a, where C_w and C_a are the radon concentrations in water and air, respectively (taken from Ref. [40]) 23
2.5 Radon Decay Chain (taken from Ref.[41]) 24
2.6 Photoelectric absorption within an atom (taken from Ref.[1]) . . 26
2.7 The illustration of Compton scattering showing the directions of the scattered photon and electron with respect to the direction of the incident photon.(taken from Ref. [43]) 26
2.8 Pair production effect (taken from Ref. [1]) 27
2.9 The range of alpha particles in silicon with their respective energy (taken from Ref. [44]) 29
2.10 Direct and indirect actions of ionizing radiation on DNA (taken from Ref. [49]) 31
2.11 Biological effects of ionizing radiation (taken from Ref. [50]) . . 33

3.1 A layout map showing the West Rand and selected mines (taken from Ref. [61]) 41
3.2 A picture taken during sample collection activity at the downstream of Driefontein mine 42

3.3 Distribution of population by age and sex, West Rand district – 1996, 2001 and 2011 (taken from Ref. [62]) 43
3.4 An Electra Gm used for background radiation level and surface radiation level on containers. 45
3.5 Sample storage 46
3.6 Filtration instrumental set-up used in sample preparation procedures. 47
3.7 Prepared samples awaiting measurements and analysis 47
3.8 LHS: The filtration of radium precipitate in solid form. RHS: Prepared samples on filter paper 48
3.9 Schematic representation of alpha spectrometry system, including associated electronics and recording devices, (taken from Ref. [65]) 53
3.10 Alpha spectroscopy chambers manufactured by CANBERRA . . 54
3.11 LHS: display with Genie 2000 software. RHS: Vacuum pump . . 54
3.12 Calibration source prepared on a stainless steel disk. 55
3.13 Energy Calibration of the detector 56
3.14 Plot of energy calibration curve for the standard source with photo-peak energies listed in Table 3.2 57
3.15 Energy peak efficiency as a function of energies for alpha spectroscopy detector 58
3.16 Two cross section examples of geometries used for Ge Detectors; (a) coaxial; (b) well or planar type. (taken from Ref. [53]) . . . 60
3.17 A typical schematic cross section of HPGE germanium detector set up cooled by a tank of nitrogen.(taken from Ref. [67]) 61
3.18 Pictures of HPGe detector situated at the NNR Environmental Laboratory 62
3.19 Schematic representation of the experimental setup of RAD7 using a grab sample and a radon-in-air monitor, an α-spectrometry method (taken from Ref. [23]) 63
3.20 A RAD-7 system aerating 250 ml water sample at Necsa's Radio-Analysis Laboratory, Pretoria. With the RAD-7 unit, RAD-H2O accessory, and An Infrared (IR) printer numbered 1-3 respectively. 64
3.21 Measurement chamber of the RAD-7 (taken from Ref. [69]) . . . 65
3.22 The internal process of the measuring chamber of the RAD-7 detector (taken from Ref. [68]) 65

3.23 Produced results summary by the RAD-7 instrument for a trial run measurement exhibiting data information, that entails time, the mean radon concentration and its standard deviation, a bar chart for the complete set of readings and a cumulative spectrum. In the cumulative spectrum, the main four windows are shown separated by dots 68
3.24 Laboratory prepared ^{226}Ra standard samples. 70
3.25 Correlation between measured ^{222}Rn and RAD-7 measured results 72
3.26 Effects of time in radon concentration yield inside the Rad-7 chamber 73

4.1 June 2019 ^{226}Ra concentration results 80
4.2 September 2019 ^{226}Ra concentration results 80
4.3 December 2019 ^{226}Ra concentration results 81
4.4 March 2020 ^{226}Ra concentration results 81
4.5 Bar graph showing the radium concentration from June 2019 to March 2020 82
4.6 Percentage composition of the total radium concentration of water samples during the seasonal survey. 84
4.7 Percentage composition of the total radium concentration per sample area for all the seasonal survey. 84
4.8 June 2019 ^{222}Rn concentration results 89
4.9 September 2019 ^{222}Rn concentration results 89
4.10 December 2019 ^{222}Rn concentration results 90
4.11 March 2020 ^{222}Rn concentration results 90
4.12 Bar graph showing the radon concentration from June 2019 to March 2020. 91
4.13 Percentage composition of the total radon concentration of water samples during the seasonal survey. 92
4.14 Percentage composition of the total radon concentration per sample area for all the seasonal survey. 92
4.15 Humidity inside the the RAD-7 chamber as the samples were counting 94
4.16 Temperature inside the the RAD-7 chamber as the samples were counting 94
4.17 ^{226}Ra and ^{222}Rn activity concentration in June 2019 98
4.18 Estimated annual effective dose due to ^{222}Rn from June 2019 to March 2020 104

4.19 Estimated annual effective dose due to ^{226}Ra exposure from June 2019 to March 2020 105
4.20 Estimated Excess lifetime Cancer risk due to ^{222}Rn from June 2019 to March 2020 105
4.21 Estimated Excess lifetime Cancer risk due to ^{226}Ra from June 2019 to March 2020 106

List of Tables

2.1 Known abundance of Radium [34] 21
2.2 Decay products of radium 21
2.3 Physical properties of ^{222}Rn [40] 22
2.4 Radioactive properties of ^{222}Rn and its short-lived progeny . . . 25
2.5 Acute effects (High dose) observed over different radiation dose exposures 34
2.6 Quality factor (Q) for several types of radiation 36
2.7 Recommended Weighting factors for body tissues or organs [55] 36

3.1 Origin and sample information of the samples under investigation 44
3.2 Calibration source with corresponding activity and photo-peak energy 56
3.3 Detector efficiency using calibration source 58
3.4 Radon standard sample concentrations (Rn-CStd) measured by Rad-7 (Rn-C_{RAD-7}) 71
3.5 Measuring time with corresponding radon activity observed in ordinary tap water 73

4.1 Activity concentration results of ^{226}Ra in the measured water samples including their uncertainties. 78
4.2 Activity concentration results of ^{222}Rn in the measured water samples including their uncertainties. 87
4.3 Activity concentration results of ^{226}Ra and ^{222}Rn in the measured water samples including the corresponding pH and Conductivity. 97
4.4 Annual effective dose for ingestion of radium and radon results. 101
4.5 Excess Lifetime Cancer Risk (ELCR) for ingestion of radium and radon results. 102
4.6 Classification of radiation dose for drinking water [68]. 107

4.7 ^{222}Rn average annual effective dose due to the ingestion (AED) of radon in river water samples and color code classification. . . 108

A.1 ^{226}Ra Activity Concentration (mBq/l) from June 2019 – March 2020 in water samples 121
A.2 ^{226}Ra Activity Concentration (mBq/l) from June 2019 – March 2020 of radon identical water samples 122
A.3 ^{226}Ra AED estimation (mSv/y) in water samples 122
A.4 ^{226}Ra ECLR estimation (mSv/y) in water samples 123
A.5 ^{222}Rn Activity Concentration (mBq/l) from June 2019 – March 2020 in water samples 123
A.6 ^{222}Rn AED estimation (mSv/y) in water samples 124
A.7 ^{222}Rn ECLR estimation (mSv/y) in water samples 125
A.8 ^{226}Ra and ^{222}Rn Activity concentration (mBq/l) in June 2019 water samples 125
A.9 ^{226}Ra and ^{222}Rn Activity concentration (mBq/l) in September 2019 water samples 126
A.10 ^{226}Ra and ^{222}Rn Activity concentration (mBq/l) in December 2019 water samples 126
A.11 ^{226}Ra and ^{222}Rn Activity concentration (mBq/l) in Mar 2019 water samples 126

Chapter 1

Introduction

1.1 Background

Radioactivity has existed since the beginning of time and is part of our planet Earth. Natural radioactivity is a source of radiation exposure to the environment and to human beings, with the two main sources being terrestrial and cosmogenic radionuclides. Naturally Occurring Radioactive Materials (NORM) which are found in rocks and soil formations emit different amounts of radiation, that human beings are exposed to via water, food and human tissue. The primary examples of NORM are ^{238}U, ^{235}U and their daughter products, and the radiation emitted by these radionuclides are mainly through alpha, beta and gamma decay.

Naturally occurring radioactive substances in the environment were discovered as a mixture of several isotopes which are often related. These are the members of series of isotopes from different radioactive elements (Uranium, Thorium, and Actinum). Uranium is the most abundant of the radioactive elements, and it consists of three isotopes ^{238}U, ^{235}U and ^{234}U. The ^{238}U and ^{234}U belong to the same family, the Uranium series while ^{235}U is the first member of series called actinum. These isotopes that are members of the radioactive series have almost the same features, series members are long-lived with a half-life that may be counted in geological time units. The final end product is lead in each case, each series consists of a gaseous member that is a different isotope of Radon element. The uranium series has the isotopes of interest in the study that is the ^{226}Ra and the gaseous member ^{222}Rn. The uranium series is called the 4n+2 chain of ^{238}U, and during it's decay process Radium (^{226}Ra) and Radon (^{222}Rn) are given out. A detailed uranium decay

chain (series) is shown in Fig. 1.1 with the radionuclides respective half-lives and they are present in any natural uranium containing sample.

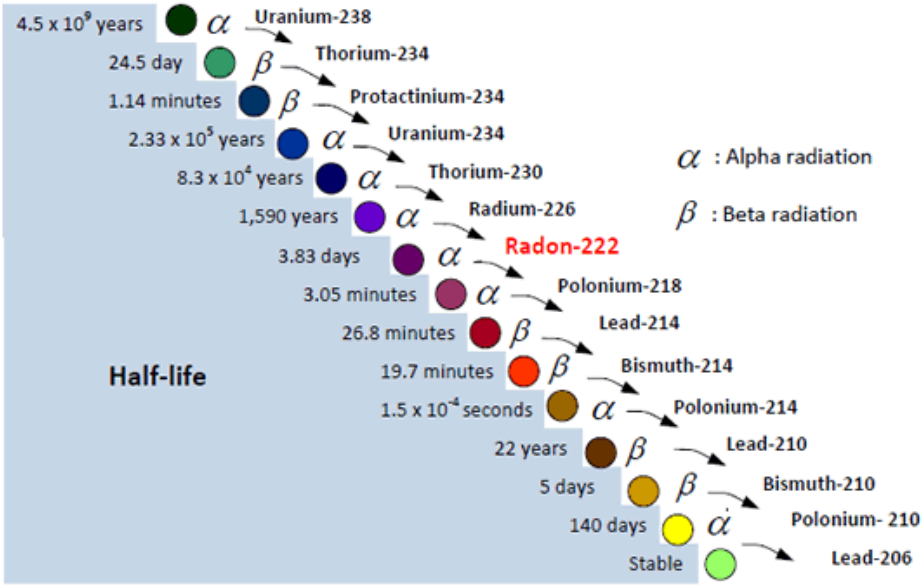


Figure 1.1: Decay chain of uranium series (taken from Ref. [4])

Radiation exposure can be received from human activities such as mining and mining processes, and they may result in situations whereby the radioactivity levels of materials that contain natural radionuclides are significant enough to warrant regulatory control [5]. In some areas in the world the radiation concentrations are high due to presence of Uranium deposits in the vicinities where mining operation took place. Uranium is widely distributed in the Earth's crust and oceans where it has an average abundance of two parts per million (ppm) and five parts per billion (ppb), respectively [6]. Some rocks contain uranium bearing minerals and are usually mined using different procedures such as conventional open pit or underground, depending on the geological condition of the ore. Natural radioactivity due to uranium and its associated decay progeny is widely spread in the Earth's crust.

Mining of radioactive ores for uranium production is common in our country. South Africa is one of largest uranium producers in Africa. Many uranium mining areas in South Africa are located in the northern part of Gauteng, the Beisa North, Buffelsfontein, The Denny Dalton, Dominion, Driefontein, Ergo, Hartebeestfontein, Karoo, KDC (Kloof), Kopanang, Mintails, Randfontein,

Rietkuil, South Deep, Vaal River and West Wits mine. Some are located in other places such as the Beafort West mine in the northern cape province of South Africa, the Moab Khotsong in North West and the proposed Springbok Flats Mine that will be located near Settlers in Southern Limpopo Province.

Uranium is passed onto humans either through inhalation of fine dust from the mine tailing or ingestion when mine waste enters rivers. In addition, these communities around West-Rand area are also directly exposed to radiation from some quantity of uranium and its radioactive daughter nuclides in the mine tailings. Although naturally occurring uranium exposure is low level and can be tolerated by humans, high levels of uranium exposure are well documented to cause health risks such as kidney damage, neurological problems and cancer.

Johannesburg is well known as the major city that is not built on a body of water, yet it has the Main Reef. The Witwatersrand mining belt is characterized by three mining areas called the West, Central and East Rand. Over a period of 90 years (1886-1976) gold was actively mined from underground workings. Historically, Johannesburg is the most productive gold reef, and precious metals have been mined from it. These mining activities have left behind a toxic inheritance of radioactivity from uranium hauled up from the mining activities. Gold and uranium occur in the same geological areas, and the Witwatersrand supergroup has more uranium than gold and has in fact also uranium mines with uranium originally a by-product of the gold mining industry [7]. Gold mining in the Wonderfonteinspruit (WFS) area of South Africa dates back to more than 120 years [8]. The WFS stream links both the West Rand and Far West Rand areas and is known for attracting media attention due to high levels of radioactive uranium related pollution.

West-Rand area is a mined out goldfield and its last operating mine was active in the 1990s, however, Far West-Rand is still being actively mined. West-Rand Consolidated company now operates these newly established goldfields. The West Rand mines are now abandoned and often contaminated. Thus, many residents in Gauteng are exposed to daily doses of uranium in the surrounding area.

1.2 Studies of Radium and Radon around mining sites

Radon naturally occurs in the environment from the decay of radioactive elements in uranium mines. Similarly, radium is a radioactive element that is found in small quantities in nature and may cause hazards to life if highly concentrated. Uranium minerals emit radon gas, and harmful highly radioactive daughter products thus making uranium mining more dangerous than other hard rock mining. It requires adequate ventilation systems if mines are not open pit. The radon level in an operating mine can be controlled by ventilation, sealing off old workings and controlling mining process water. The radioactivity level in a mine can rise when the mine is abandoned. Extensive data on quantitative risks of lung cancer associated with radon progeny exposure in underground mines have been provided by investigations of uranium [9]. Underground miners not only inhale radon progenies but also dust and blasting fumes, thus inflammation of the airways with increased cell proliferation may result.

It was pointed out in Ref. [10] that in the uranium mining industry, radiological exposures to ^{222}Rn daughters are the most significant hazard. Radon gas also appears in the natural radiation environment wherever natural uranium exists in surface rocks and ores. Radon-222 and its daughters present a unique problem and hence much instrumentation developed for their measurement is unique .

Uranium mining in South Africa has resulted in large amounts of tailings which are deposited in impoundments. The tailings mostly escape and seep into running water or dams adversely affecting water quality. An investigation of evaluation of radiological hazards from gold mine tailings in the province of Gauteng in South Africa was reported in Ref. [11]. This study used gamma spectroscopy to measure the activity concentrations of these radionuclides in 56 soil samples from the mine tailings and 10 soil samples from the control area. It was found that the average activity concentrations in Bq.kg^{-1} for ^{238}U, ^{233}Th, and ^{40}K from the mine tailings were 785.3 $\pm$ 13.7, 43.9 $\pm$ 1.0 and 427.0 $\pm$ 13.1, respectively. Radiological hazard parameters calculated from these activity concentrations were higher than recommended safe limits. In particular, calculated average values for the external hazard (Hex) and the

internal hazard (Hin) from the mine tailings were found to be 2.4 and 4.5. Both these values were higher than unity, posing a significant health risk to the population in the area.

Many studies have been conducted elucidating potential risk to exposure of radon, radium and their genotoxic effects among people and the environment. Uranium has been actively mined and milled in the area and many people had been repeatedly exposed to radioactivity fallout. The environment had been contaminated through a number of activities including open pit mining process, transportation to and from milling sites, milling and processing of ore and open-air storage of radioactive and non-radioactive mining wastes. That result to exposure to a variety of hazardous materials and radon was found in high levels.

In Ref. [12], charcoal canisters and sodium iodide detectors were used to determine concentration levels and the effective exposure dose of radon in mining industries. Radiological risk of radon exposure was assessed in selected areas. Concentration levels of radon were found to vary from 28±1 to 97±5 Bq m^{-3} and the effective dose varied from 0.71±0.03 to 2.44±0.13 $mSvy^{-1}$, respectively. The mean radon concentration values reported were below the United Nations Scientific Committee on the Effects of Atomic Radiation (UNSCEAR) and International Commission on Radiological Protection (ICRP) recommended action level of 200 mBq/l. Some radon concentration results were close to 100 mBq/l an action level recommended by the World Health Organization (WHO), that implied that radon concentration levels were still within limits.

Witwatersrand gold or uranium mines have natural radioactivity in their tailing impoundments, posing a potential source of contamination of environmental waters. This results from the presence of large activities, although at low concentrations of ^{226}Ra, giving out ^{222}Rn in the Witwatersrand mines. Detection of partition function (K_d) in the tailings impoundments takes place in field and laboratory studies, from which mobility of radium ore is deduced.

An international research study reported in Ref. [1] was also conducted to assess ^{222}Rn and ^{226}Ra activity concentrations in drinking water sources using active and passive detection methods. The measurements were carried out by using RAD-7 [1] as an active method for alpha analysis and a permeable cup provided with a CR-39 alpha nuclear track detector as a passive method.

Sodium iodide NaI(Tl) detector was used as an active method for gamma spectrometry for radium (^{226}Ra) activity concentration measurement for the same water samples. The results revealed that values of radon concentration in water samples were mostly below the maximum contamination level 11.1 Bq/l recommended by US-EPA. The results for radium demonstrated that some well water had higher than the maximum contamination level of 555 mBq/l suggested by US-EPA, whereas other samples mostly from surface water were lower than 555 mBq/l.

1.3 Problem statement

Water is the most fundamental source of life on earth, and makes up 70 - 75% of total body weight. Whereas out of about 70% of the earth surface covered by water, only 0.3% of the total water resources on earth is suitable for daily use. Therefore, water is one of the most valuable resources. Monitoring water quality based on radium and radon investigations and estimations is among one of the essential public health studies, as it reveals the extent of population exposure to radiation. Hence, this attempt at radioactivity assessment of radium and radon water sources around former uranium mines in the West-Rand area of Johannesburg was attempted in this study. According to the World Health Organization (WHO), through meticulously measured activity of radionuclide-specific concentrations of natural $\alpha-$emitters, radionuclide-specific concentrations should be brought into compliance with WHO guidance levels which are 1 Bq/L for ^{226}Ra and 100 Bq/L for ^{222}Rn [13].

Studies of radium and radon concentration in different types of water such as groundwater, drinking water, boreholes and few rivers have been carried out over the past decade. These studies were conducted to measure the quality of water from active and former mines [1] and also from aquifers and rivers. A research study by Ava Nourian Dehkordi (University of the Witwatersrand - Johannesburg 2012) [14], investigated radiation doses to the West Rand public due to inhalation of ^{222}Rn and its daughter products. This study presents the results of radon monitoring carried out in selected houses close to gold and uranium mining operations in the West rand. Monitoring of radon and its progeny was carried out inside selected houses that were built about 100 years ago, using a calibrated AlphaGuard PQ2000PRO active instrument. The results were compared with long-term measurements performed in the same

areas using the passive RGM (Radiation Gas Monitor) caps. Dose assessment as a result of inhaling air possibly contaminated by radon and its progeny was based on the obtained results of radon monitoring and the doses were also compared to internationally accepted intervention and action levels established by International Commission of Radiological Protection 65 (ICRP) and various regulatory authorities throughout the world [14].

Uraniferous ores are radioactive in nature and may result in occupational hazards to the mine workers and the environment. Uranium decay products are considered as major causes of health and safety concern for miners. Uranium ore consists of ^{226}Ra (decay by-product) and it is a natural source that emits high levels of radiation in uranium mines.

^{226}Ra has a long half-life of 1600±7 years, therefore it acts as an effective source of radon (^{222}Rn) gas with a relatively short half-life of 3.83 days in a mine atmosphere. ^{222}Rn in the uranium decay series is the only gaseous member and it decays through a series of short-lived decay products namely, ^{218}Po, ^{214}Pb, ^{214}Bi and ^{214}Po [15]. When radon has been inhaled, its daughter products which are atoms of heavy metals are deposited in the respiratory system and irradiate the lung tissue for a relatively long time. In addition, radon and its daughter products emitting alpha particles are recognized as main causes for lung cancer when high radon doses are inhaled. In Ref. [16], it was suggested that radon concentration in underground uranium mine atmosphere mainly depends on the emission of radon from an ore body, broken ore, backfill milling tailings, and mine water. The different sources that emit radon into mine atmosphere depend on various factors such as the type of mineralization, grade, radium content, porosity and moisture content of the ore as well as atmospheric pressure, ventilation rate and temperature.

In view of previous studies of radium and radon in water, the current study was done to broaden the scope and determine whether ^{226}Ra and ^{222}Rn concentration in the mines around the West-rand from the former mining activities is elevated. This was done by measuring radium and radon concentration from different water samples. The study covers mainly former uranium mines from western side of Gauteng province, South Africa. The Aim of this study was to assess the radium and radon concentrations in water sources at and near selected former uranium mines in the West-Rand area. The Objectives were

to:

1. Investigate radiation exposure through ingestion of contaminated water.
2. Evaluate the quality of water in respect of its radioactivity concentration.
3. Estimate biologically harmful radiation indices (annual effective dose dose)r different age groups.

1.4 Scope of the dissertation

The structure of this dissertation is as follows:

Chapter 1 introduces the context and the objectives of this study.

Chapter 2 describes the theoretical backgrounds related to the study. This includes characteristics of radium and radon and its properties, the radium and radon progeny decay series which also covers the origin of the isotopes of interest and their propagation in nature. Chapter 2 then continues with discussions concerning radiation dosimetry, health effects, radiation protection and exposure limits for members of the public.

Chapter 3 discusses the set-ups and experimental aspects of measuring radium and radon in this work. This includes the equipment used for analysis in this study and a detailed description of the experimental procedures. These techniques include alpha spectrometry and γ-ray spectrometry.

Chapter 4 outlines the analysis of the data and presentation of the experimental results obtained.

Chapter 5 presents the discussions of the findings and elaborate the conclusions of this study.

Chapter 2

Theoretical Considerations

Radionuclides of interest in this study, that is, radium and radon are disintegration products of uranium, hence this chapter discusses the origin of these radionuclides and their propagation in nature. In addition, applicable theoretical aspects in understanding radioactivity as well as major radiation protection concepts are addressed.

2.1 Radioactive decay

Towards the end of the 19^{th} century, minerals were found to darken a photographic plate even in the absence of light [17]. This phenomenon is now well known as radioactivity and has existed since the creation of the Earth. An unstable nuclei can decay by α-particle, β-particle or γ-ray emission to become a nuclei [18], that may in turn be also radioactive. Therefore a decay series can arise. Below are the example equations of each radiation emission [19].

$$^{210}_{84}Po \longrightarrow {}^{4}_{2}He + {}^{206}_{82}Po \tag{2.1}$$

$$^{131}_{53}I \longrightarrow {}^{0}_{-1}e + {}^{131}_{54}Xe + {}^{0}_{0}\gamma \tag{2.2}$$

$$^{60}_{27}Co \longrightarrow {}^{0}_{0}\gamma + {}^{60}_{27}Co \tag{2.3}$$

These are the three classified emissions, α, β- and γ-decay as illustrated by equations 2.1 to 2.3.

2.1.1 Alpha Decay

Alpha decay is the nuclear decay process in which unstable atomic nuclei dissipate excess energy by spontaneously ejecting an α-particle. During alpha decay, an atomic nucleus emits an α-particle and decays into a different atomic nucleus, with mass number reduced by 4 and atomic number reduced by 2. The α-particles are emitted as decay products of many radionuclides that possess a large nucleus, predominantly with an atomic number greater than 81 [20]. It is known that the α-particles do not penetrate far into a material and can be stopped quite easily; however they are able to break chemical bonds (which can cause chemical or biological damage) when they strike a molecule because of their size, mass, and charge. The penetration depth of α-particles depends upon the energy emitted at and the penetrating material. Thus, because α-particles can be stopped by thin barriers such as a piece of paper or skin, α-emitters are most damaging if ingested or inhaled into the lung [21]. The decay process is:

$$ {}^{A}_{Z}X_{N} \longrightarrow {}^{A-4}_{Z-2}X^{|}_{N-2} + {}^{4}_{2}He_{2} + E \tag{2.4} $$

where X and $X^{|}$ are the initial and final nuclei, A is the total mass number, N is the number of neutrons, Z is the number of protons in the nucleus and E is the energy given out. The released energy Q from decay emerge from a total loosed masses $M_{X,N}$, $M_{X^{|},N}$ and $M_{He,N}$ of the parent, daughter, and Helium nuclei:

$$ Q = M_{X,N} - M_{X^{|},N} - M_{He,N} \tag{2.5} $$

The Q value is shared by alpha and the recoil daughter nucleus. Since the parent nucleus was at rest, the momenta of the two decay products must be opposite and equal. Making m and v represent the mass and initial velocity of the alpha particle and M and V those of recoil nucleus [22], thus

$$ mv = MV \tag{2.6} $$

Since the initial kinetic energy of the products must be equal to the energy released in the decay, it follows

$$ \frac{1}{2}mv^{2} + \frac{1}{2}MV^{2} = Q \tag{2.7} $$

Substituting $V = \frac{mv}{M}$ from Eq. (2.6) into Eq. (2.7) and solving for v^2, one

finds

$$v^2 = \frac{2MQ}{m(m+M)} \tag{2.8}$$

Thus, the alpha particle energy obtained is,

$$E_\alpha = \frac{1}{2}mv^2 = \frac{MQ}{m+M} \tag{2.9}$$

With the roles of the two masses interchanged, the recoil energy of the nucleus is as follows

$$E_N = \frac{1}{2}MV^2 = \frac{mQ}{m+M} \tag{2.10}$$

As a check, we see that $E_\alpha + E_N = Q$ (from equation 2.7). The Q value for the less frequent alpha particle can be found from Eq. (2.9)

$$Q = \frac{(m+M)E_\alpha}{M} \tag{2.11}$$

If E_α represents kinetic energy of the alpha particle, the value of Q may be written as $Q = E(\frac{m}{M} + 1)$, Thus E:

$$E = \frac{Q}{1 + (\frac{m}{M})}. \tag{2.12}$$

E is slightly less than the Q-value, that implies nearly all the energy released in the decay is carried away as kinetic energy of the light particle.

2.2 Radioactivity Kinetics

The radioactivity of a known sample decreases in time, in other words, the number of nuclei in a radioactive sample that disintegrates during a given time interval decreases exponentially with time. Radioactivity is the number of times a radioactive decay occurs in the sample per unit time, and the standard unit for activity is the number of decays per second (Bq). This decay rate serves as a very useful means of identifying a given nuclide. Therefore, radioactive decay is a transformation of unstable radioactive nuclei to more stable nuclei, which may also be radioactive is an irreversible event.

2.2.1 Decay Equations

Radioactive decay rate is proportional to the number of each type of nuclei present in a given sample. A radioactive nucleus has a probability per unit time to decay and this is termed the decay constant, given by the symbol λ. The decay constant depends on the particular decay process occurred. From this, the Radioactive Decay Law can be derived as follows.

Let $N(t)$ be the number of radioactive nuclei in the sample at time t, the number of nuclei that decay in a time Δt equals $N(t)$ times the probability that one will decay in the time Δt. This is expressed in the equation below:

$$N(t) - N(t + \Delta t) = N(t)\lambda\Delta t \tag{2.13}$$

On dividing with Δt and multiplying by -1, we have

$$\frac{N(t) - N(t + \Delta t)}{\Delta t} = -\lambda N t \tag{2.14}$$

Taking a limit as Δt goes to zero, we obtain a simple differential equation for $N(t)$:

$$\frac{dN}{dt} = -\lambda N \tag{2.15}$$

Note that N is constantly reduced in magnitude as a function of time. Rearrangement of 2.15 to separate the variables gives [22];

$$\frac{dN}{N} = -\lambda dt \tag{2.16}$$

At $t = 0$, N_0 radioactive nuclei is present, then the integration of Eq. (2.16) gives the radioactive decay law:

$$N(t) = N_o e^{-\lambda t}. \tag{2.17}$$

The halt-life is related to the decay constant using the expression:

$$\tau = \frac{\ln 2}{\lambda} \tag{2.18}$$

This relationship allows us to determine the decay constant by measuring the half-life of a radioisotope.

In order to determine how many radioactive nuclei in the sample, the rela-

tion between activity and the decay constant is used. Let activity be $A(t)$ be the number of decays per unit time or decays/sec. Consider measuring for a time Δt, in terms of the number of radioactive nuclei at time t, $N(t)$, it can be noted that

$$A(t) = \frac{N(t) - N(t + \Delta t}{\Delta t} \tag{2.19}$$

Taking limit as Δt goes to zero, thus:

$$A(t) = -\frac{dN}{dt} = -\frac{d(N_o e^{\lambda t})}{dt} = \lambda N t, \tag{2.20}$$

which can be written as

$$A = \lambda N = \frac{N \ln 2}{\tau}. \tag{2.21}$$

This relationship assists in measuring the activity of a sample and the number of radioactive nuclei knowing the half-life of the isotope. Evaluation of the counting rate that is given by the detector as a function of time t, or the activity of a given sample can be determined. The counting rate in the radiation detector, C, is equal to the rate of disintegration of radioactive nuclei present in a sample denoted as Activity (A) multiplied by a constant related to the efficiency of the radiation system. Thus

$$C = \varepsilon A = \varepsilon\Big(- \frac{dN}{dt}\Big) = \varepsilon \lambda N \tag{2.22}$$

where ε is the efficiency. Substituting C into Eq. (2.17) yields:

$$C = C_0 e^{-\lambda t}, \tag{2.23}$$

where C is the counting rate at some time t due to radioactive sample that gave counting rate C_0 at time $t = 0$.

2.2.2 Two-Stage Radioactive Decay

The equations governing the decay of a radionuclide when the product of decay, the daughter nuclide is considered stable, are expressed in Section 2.7.1. Consider radioactivities where the daughter itself is radioactive. Suppose that $N_1(t)$ is the number of nuclei of the original radionuclide (parent) as a function of time and that λ_1 is its decay constant. Also, suppose $N_2(t)$ represents the number of nuclide of the daughter as a function of time and that λ_2 is its decay constant.

At equilibrium, the activity of the parent and daughter is equal to that of the daughter, and their ratio of decay constants are in the inverse ratio of the equilibrium concentrations of the parent and daughter. That is

$$\lambda_1 N_1(t) = \lambda_2 N_2(t) \tag{2.24}$$

For the original radioactive nuclide, the time rate of change of the number of atoms is [23],

$$\frac{dN_1(t)}{dt} = -\lambda_1 N_1(t) \tag{2.25}$$

But the case of daughter:

$$\frac{dN_2(t)}{dt} = -\lambda_2 N_2(t) + \lambda_1 N_1(t) \tag{2.26}$$

Note from equation (2.17), $N_1(t) = N_o e^{-\lambda_1 t}$, then

$$\frac{dN_2(t)}{dt} = -\lambda_2 N_2(t) + \lambda_1 N_0 e^{-\lambda_1 t} \tag{2.27}$$

On multiplying through by $e^{\lambda_2 t}$ and collecting the terms with N_2 on LHS thus,

$$e^{\lambda_2 t}\frac{dN_2(t)}{dt} + e^{\lambda_2 t}\lambda_2 N_2(t) = \lambda_1 N_0 e^{(\lambda_2 - \lambda_1)t} \tag{2.28}$$

Note that $\frac{d(e^{\lambda_2 t} N_2(t))}{dt} = e^{\lambda_2 t}\frac{dN_2(t)}{dt} + e^{\lambda_2 t}\lambda_2 N_2(t)$ which is equal to the LHS of equation (2.35), so the equation 2.35 becomes

$$\frac{d(e^{\lambda_2 t} N_2(t))}{dt} = \lambda_1 N_0 e^{(\lambda_2 - \lambda_1)t} \tag{2.29}$$

On integration, both sides gives:

$$e^{\lambda_2 t} N_2(t) = \frac{\lambda_1}{\lambda_2 - \lambda_1} N_0 e^{(\lambda_2 - \lambda_1)t} + C \tag{2.30}$$

Where C is the integration constant.

To find C, we use the boundary condition, $N_2 = 0$ at $t = 0$, we have

$$e^{\lambda_2 (0)} N_2(0) = \frac{\lambda_1}{\lambda_2 - \lambda_1} N_0 e^{(\lambda_2 - \lambda_1)0} + C \tag{2.31}$$

therefore

$$C = N_2(0) - \frac{\lambda_1}{\lambda_2 - \lambda_1} N_0 \tag{2.32}$$

when $N_2(0) = 0$

$$C = -\frac{\lambda_1}{\lambda_2 - \lambda_1} N_0 \tag{2.33}$$

Thus,

$$e^{\lambda_2 t} N_2(t) = \frac{\lambda_1}{\lambda_2 - \lambda_1} N_0 e^{(\lambda_2 - \lambda_1)t} - \frac{\lambda_1}{\lambda_2 - \lambda_1} N_0 \tag{2.34}$$

finally,

$$N_2(t) = \frac{N_0 \lambda_1}{\lambda_2 - \lambda_1} (e^{-\lambda_1 t} - e^{-\lambda_2 t}) \tag{2.35}$$

The activity of the parent is $N_1(t) \times \lambda_1$ and the activity of the daughter is found by multiplying the above expression by λ_2.

When both sides of Eq. (2.35) are multiplied by λ_2, then the expression for the activity of the daughter becomes:

$$\lambda_2 N_2(t) = \frac{N_0 \lambda_1 \lambda_2}{\lambda_2 - \lambda_1} (e^{-\lambda_1 t} - e^{-\lambda_2 t}) \tag{2.36}$$

For cases in which the half-life of the parent is very much greater than that of the daughter that is, when $\lambda_1 \ll \lambda_2$, Equation (2.36) approaches the condition of secular equilibrium. The quantitative relationships prevailing during transient equilibrium may be inferred from Eq.(2.36) when λ_2 is greater than λ_1, then, after some long time, $e^{-\lambda_2 t}$ will become much smaller than $e^{-\lambda_1 t}$, equation Eq.(2.36) may be rewritten as

$$\lambda_2 N_2(t) = \frac{N_0 \lambda_1 \lambda_2}{\lambda_2 - \lambda_1} e^{-\lambda_1 t} \tag{2.37}$$

By application of Eq.(2.17), the expression for transient equilibrium, Eq(2.37) may be rewritten as

$$\lambda_2 N_2(t) = \frac{N_1 \lambda_1 \lambda_2}{\lambda_2 - \lambda_1} \tag{2.38}$$

2.2.3 Secular Equilibrium

Secular equilibrium in a radioactive decay chain can only occur if the half-life of the parent radionuclide is much greater than the half-life of the daughter radionuclide, that is $\lambda_1 \ll \lambda_2$. In such a case, the half-life of the parent is so long that there is a negligible decrease in the activity of the parent for the real-time observation [24]. Most nuclear techniques that are used for measuring parent radiation are underpinned by secular equilibrium indirectly through the progeny produced.

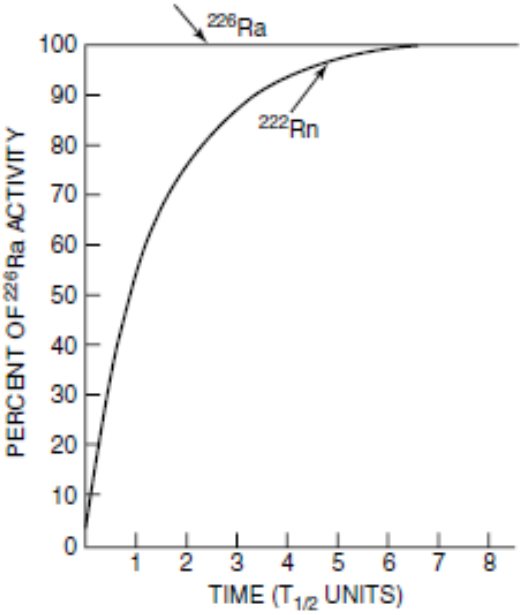


Figure 2.1: Growth of activity and secular equilibrium of ^{222}Rn produced by the decay of ^{226}Ra (taken from Ref. [25])

The growth of activity and the activity at equilibrium for ^{222}Rn produced in a closed environment is illustrated in the Fig. 2.1. Several half-lives of ^{222}Rn must elapse before the activity equals 99% of the parent activity [25]. The equation for the activity of the daughter in equilibrium is given by the Bateman equations. At any time t_0, the activity of the parent is $\lambda_1 N_1$ and the activity of the daughter is $\lambda_2 N_2$ [24]. If N_1 and N_2 are the numbers of atoms of each at any time t_0, then

$$\frac{dN_1}{dt} = -\lambda_1 N_1 \tag{2.39}$$

and

$$\frac{dN_2}{dt} = -\lambda_2 N_1 + \lambda_1 N_1. \tag{2.40}$$

Integrating Eq.(2.40) yield a solution for the number of atoms of daughter N_2 at any time t:

$$N_2(t) = N_1(t_0)\frac{\lambda_1}{\lambda_2 - \lambda_1}(e^{-\lambda_1 t} - e^{-\lambda_2 t}) + N_2(t_0)e^{-\lambda_2 t}. \tag{2.41}$$

Reformulating Eq. (2.41) in terms of activity by the use of the two equations expressing activity of the daughter and parent in the form of N_2 and N_1:

A_2=$\lambda_2 N_2$ and A_1=$\lambda_1 N_1$. Substitution into the following form for activity of the daughter at any time t yields:

$$A_2(t) = A_1(t_0)\frac{\lambda_2}{\lambda_2 - \lambda_1}(e^{-\lambda_1 t} - e^{-\lambda_2 t}) + A_2(t_0)e^{-\lambda_2 t} \tag{2.42}$$

Now for secular equilibrium, after a period of time t, and several half-lives, the term $e^{-\lambda_2 t}$ will be approximately zero[24]. With this approximation and the activity of the parent nucleus $A_1(t) = A_2(e^{-\lambda_1 t})$ the secular equilibrium is derived mathematically:

$$A_1(t) \approx A_2(t) \tag{2.43}$$

2.3 Occurrence of Radium and Radon

The concept of radioactivity and radium was discovered by Marie and Pierre Curie while studying radioactivity [26] in pitchblende. The mineral was found radioactive even after removal of uranium from it. Understanding the occurrence of radium can lead to better understanding the occurrence of radon. Ample radiological and epidemiological studies worldwide have been carried out on radium and radon as subjects [27].

The various radioactive isotopes of naturally occurring radium are ^{223}Ra, ^{224}Ra, ^{226}Ra and ^{228}Ra. Figure 2.2 presents the three decay series namely Uranium series, Thorium series and Actinum series. ^{224}Ra, the 5^{th} radionuclide in the ^{232}Th decay series, is derived from the decay of ^{228}Th and has the shortest half-life (3.64 days) as compared to that of ^{223}Ra (11.43 days) in the ^{235}U series. ^{228}Ra and ^{226}Ra has half-lives 5.7 years and 1602 years, from ^{232}Th and ^{238}U decay series, respectively. These isotopes are the most long-lived isotopes of radium. ^{223}Ra, ^{224}Ra and ^{226}Ra decay by emitting an alpha particle, whereas ^{228}Ra emits a beta particle in decaying to ^{228}Ac. Radium is relatively insoluble or immobile in water whereby its concentration is controlled by uranium content of the encasing rocks and the recoil process from the alpha-decay of ^{230}Th, depending on the water chemistry, including the ion concentrations of Ca^{2+}, Mg^{2+}, Ba^{2+}, Cl^{-1} and SO_4^{2-}, salinity and pH [27]. Ref. [27], further states that radium can be ingested in water sources and the resulting dose can be of concern in areas contaminated by mining industries or by radium processing plants. Radium in drinking water enhances cancer risks, primary bone and sinus cancers.

Two isotopes of concern in drinking water have been indicated in Ref. [28], and those are ^{226}Ra and ^{228}Ra. ^{226}Ra is a member of ^{238}U series with parent ^{230}Th and daughter ^{222}Rn, decaying through alpha emission.

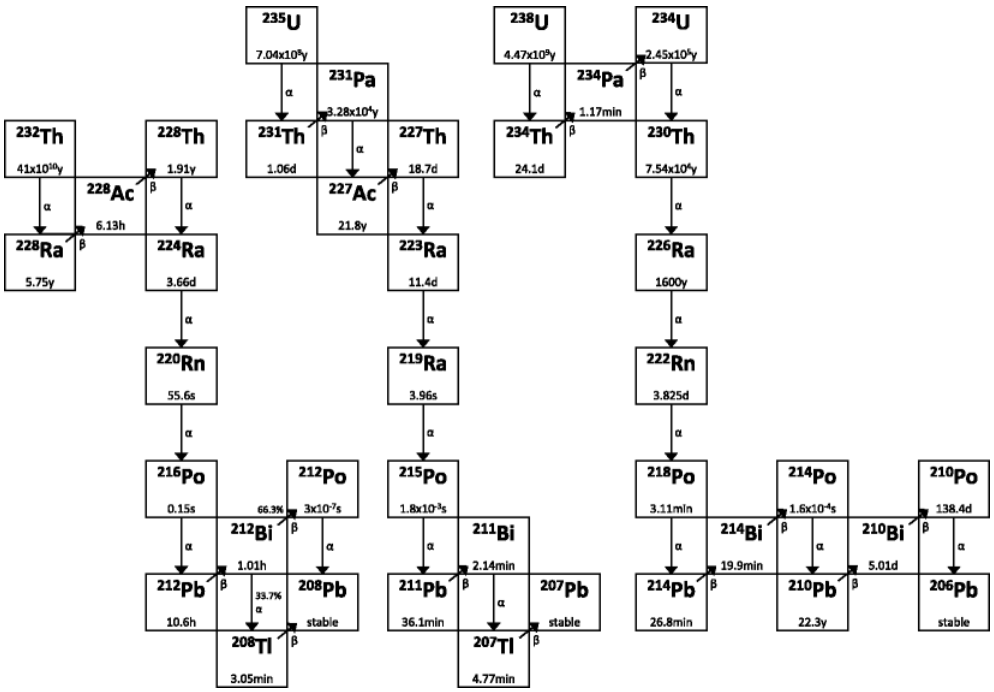


Figure 2.2: Decay series of uranium-238 (^{238}U), uranium-235 (^{235}U), and thorium-232 (^{232}Th). Time shown are half-lives inside the squares and mode of decay indicated (taken from Ref. [29])

Fredrich Dorn firstly discovered radon in 1900 [30], whilst he was working with the element radium. Radon's longest-lived isotope is ^{222}Rn, with half-life of 3.83 days in the ^{238}U decay series depicted in Fig. 2.2. Thoron ^{220}Rn and actinon ^{219}Rn are other natural radon isotopes, with half-lives 56.6 seconds and 3.96 seconds, respectively. These isotopes arise from ^{232}Th and ^{235}U decay series, respectively as shown in Fig. 2.2. Uranium and radium concentrations largely control the rate of release of radon from rocks and soils. Radon decays to form short-lived radioactive particles that can enter the body through inhalation.

^{222}Rn is a noble, colorless and odorless radioactive gas that is produced by the alpha decay of the radioactive alkaline earth metal ^{226}Ra [31]. Alpha radiation is a product of radioactive decay in which a helium nucleus ${}^{4}_{2}He^{2+}$

(the alpha particle) is emitted. This is illustrated below by the disintegration processes of ^{238}U and ^{226}Ra [22, 32]:

$$^{238}_{92}\mathrm{U} \longrightarrow {}^{234}_{90}\mathrm{Th} + {}^{4}_{2}\mathrm{He}^{2+} + 4.274MeV \tag{2.44}$$

$$^{226}_{88}\mathrm{Ra} \longrightarrow {}^{222}_{86}\mathrm{Rn} + {}^{4}_{2}\mathrm{He}^{2+} 4.785MeV \tag{2.45}$$

Equation (2.45) represents the production of ^{222}Rn which can be isolated through radioactive alpha decay of ^{226}Ra. The transformation or decay of ^{226}Ra into ^{222}Rn is shown in Fig 2.3. The decay scheme shows two alpha particles of different energies from the radioactive transition of ^{226}Ra. The first (4.78 MeV) occurs in 94% of the transformations and leads directly to the ground state of ^{222}Rn; the other (4.59 MeV) occurs 6% of the time and leaves the product nucleus in an excited state. The excited nucleus reaches the ground state by emitting a gamma-ray of 0.186 MeV with a yield of 3.59% (internal conversion accounts for the other 2.1% by this route). The existence of these two different alpha particle energies and the gamma ray demonstrates the importance of discrete nuclear energy states. The alpha particles for a given transition are monoenergetic, i.e., they all have the same energy [33].

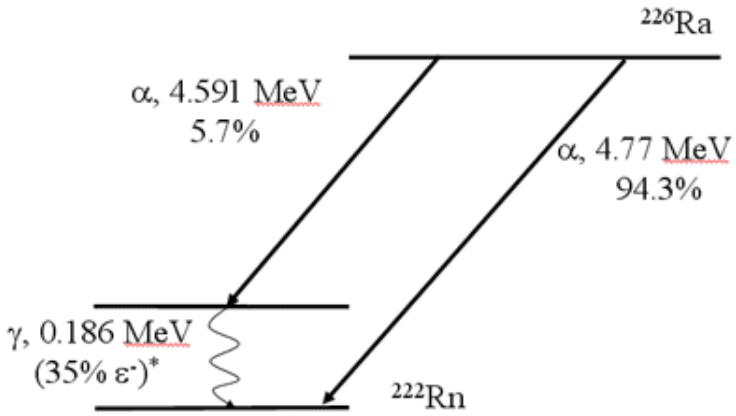


Figure 2.3: Decay scheme of ^{226}Ra into ^{222}Rn with corresponding alpha and gamma decay energies (taken from Ref. [33])

2.4 Radium and Radon Properties

Radium is a silvery, lustrous, soft, intensely radioactive chemical element with atomic number 88. It has an atomic weight of 226.0254 g/mol [34] and its normal phase is solid. Radium is an alkaline earth metal that is found in trace amounts in uranium-bearing ore [35]. Its appearance is almost pure white but turns black when it is oxidized with exposure to air. Radium is the heaviest of alkaline earth metals and resembles barium in its chemical behaviour [35]. It can be confirmed from Fig. 2.3 that radium emits an alpha particle and when the alpha particle is mixed with beryllium, it produces neutrons which are useful for physics experiments. Radium reacts violently with water and oil to form radium hydroxide and is slightly more volatile than barium. Its most stable and longest-lived isotope is ^{226}Ra ($T_{1/2}$=1602 years), that occurs in the disintegration of ^{238}U series and decay into radon gas (^{222}Rn).

The element radium exhibits only one oxidation state (+2) in a solution. The ion is not easily complexed because of radium's basic character. Hence, most radium compounds are simply ionic salts, which are white when freshly, turning yellow and ultimately dark with aging owing to self-decomposition from alpha radiation [36]. The nitrate, bromide, and chloride of radium are soluble in water, but their solubilities decrease with increasing concentration of the respective mineral acid.

Radium metal is found in small-scale in the uranium ore "Pitchblende", and other various uranium minerals. All isotopes of radium are radioactive and short-lived on a geological time scale, any primeval radium would have disappeared long ago. Therefore, radium occurs naturally only as a disintegration product in the three natural radioactive series (Uranium, Thorium and Actinum series) [34]. Radium is a decay product of the Uranium series and therefore can be found in uranium processing waste. Table 2.1 lists the known abundance of radium.

Table 2.1: Known abundance of Radium [34]

Location	ppp by weight	ppp by atoms
Universe	0	No data
Sun	No data	No data
Meteorite (Carbonaceous)	No data	No data
Crystal rocks	0.00010	0.00001
Sea water	0.00000001	0.0000000003
Streams	0.0000004	0.000000002
Humans	0.0000011	0.00000003

Radium has no stable isotope, therefore standard atomic mass cannot be given, though it is usually given as 226.0 g/mol. Radium having the same mass as Uranium is over 1 million times more radioactive, it decays in at least seven stages [34]. The successive main products have been studied and were called "radium emanation" (now identified as radon), and these decay products were known as radium A, B, C, etc. These are now known to be isotopes of other elements as shown in Table 2.2. These solids products are radioactive elements, each with an atomic number lower than its predecessor.

Table 2.2: Decay products of radium

Radium emanation	^{222}Rn
Radium A	^{218}Po
Radium B	^{214}Pb
Radium C	^{214}Bi
Radium C_1	^{214}Po
Radium C_2	^{210}Ti
Radium D	^{210}Pb
Radium E	^{210}Bi
Radium F	^{210}Po

Radon is a radionuclide that has no smell, no color, tasteless noble gas that cannot be detected by human senses. Its presence or absence can be detected by radioactivity detectors [37]. Radon gas is located in group 18 or group 0 and fits the criteria to be classed as a noble element. It is the heaviest of the gases in group 18 and the only noble "inert" gas that is naturally radioactive. Radon gas is easily converted into a liquid and become solid at the relatively high temperature of $-71\,^{\circ}$C [38]. As a solid, it glows with a yellow light color and its melting point is $-71\,^{\circ}$C. Some physical properties of ^{222}Rn are listed in Table 2.3. At standard temperature and pressure, radon forms a monoatomic gas with a density of about 9.73 kg/m^3. Also, at standard temperature and

pressure, radon has no color, but when it is cooled down below its freezing point of 202 K (−71 °C; -96 °F), it has a brilliant phosphorescence which turns yellow as the temperature is lowered, and becomes orange-red as the air liquefies at temperature below 93 K (−180.1 °C; -293.3 °F). Radon glows upon condensation because of the intense radiation it produces.

Although ^{222}Rn is quite unstable, it is readily measurable in the atmosphere because of its continuous generation by the decay of ^{226}Ra in rock and soil [39]. Since radon is an inert gas, it cannot be transported through food chains and does not generally concentrate in biological tissues, but this is an exception for ^{222}Rn, which can reside in fatty tissues if generated within an organism by the decay of ^{226}Ra. Radon progeny tend to attach onto small dust particles, which can affix on biological surfaces and of particular concern is their inhalation [39]. The radon progeny in the lung leads to irradiation of the lung tissues, which induce cancer in uranium miners and members of the public exposed to it. Radon is often the single largest contributor to an individual's background radiation dose and varies from location to location.

Table 2.3: Physical properties of ^{222}Rn [40]

Property	Value
Boiling point	−61.8 °C
Melting Point	−71 °C
Relative atomic Mass	222.02
Critical temperature	104 °C
Critical Pressure	62 atmospheres
Density	9.96 kg m^{-3}
Volume of 27.03 pCi at normal temperature and pressure	1.6× 10^{-20} m^3

^{222}Rn forms and collects few inches below the surface of the ground and is often found trapped in pockets of air, escaping through porous soils and crevices [38]. The Earth's atmosphere is just 1.00×10^{-19} % radon, but because radon is 7.5 times heavier than air, it can be collect in basements and low places in buildings and homes. Radon is sparingly soluble in water and it's solubility decreases with increasing temperature as shown in the Fig. 2.4 below.

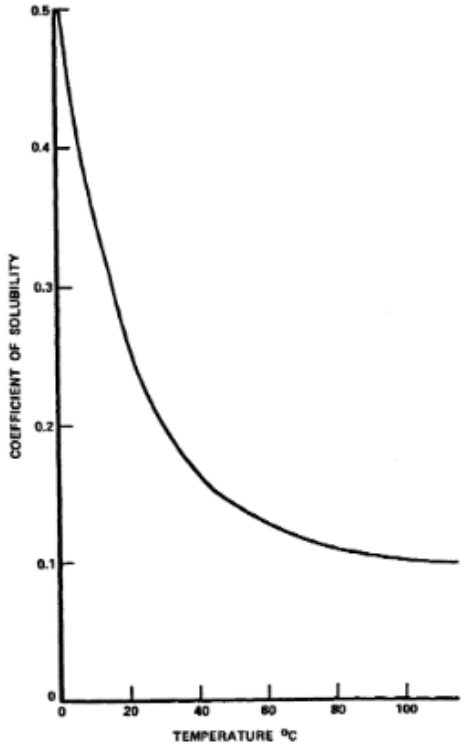


Figure 2.4: Plot of the coefficient for radon as a function of water temperature. The solubility coefficient in water is defined as the ratio C_w/C_a, where C_w and C_a are the radon concentrations in water and air, respectively (taken from Ref. [40])

2.4.1 Radium, Radon and their Progeny Decay Series

The α-decay process release an α-particle that is structurally equivalent to the nucleus of helium (He) atom [20]. As shown in section 2.2 Fig.2.3, ^{226}Ra decays to ^{222}Rn, when the lower energy particle is emitted the radon nucleus is left in an excited state with energy 0.186 MeV above the ground state [22]. When ^{222}Rn decays, it forms a number of short-lived radioactive decay daughters as shown in the chain below:

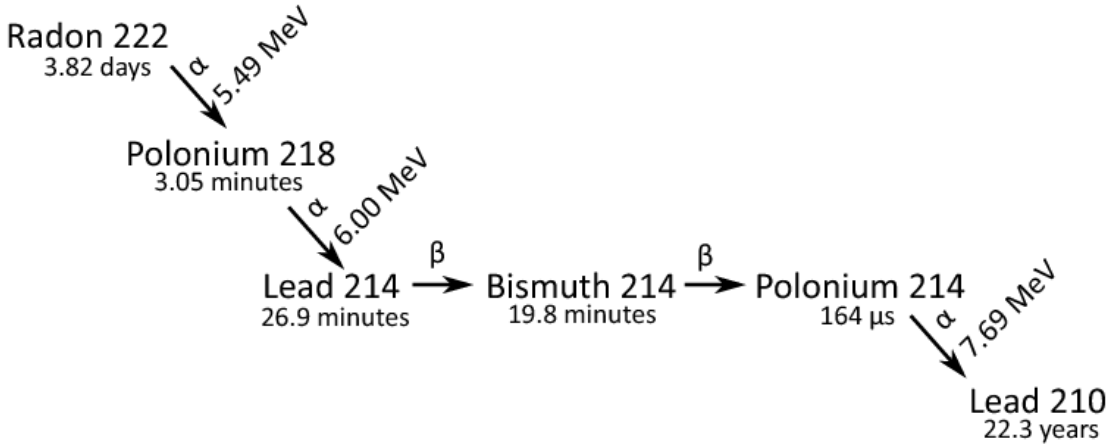


Figure 2.5: Radon Decay Chain (taken from Ref.[41])

The examples of α-decay equations of ^{222}Rn, ^{218}Po and ^{214}Po from the decay series of radon are presented by mass-energy balance equations as follows:

$$^{222}_{86}Rn \longrightarrow ^{218}_{84}Po + ^{4}_{2}\mathrm{He}_2 + 5.49MeV \tag{2.46}$$

$$^{218}_{84}Po \longrightarrow ^{214}_{82}Pb + ^{4}_{2}\mathrm{He}_2 + 6.00MeV \tag{2.47}$$

$$^{214}_{84}Po \longrightarrow ^{210}_{82}Pb + ^{4}_{2}\mathrm{He}_2 + 7.69MeV \tag{2.48}$$

According to Ref. [22], ^{226}Ra decays into a series of short-lived daughters, two of which, ^{218}Po and ^{214}Po, are α-emitters. When an α-particle is emitted in the lung, it deposits all of its energy locally within a small thickness of adjacent tissue. An α-particle from ^{214}Po, for example, deposits its 7.69 MeV of energy within about 70 μm. A 1-MeV beta particle from ^{214}Bi, on the other hand, deposits its energy over a much larger distance of about 4000 μm [22]. Thus, the dose to the cells of the lung from beta and gamma radiation from radon daughter radionuclides is very small compared with that of the alpha particles radiation. Therefore radon health hazard is closely related to the air concentration of the potential alpha-particle energy of the short-lived daughters.

The ^{222}Rn disintegration decay is represented by the value of 5.49 MeV. ^{226}Ra alpha emitters have discrete energies from about 4-10 MeV, spanning a range of about a factor of 2, but half-lives ranging from 10^{-6}-10^{17}s, spanning

a range of about a factor of 10^{23}. Short-lived alpha emitters have the highest energy as indicated in Table 2.4 below [23].

Table 2.4: Radioactive properties of ^{222}Rn and its short-lived progeny

α-emitter	A (amu)	$T_{1/2}$ (S)	λ (s^{-1})	Q-value (Mev)	E (Mev)
^{222}Rn	222.0176	3.3×10^{5}	2.1×10^{-6}	5.49	5.39
^{218}Po	218.0090	183	3.8×10^{-3}	6.00	5.89
^{214}Po	213.9920	0.164	2.23	7.69	7.56

2.5 Radiation interaction with matter

Radiation interaction is the mechanism through which the ionizing radiation, such as α or β particles and γ-ray passes through materials and loses energy. Radiation probability to interact with matter is shown as a cross-section. Alpha and beta particles interact mainly directly with electrons in matter through the Coulomb force and, as a result, the electrons are excited to a higher atomic state. This leads to ionization in the medium. The mean distance travelled by α and β-particles, ejected in natural decay, in air or solid materials is in the range of micrometers and a few centimeters, respectively [1]. The γ-rays are electrically neutral and interact with matter through three processes namely Photoelectric effect, Compton scattering and Pair production.

2.5.1 photoelectric effect

The photoelectric effect occurs in the low-energy range of 10 keV to 100 keV [42]. During photoelectric effect, a γ-ray photon is absorbed completely by a bound atomic electron and as a result, a photo electron is released. The electron is released at an energy equal to the energy of the incident photon less the binding energy of the electron. Fig. 2.6 illustrates the photoelectric absorption process.

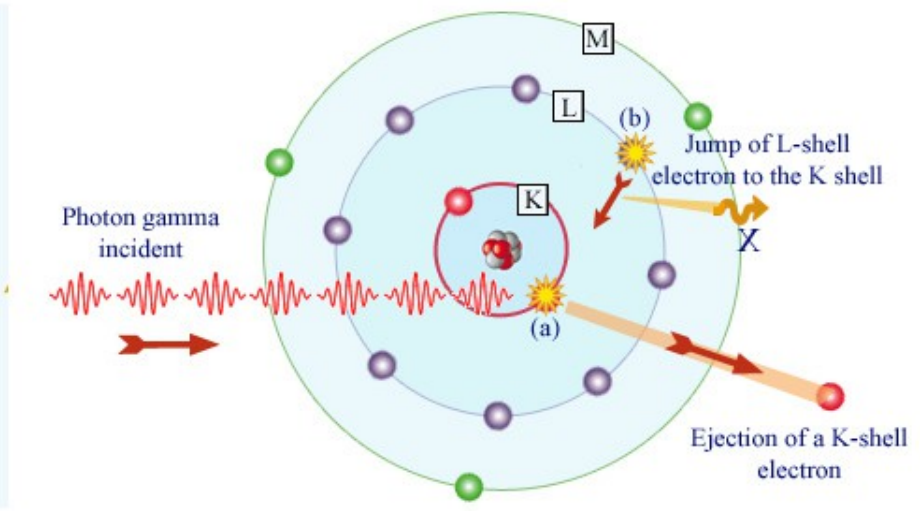


Figure 2.6: Photoelectric absorption within an atom (taken from Ref.[1])

2.5.2 Compton Scattering

Compton scattering is a mechanism through which an incident gamma photon interact with an electron in the absorbing material. The process occur at higher energy (0.1 - 3 MeV) [42]. The process is illustrated in Fig.2.7, which depicts an incident gamma photon deflected through a given angle θ (scattering angle) from its original direction [43]. The incident photon transfers a fraction of its energy to the electron (assumed at rest), which is then known as recoil electron. So in this case the gamma ray loses only part of its energy as compared to the photoelectric effect where all the energy is lost.

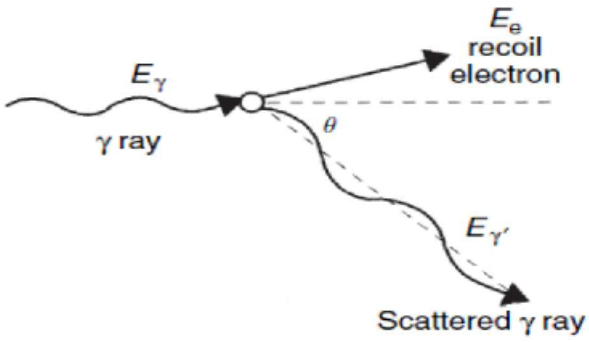


Figure 2.7: The illustration of Compton scattering showing the directions of the scattered photon and electron with respect to the direction of the incident photon.(taken from Ref. [43])

2.5.3 Pair Production

When a photon with excess energy greater than 1.022 MeV enters matter, it may interact with the nucleus in a process leading to pair production that is, an electron and are created. The excess energy carried in by the incident photon above the 1.02 MeV required to create the pair, is transferred as kinetic energy of the produced particles [43]. The positron subsequently annihilate after slowing down in the absorption medium, leading to production of two annihilates photons that are considered as secondary products of the interaction. Fig. 2.8 shows this interactive process, the photon energy is shared by two particles.

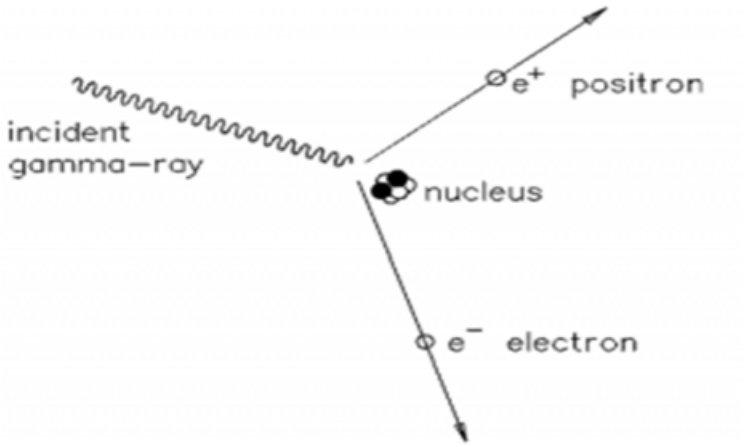


Figure 2.8: Pair production effect (taken from Ref. [1])

2.5.4 Alpha radiation on Materials of the Detector

To understand how to maximize the functionality of the detector, it is important to comprehend the behavior of alpha radiation when it interacts with the detector material. Hence, it is noticed that for most precise results in determining alpha particles energy distribution, minimum detectors are suitable. Presently, detectors made from silicon semiconductor are extensively used. On account of instrumental improvements and success in spectrum evaluation system, alpha spectrometry using Si detectors with high-resolution were on the market. Proportional counters and Ionization chambers have been used in alpha spectrometry among gas ionization detectors, and a gas detector is used for the determination of the pulse-height distribution of alpha particles.

When alpha particles enter the detector, they immediately interact with the atomic electrons of the detector material. The main results of this interaction are excitation and ionization. In the latter case, an electron and positron ion (cation/hole) pair is formed. Along its path through the detector, the high-energy alpha particle will create a large number (N) of electron-cation pairs [44]. N can be expressed as

$$N = \frac{E_\alpha}{\varepsilon} \tag{2.49}$$

where E_α is the energy of the alpha particle and ε is the energy needed to form one electron-cation pair as defined in Ref. [44]. Since E_α is in the range of a few MeV and ε depends on the type of detector in the range of 1 eV to 100 eV, a single alpha particle can produce 10 000 to 1 000 000 charge carriers while it loses its energy before it is stopped [44]. The track of the alpha particles in the detector is almost straight because heavy particles are not significantly deflected by the interacting electrons. The specific energy loss of the alpha particle, also called the stopping power, is described by the Bethe formula introduced in Eq. (2.19). This formula yields the amount of the energy loss per unit length [45]:

$$\frac{dE}{dx} = \left(\frac{e^2}{4\pi\varepsilon_o}\right)^2 \frac{4\pi z^2 N_o z_\rho}{mc^2\beta^2 A}\left[ln\frac{2mc^2\beta^2}{I} - ln(1-\beta^2) - \beta^2\right] \tag{2.50}$$

where ν=βc is the velocity of the particles, ze is its electric field charge, Z, A and ρ are the atomic number, atomic weight, and density of the stopping material, respectively. N_o is the Avogadro's number and m is the electron mass. The parameter I represents the excitation energy of the atomic electrons, which could in principle be computed by averaging over all atomic ionization and excitation processes [45]. In practice, I is regarded as an empirical constant measured in eV.

The alpha particle interaction with the detector is characterized by a range or distance beyond which no particles penetrate. This range depends on the energy of the alpha particle and the type of detector, i.e. its atomic number and density [44]. As an example, the range of alpha particles in Si is shown as a function of alpha energy in Fig. 2.9 below [44].

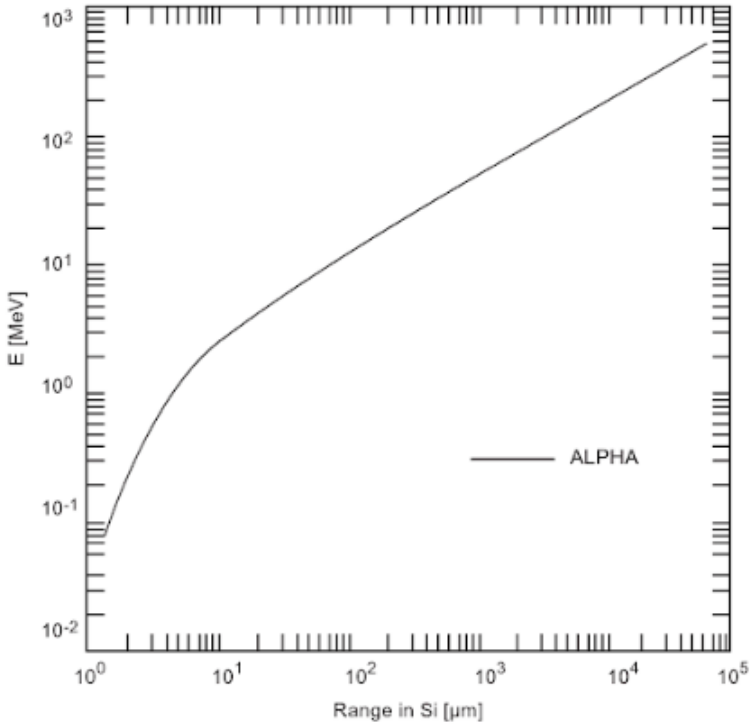


Figure 2.9: The range of alpha particles in silicon with their respective energy (taken from Ref. [44])

Alpha energies emitted from radionuclides are not higher than 10 MeV, they are completely absorbed in Si layers of 100-mm thickness [44]. Hence, Si detectors should not be significantly thicker if they are used for the measurement of alpha-emitting radionuclides. In the case of gas detectors, the detector thickness depends on the type and especially on the pressure of the gas in the detector chamber. Around atmospheric pressure, the range of 10 MeV alpha particles is about 5–10 cm, and so this is the desired detector size [44]. The very short range of alpha radiation enables the design of detectors, which can completely absorb the incident radiation, without requiring large detector volumes. This fact, combined with a large number of charge carriers that are produced, is responsible for the higher counting efficiency that is typical of alpha spectrometry.

However, the limited range of alpha radiation is also responsible for the major challenge in alpha particle detection, which is ensuring that alpha particles reach the active volume of the detector without significant losses [44]. This means the reduction or elimination of absorption in the source, any absorbent

layers between source and detector, and in the detector window. Absorption and self-absorption in the detection procedure can be reduced by ensuring direct contact between the source and the detector, e.g., by placing the source inside the detector gas chamber or by dissolving the source in a liquid detector, as in the case of liquid scintillation counting (LSC). In the case of silicon detectors, absorption can be reduced by the use of a vacuum in the chamber surrounding the detector and the alpha source.

2.6 Radiation Health effects

Ionizing radiation can cause damage in cells and induce chemical changes. Some cells die or become abnormal temporarily or permanently. Radiation damage starts at the cellular level. Any molecule in the cell may be disrupted by radiation except DNA, the most sensitive biological target due to limited redundancy of the genetic information it contains [46]. Evidence indicates that damage to DNA is what causes cell death, mutation, and carcinogenesis [47].

The extent of damage to health caused by ionizing radiation is based on amount of energy given to a tissue, by alpha or beta particles, neutrons or photons. This energy can induce chemical reactions in the tissues, such as DNA breakage or the formation of free radicals that can further damage DNA strands [48]. The cells normally repair themselves, if the cells are not able to repair DNA damage properly, early senescence, apoptosis or mutations occur, the latter of which may lead to cancer [48]. An absorbed dose of radiation is sufficient to kill the average dividing cell-2 gray (Gy)-suffices to cause hundreds of lesions in its DNA molecules. Most such lesions are repairable, but those produced by densely ionizing radiation (for example a proton or alpha particle) are generally less repairable than those produced by sparsely ionizing radiation (for example an x-ray or γ-ray) [46]. Densely ionizing (high linear energy transfer (LET)) radiations, therefore typically have a higher relative biological effectiveness (RBE) than sparsely ionizing (Low LET) radiations for most form of injury. Illustrated in Fig. 2.10 are schematics of direct and indirect actions of ionizing radiation on DNA structure.

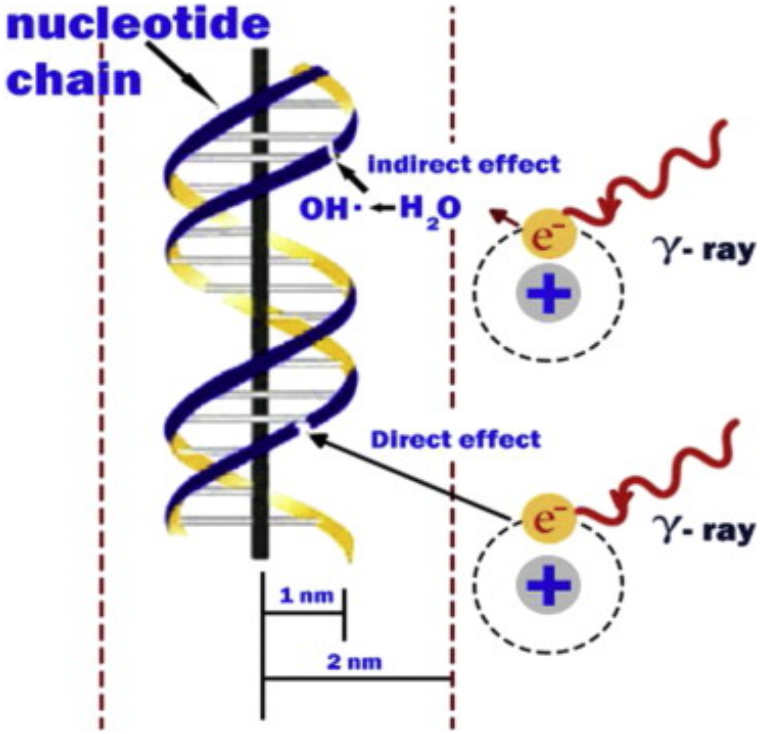


Figure 2.10: Direct and indirect actions of ionizing radiation on DNA (taken from Ref. [49])

Radiation damage to the cell can be caused by the direct or indirect action of radiation on the DNA molecules. In the direct action, the radiation hits the DNA molecule directly, disrupting the molecular structure [49] causing ionization of atoms in the DNA molecule. Such structural change leads to cell damage or even cell death. Damaged cells that survive may later induce carcinogenesis or other abnormalities. This process becomes predominant with high-LET (linear energy transfer) radiations such as α-particles and neutrons, and high radiation doses. In the indirect action, the radiation interacts with the non-critical target atoms or molecules such as water molecules, the major constituent of the cell, and other organic molecules in the cell, whereby free radicals such as hydroxyl (HO•) and alkoxy (RO2•) are produced [49]. These free radicals are characterized by an unpaired electron in the structure, which is very reactive and can attack the critical target which is the DNA molecule and cause molecular structural damage. Hydrogen peroxide, H_2O_2, is also toxic to the DNA molecule. The result of the indirect action of radiation on DNA molecules is the impairment of function or death of the cell. The number of free radicals produced by ionizing radiation depends on the total dose. It has been found that the majority of radiation-induced damage results from

the indirect action mechanism because water constitutes nearly 70% of the composition of the cell [49].

When the DNA is attacked, either via direct or indirect action, the damage is caused to the strands of molecules that make up the double-helix structure. Most of this damage consists of breaks in only one of the two strands and is easily repaired by the cell, using the opposing strand as a template. If, however, a double-strand break occurs, the cell has much more difficulty repairing the damage and may make mistakes. This can result in mutations, or changes to the DNA code, which can result in consequences such as cancer or cell death. Double-strand breaks occur at a rate of about 1:25 single-strand breaks. Thus, most radiation damage to DNA is reparable.

2.7 Radiation Exposure effects

The extent of damage to the cells depends upon the dose and duration of the exposure, as well as the organs exposed. There are two broad categories of health effects; the Acute (short-term) and Chronic (long-term) effects. Figure 2.11 shows the biological effects of ionizing radiation, categorized in relation to the characteristics of effect, occurring times and the objects or organs that shows the effect. The types of biological effects can further be expanded to be deterministic and stochastic effects. These biological effects are to be categorized in relation to the characteristics of effects, occurring times and the object that shows the effects as shown in Fig. 2.11.

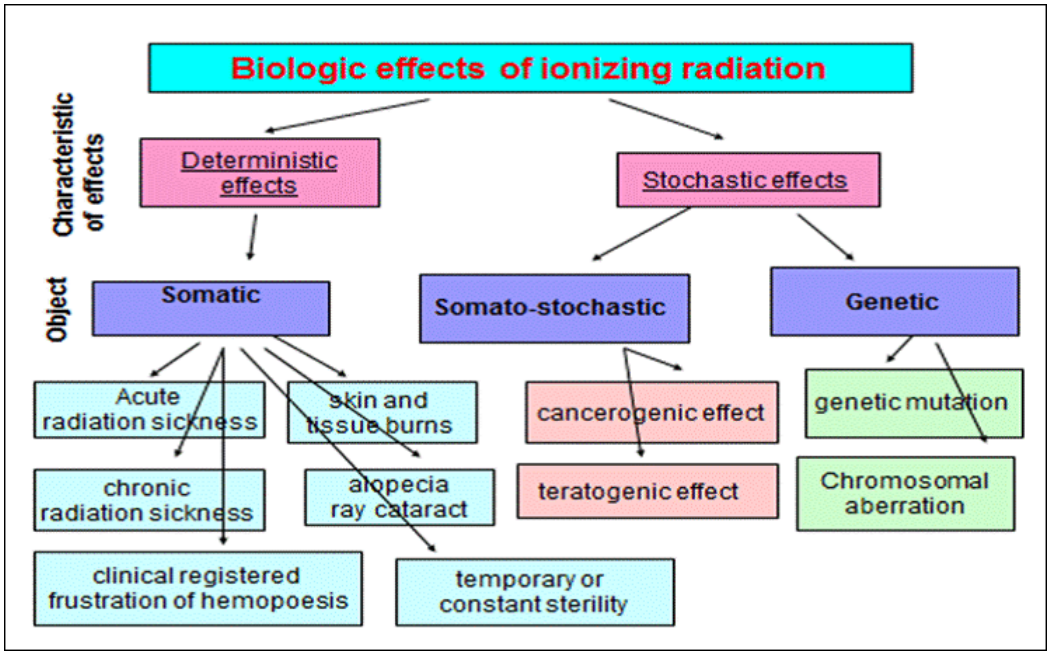


Figure 2.11: Biological effects of ionizing radiation (taken from Ref. [50])

2.7.1 Acute effects

This occurs when there is sudden radiation exposure for a short period which results in acute radiation effects. This occurs in exposure to radiation resulting from nuclear explosions such as atomic bombs; consequently, a very high dosage is produced. Radiotherapy may also pose an acute health effect on humans [47]. A very large amount of radiation exposure (acute exposure) may cause sickness or even death within hours or days. High dose can kill too many cells such that tissues and organs are smashed, and this sequence may bring about a rapid whole body response frequently called the Acute Radiation Syndrome (ARS) [50].

An acute, whole-body, gamma-ray dose of about 4 Gy without treatment would probably be fatal to about 50% of the people exposed [22]. This dose is known as the LD50-(Lethal Dose) to 50% of a population. More specifically, it is also sometimes called the LD50/30, indicating that the fatalities occur within 30 days. If a group of people is exposed to a whole body penetrating radiation dose, the listed effects in Table 2.5 might be observed [51].

Table 2.5: Acute effects (High dose) observed over different radiation dose exposures

Dose (Rad)	Effects Observed
15-25	Blood count changes in a group of people
50	Blood count changes in an individual
100	Vomiting (threshold)
150	Death (threshold)
320-360	LD 50/60 with minimal care
480-540	LD 50/60 with supportive medical care
1,100	LD 50/60 with intensive medical care (bone marrow transplant)

2.7.2 Chronic effects

Chronic exposure is continuous exposure to radiation over a long period of time. With chronic exposure, there is a delay between the exposure and the observed health effect. These effects can include cancer and other health outcomes such as benign tumors, cataracts, and potentially harmful genetic changes [47]. Chronic exposure effects signify exposure to low doses of radiation over a prolonged period of time, producing chronic or long-term effects.

2.8 Radiation Dosimetry

Radiation dosimetry deals with measurement of the absorbed dose received by human body tissue or organ resulting from the exposure to ionizing radiation. Ref. [19], further explains that it strongly refers to the determination (i.e., by measurement or calculation) of these quantities, as well as any of the other radiologically relevant quantities such as exposure, kerma, fluence, dose equivalent, energy imparted, and so on. Radiation effect is measured in terms of exposure, absorbed dose, equivalent dose and effective dose [52].

2.8.1 Exposure

Radiation exposure is defined as charge released per unit mass of air [53]. It is a measure for gamma and X rays in terms of the amount of ionization produced in air [33]. Exposure is measured by the unit Roentgen (R) which was originally defined as that amount of gamma- or X-ray radiation that produces ionization of the electrostatic unit of either positive or negative charge per cubic centimeter of air at 0°C and 760 mm Hg, standard temperature and

pressure (STP) [54]. Because 1 cm^3 air weights 0.001293 g at STP and a charge of either sign carries 1.6×10^{-19} C [54]. It can be written as:

$$1R = 2.58 \times 10^{-4} Ckg^{-1}. \tag{2.51}$$

However it can be shown that 1 esu cm^{-3} in air at STP is equivalent to the definition (2.51) of 1R of exposure. Since the density of air at STP is 0.001293 g cm^{-3} and 1 electrostatic unit (esu) = 3.34×10^{-10} C, thus [33]:

$$\frac{1esu}{cm{-}^3} = \frac{3.34 \times 10^{-10} C}{0.001293g \times 10^{-3} kgg^{-1}} = 2.58 \times 10^{-4} Ckg^{-1}. \tag{2.52}$$

2.8.2 Absorbed Dose

The absorbed dose is the primary physical quantity used in dosimetry. It is defined as the energy absorbed per unit mass from any kind of ionizing radiation in any target [33]. Nowadays, the SI unit of absorbed dose, J kg^{-1}, is called the gray (Gy). And it can be expressed as:

$$1Gy = 100rad \tag{2.53}$$

Conversely, 1.0 rad= 0.01 Gy. For human health protection, however, the important thing is not the measurement of energy deposited (the absorbed dose) but the biological effects due to radiation exposure [53]. The International Commission on Radiological Protection (ICRP), National Council on Radiation Protection and Measurements (NCRP), and ICRU introduced the concept of dose equivalent for radiation-protection purposes [22], which takes into account the biological effects of radiation.

2.8.3 Dose Equivalent

The dose equivalent given by H, at any point in a tissue is defined by equation (2.54) [19]. The Q factors for various radiations that are commonly encountered are listed in Table 2.6.

$$H = DQN \tag{2.54}$$

where D is the absorbed dose, Q is the quality factor for the specific radiation type, and N is the product of all other modifying factors, with suggested value of 1 [19].

Table 2.6: Quality factor (Q) for several types of radiation

Type of Radiation	Quality factor (Q)
X-rays	1
γ-rays	1
Beta particles	1
Electrons	1
Positrons	1
Photons (E<14 MeV)	10
Alpha particles (E<10 MeV)	20

However, if D is given in J/kg, then so is H, since Q is dimensionless, thus the unit of dose equivalent is joule per kilogram (J. kg^{-1}, with its special name known as Sievert (Sv)). [19].

2.8.4 Effective Dose

Beside several factors such as type and energy of radiation, sensitivity of irradiated body organ or tissue must also be taken into account when dealing with the biological effects of ionizing radiation. The effective dose, E, is defined by the weighted sum of tissue or organ equivalent doses, given by equation [48]:

$$E = \sum_T W_T H_T \tag{2.55}$$

where W_T is the tissue weighting factor. The equivalent dose and the effective dose are both measured Sievert(Sv). The tissue weighting factors for different organs of the body are listed in Table 2.7 [55].

Table 2.7: Recommended Weighting factors for body tissues or organs [55]

Tissue	W_T
Bone-marrow (red), Colon, Lung, Stomach, Breast, Remainder tissues *	0.12
Gonads	0.08
Bladder, Oesophagas, Liver, Thyroid	0.04
Bone surface, Brain, Salivary glands,Skin	0.01

*Remainder tissues: Adrenals, Extrathoracic (ET) region, Gall bladder, Heart, Kidneys, Lymphatic nodes, Muscle, Oral mucosa, Pancreas, Prostate, Uterus/Cervix, Spleen, Small intestine, Thymus [55].

Considering the linkage between the cancer risk and effective dose, the International Commission on Radiological Protection had assessed the detriment-adjust cancer risk to be 5.5×10^{-2} Sv^{-1} for the whole population and 4.1×10^{-2} Sv^{-1} for adult workers. This means that if a person is exposed to an effective dose of one sievert, his or her cancer risk increases by 5.5 percentage points over a long period of time. The dose response relationship is hence considered to be linear [48].

In the present study, effective doses through ingestion of uranium radionuclides in water were assessed for the adults age group. The annual radiological dose for a person drinking water that may contain a certain level of radioactivity is calculated by an apparent simple equation that follows:

$$AED_{Rn}(mSv/y) = C_{Rn}W \times I_a \times Df \tag{2.56}$$

where

AED_{Rn} is the committed annual effective dose from drinking water containing ^{222}Rn (mSv/y),

$C_{Rn}W$ (mBq/l) is the radon concentration in water,

I_a is the water consumption rate per year taken to be 60 litres for ^{222}Rn,

Df is the ingestion dose conversion factor for ^{222}Rn (nSv/Bq), equal to 1×10^{-8} Sv/Bq as recommended by UNSCEAR [56].

2.9 Radiological Hazard Indices

To limit external and internal health effects due to gamma radiation exposure from terrestrial radionuclides to a maximum permissible limit of 1 $mSv.y^{-1}$ for the individual member of the public and 20 $mSv.y^{-1}$ for radiation workers, the radiological hazard indexes known as External Hazard Index (H_{ext}) and Internal Hazard Index (H_{int}) were introduced [57, 58]. In order to keep the radiation hazard negligible, the value of this H_{ext} must be less than unity. This means that the maximum value of H_{ext} equal to unity must correspond to the upper limit of radium equivalent activity of 370 $Bq.kg^{-1}$ [11]. The external hazard index is defined by Eq. (2.57) as:

$$H_{ext} = \frac{C_{Ra}}{370Bq..kg^{-1}} + \frac{C_{Th}}{259Bq.kg^{-1}} + \frac{C_K}{4810Bq.kg^{-1}} \tag{2.57}$$

where C_{Ra}, C_{Th} and C_K are the activity concentrations in $Bq.kg^{-1}$ of ^{226}Ra, ^{232}Th and ^{40}K, respectively.

Inhalation of alpha particles emitted from the short-lived radon (^{222}Rn), the daughter product of radium (^{226}Ra) and progenies are hazardous to the respiratory organs[59]. This hazard can be controlled by the internal hazard index (H_{int}), which is given by Eq. 2.58:

$$H_{int} = \frac{C_{Ra}}{370Bq.kg^{-1}} + \frac{C_{Th}}{259Bq.kg^{-1}} + \frac{C_K}{4810Bq.kg^{-1}} \tag{2.58}$$

where C_{Ra}, C_{Th} and C_K are the activity concentrations in Bq.kg^{-1} of ^{226}Ra, ^{232}Th and ^{40}K respectively. Similarly, the H_{int} value must be less than 1 to keep the radiation hazard insignificant [52].

2.9.1 Excess Life Time Cancer Risk (ELCR)

An exposure to ionizing radiation can cause cancer over time. Estimating the excess lifetime cancer risk (ELCR) gives the probability of developing cancer over a lifetime[59]. The ELCR can be estimated using Eq. 2.59:

$$ELCR(mSv.y^{-1}) = AEDE \times DL \times RF \tag{2.59}$$

where
$AEDE$ is the committed annual effective dose from drinking wate (mSv/y), DL is the average life expectancy (70 years), and RF is the risk factor (Sv) [59]. The ICRP publication 106 uses a value of $RF = 0.057$ for members of the public.

2.10 Radiation Protection and Exposure Limits

Radiological protection is the science and practice of protecting people and the environment from the harmful effects of ionizing radiation. Fundamental to radiation protection is the reduction of expected dose and the human dose uptake that can be measured. ICRP Publication 103 [55] explains that most adverse health effects of radiation exposure may be grouped into two general categories [55], deterministic and stochastic effects. These are explained in detail in Section 2.7.

2.10.1 The radiological protection principles

To avoid unnecessary exposure causing the biological effects of radiation to radiation workers and the general public, there should be guidelines or principles to be followed and adhered to. Three basic general radiological protection principles for any practice resulting in increased exposure to radiation (ICRP Publication No. 103) [55], and those practises should be carefully planned in accordance to these principles [55, 60]. The first principle is Justification of a practise [55], which, in this context means that any new practice involving exposure should be justifiable, i.e, it produces more benefit to the exposed individual or society than harm. Secondly, Optimization of Protection. This principle sets out that the magnitude of individual doses and the number of people exposed should be kept As Low As Reasonably Achievable (ALARA) considered with economic and social factors [55]. Thirdly, the Application of Dose Limit principle. ICRP Publication No. 103 recommended implementation of interventions in unlikely event of a nuclear accident resulting in an increase of environmental radiation level, i.e. human activities to reduce the overall exposure by altering the existing causes of exposure. Individuals should receive exposure dose within the recommended limits, these are enumerated below [55].

- For uniform irradiation of the whole body, the annual effective dose that the whole body must receive from occupational exposure should be expressed as an effective dose of 20 mSv per year, averaged over defined 5 year periods (100 mSv in 5 years), with the further provision that the effective dose should not exceed 50 mSv in any single year.
- For a member of public, the dose exposure is set at 1 mSv per year.
- To prevent non-stochastic effects, occupational equivalent dose limits for lens of the eye, skin, the hand and the feet of 150, 500, and 500 mSv per year, respectively, are recommended.
- The annual equivalent doses for the individual member of the public are limited to 50 mSv per year for the skin and 15 mSv per year for the lens of the eye.

However, for non-uniform irradiation of the body, the tissue weighting factors of various organs as listed in Table 2.7 are used for determining the detrimental effects that contribute to each individual organ due to their different sensitivities to radiation.

Chapter 3

Experimental Methods

There are several techniques and methods for measuring the effective activity and concentration of Radium and Radon specifically ^{226}Ra and ^{222}Rn from water samples collected in the West-Rand area (Witwatersrand) of Johannesburg in the Gauteng province, South Africa. A review of some of these techniques is presented in this Chapter. Likewise, the set-ups and methodologies of measuring radium and radon that are used in this study are presented. These techniques include alpha spectrometry using alpha spectroscopy (subsection 3.4.1), α-spectrometry using a Durridge RAD7 radon monitor (section 3.6), and γ-ray spectrometry using a HPGe detector (section 3.5).

3.1 Study Area

As mentioned in the Introduction Chapter, the West Rand mines are now abondoned and often contaminated. Figure 3.1 shows the location of this district with the selected uranium mines in the West Rand and Far West Rand area of Johannesburg [61].

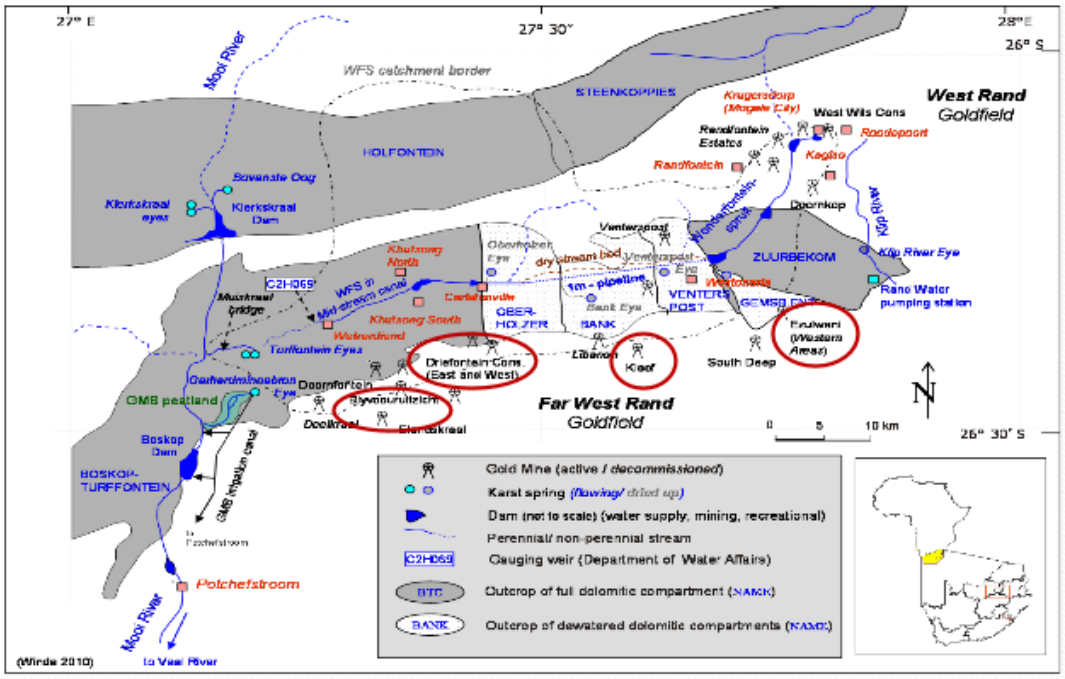


Figure 3.1: A layout map showing the West Rand and selected mines (taken from Ref. [61])

During June 2019, a total of seven samples were collected in the first batch: these include 3 samples from different sampling points in Blyvooruitzich mine area, 1 drinking water samples Near Driefontein waste water treatment facility, 3 samples coming from downstream operations of Kloof, Driefontein and Ezulwini mines. More sampling points were added within the same mining sites for stastical purposes, this escalated to a total of 10 samples collected for the three remaining seasons. The mines in the West Rand are no longer operational or there are no legal mining activities. The Blyvooruitzich mine is in contract with a neighbouring company (Anglo Gold Ashante) to pump out water from the underground as to avoid flooding and damages that may arise, so it called Covalent Water Company. Depicted in Fig. 3.2 is one of the pictures taken during the collection of first batch of water samples. Water from Downstream of the mining sites flows via Wonderfontein Catchment Area (WCA) depending where the mining site is located, and eventually all end in the Vaal river.



Figure 3.2: A picture taken during sample collection activity at the downstream of Driefontein mine

3.1.1 Demography

Based on figures from the Municipalities of South Africa from 2012-2019, the town had an estimated total population of 838 594 in 2016 and 820 995 in 2011. Figure 3.3 illustrates the pyramid for West rand district. The pyramid shows that the majority of the population is in the adult ages.

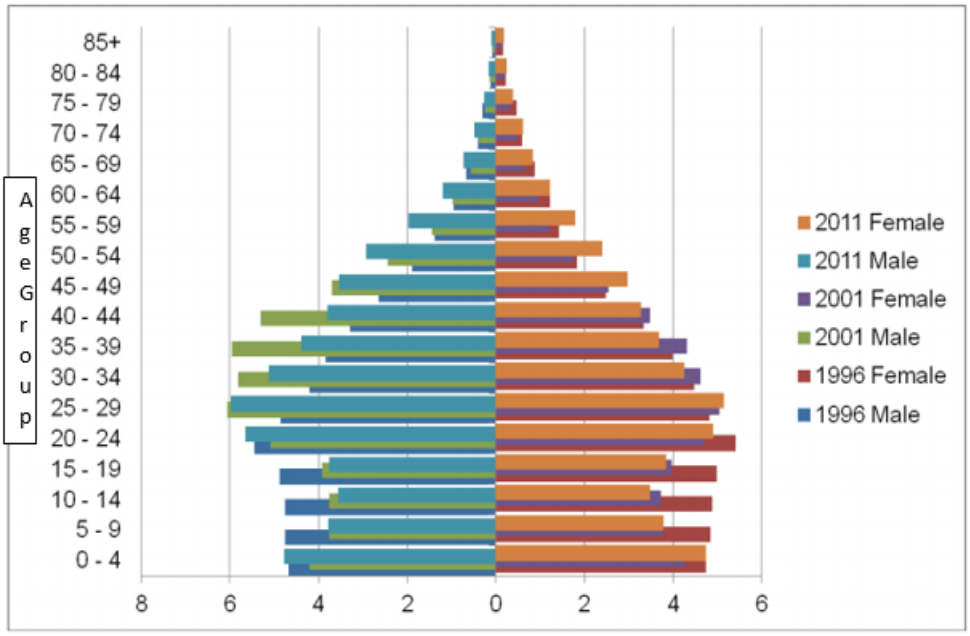


Figure 3.3: Distribution of population by age and sex, West Rand district – 1996, 2001 and 2011 (taken from Ref. [62])

3.1.2 Climate

The area is said to offer one of the world's best climates: summer days are warm and wind free and winter days are crisp and clear. There are about six weeks of chill in mid-winter (from July to August) and summer offers warm sunshine followed by balmy nights (October to March). The rainy season is in summer rather than winter. Rainstorms are often harsh accompanied by much thunder and lightning and occasional hail, but they are brief and followed by warm sunshine. Summer days are hot, though rarely to the point of discomfort. The average climates are:

- January: maximum 26°C (79°F); minimum 15°C (60°F)
- June: maximum 16°C (61°F); minimum 4°C (39°F)
- Annual precipitation: 713 mm (28 inches)

3.2 Sample collection

The water samples under investigation were collected from the former uranium mines in the West-Rand area of Johannesburg. These samples were collected

in four consecutive seasons. This was done as to observe seasonal variations, to evaluate the effect of climate in observed results. Several tools such as 5L bucket tied with a rope, gloves, markers were used to fill the 2 litre sample bottles. The rope bucket assist is getting water from deep ends, gloves for sample handling and markers to mark the samples immediately after collection. To prevent nuclide absorption, an addition 10 ml of HNO_3 per liter of water was added to reduce the pH of the water to less than 2. This is done within 12 hours after collection. Samples are stored in a cooler box container, as it is recommended that the water samples must always be stored at temperatures between 1 °C and 5 °C. The sample information is summarized in Table 3.1. below.

Table 3.1: Origin and sample information of the samples under investigation

Sample Matrix	Water	Sample detail
Sample ID.	Facility name	Sample Description
Bly4	Blyvooruitzich	Downstream water discharging from shaft4
Bly6	Blyvooruitzich	Downstream water discharging from shaft6
Bly comb	Blyvooruitzich	Combined downstream water from all operations
Drie down	Driefontein	Downstream of operations (grazing cows and people performing tradition were observed)
Drie Settl	Driefontein	Water from settling ponds
Drie8	Driefontein	Water from discharging from shaft 8
Kloof10	Kloof	Water from shaft 10
Kloof down	Kloof	Downstream of operations
Ezul	Ezulwini	Peter Wright Outlet
Ezul in	Ezulwini	Peter Wright Inlet
Drink	Driefontein	Drinking water sample from a nearby Waste water treatment facility. People were seen performing ritual at this sampling point

3.2.1 Sample receipt and storage

Samples were received at the National Nuclear Regulator (NNR), by the laboratory sample custodian and followed their sample receipt procedures. Initially

the background radiation level of the room that the samples were surveyed in was measured. Samples were labelled directly on the container with a marker that would not easily come off. A standard safety procedure for received samples at the laboratory was followed. The samples were externally scanned and recorded in the lab data base books. The scanning procedure is as stipulated in these steps:

- Visually scanned the package for signs of material leakage or sample container breakage.
- Obtained a calibrated Electra Gm portable radiation meter, calibrated in 05/04/19 by National Metrology Institute of South Africa (NMISA). As the samples were collected in different seasons, a different Electra Gm with a newer calibration date was used. This is done to ensure accurate test findings.
- Measured the radiation level 50 cm away from the sample bottle.
- Measured the surface contamination levels of the each sample bottle.



Figure 3.4: An Electra Gm used for background radiation level and surface radiation level on containers.

Samples were then stored on White area shelves, in a storage room for liquid environmental samples.



Figure 3.5: Sample storage

.

3.2.2 Sample Preparation for alpha and gamma spectroscopy

Sample preparation is a sensitive significant part of the analytical procedure. To guarantee homogeneity, 500 ml of the preserved samples were filtered at the NNR lab. This is done to remove any mud or silt and other foreign materials within the water samples before being subjected to measurements and analysis. The filter funnels were washed with distilled water, the filter papers were changed before filtering new samples so as to avoid cross contamination between samples. The filtering instruments used are shown in Fig. 3.6. The filtered samples were then transferred into sealed bottles, re-tagged, and stored for radium precipitate extraction. Figure 3.7 shows the new 500 ml container that prepared samples were bottled in.



Figure 3.6: Filtration instrumental set-up used in sample preparation procedures.



Figure 3.7: Prepared samples awaiting measurements and analysis

Before counting of samples in Alpha Spectrometry, radium is chemically separated from the prepared samples. During this process, radium in water sample

is separated from the bulk by adding lead and barium carriers to the sample, and then precipitating these together as a mixed sulphate. The precipitate is purified from the ions by washing, and then dissolved again by adding a complexing agent. The barium and radium are again precipitated and filtered in form of sulphate as illustrated in Fig.3.8, while the lead is kept in solution by careful control of the pH value. The fraction of barium and radium that is present in the sample, and recovered in the final precipitate, is determined by adding a known activity of ^{133}Ba tracer to the sample, and measuring the precipitate by gamma counting using the HPGE detector. The final $BaSO_4$ precipitate which includes radium-226 is counted on the alpha spectroscopy to determine the disintegration rate of ^{226}Ra.

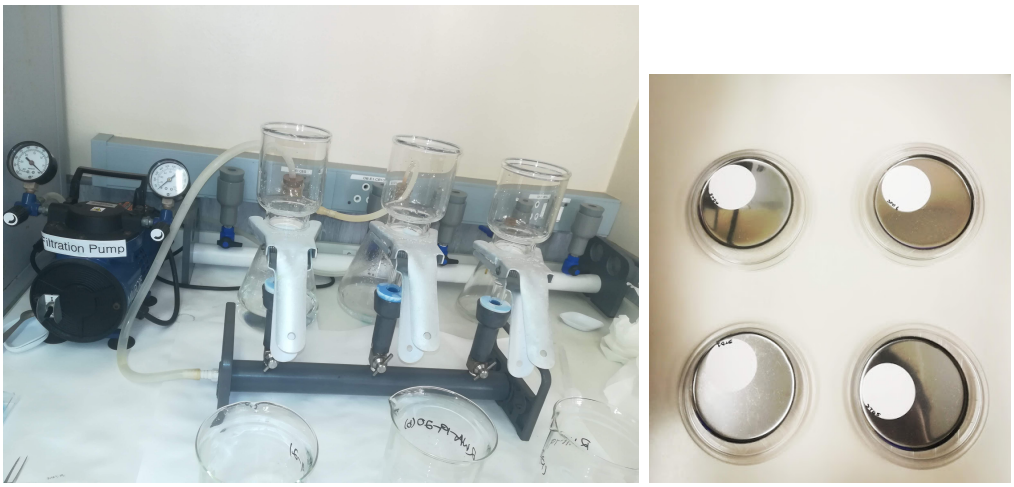


Figure 3.8: LHS: The filtration of radium precipitate in solid form.
RHS: Prepared samples on filter paper
.

3.3 Detection System

The function of the detector is to produce a signal for every particle passing into it. A detector works according to the principle of the interaction of particle radiation with matter. Krane et.al [45], further explained in this manner, "the radiation enters the detector, interacts with the atoms of the detector material (losing part or all of its energy), and releases a large number of a relatively low-energy electron from their atomic orbits. These atoms are then collected and formed into voltage or current pulse for analysis by electronic circuitry".

3.3.1 Semiconductor Silicon Detectors

The basic medium of silicon (Si) semiconductor detectors is a solid semiconductor material. The passage of ionization radiation produces electron-hole pairs which are then collected by an electric field [63]. The use of a solid medium has the advantage that the dimensions of the detector can be kept small. In α-spectrometry, this means that a 100% intrinsic efficiency can be reached with Si detector of 100-μm thickness [44]. The amount of ionization produced for given energy has greater magnitude resulting in increased energy resolution. Moreover, because of their great density, they have greater stopping power. The high-energy resolution of semiconductors is a major advantage. A drawback includes the limitations on size and their high susceptibility to radiation-induced damage resulting in spectrum degradation.

A common fabrication procedure for Silicon detectors is, to begin with, a sample of p-type material and diffuse into its surface a concentration of Li (Lithium) atoms, which tend to form donor states and thereby create a thin n-type region. Under reverse bias, and at a slightly elevated temperature, the Li drifts into the p-type region, making quite a large depletion region [45]. Such detectors are known as Lithium-drifted Si detectors (Si(Li)).

The n-type layer created in producing Si(Li) detectors is of order 1 mm thick, which is easily penetrable by medium-energy γ rays (the range of a 100-keV photon in Si is about 2 cm). However, for charged particles, the range is much smaller (for a 1-MeV electron, the range is about 1 mm in Si: for a 5-MeV α particle, the range is only 0.02 mm in Si) and such a layer would prevent the particle from reaching the depletion region [45].

3.3.2 Scintillation Detectors

Ahmed et.al [64] explained that "The basic process is very simple: when the atoms of incident radiation interact with atoms of these so-called scintillation materials, they transfer some of their energy to atoms. As a result, these excited atoms go into short-lived excited states. When they return to the ground state they emit photons, mostly in the visible and ultraviolet region of the spectrum". This provides an alternative mechanism to the ionization to detect and measure radiation. Scintillation gamma spectrometry was a basic tool until the 1980s, but it was gradually replaced by semiconductor spectrometry of much better energy resolution [44]. At present, most of the

applications are related to gross counting of alpha, beta, and gamma radiation due to typical high counting efficiency and the low cost of the instrumentation while radiation spectroscopy is limited by the insufficient energy resolution of the scintillators to allow the identification of the radionuclides in an isotope mixture [44].

The basic steps involved in scintillation detection of radiation are [64];

- Interaction of radiation with the scintillation material
- Transfer of energy to the bound states of the material.
- Relaxation of the excited states to the ground state resulting in the emission of the light photons.
- Collection of photons by the photodetector.
- Detection of the photodetector signal by associated electronics.

The main parts of a scintillation detector are the scintillator, which converts the radiation energy to visible light photons, and the photoelectron-multiplier (PM) tube containing the photocathode, the multistage electron-multiplying section made of a series of electron-multiplying dinodes and an anode for collection of the amplified charge situated in a glass vacuum envelope [44]. Photocathodes are responsible for converting the energy of the photons into electrons. If the light appears as a pulse, the photoelectrons produced will also form a pulse in a similar time duration. The number of electrons emitted by the cathode is multiplied on the dinodes where the multiplication factor can be as high as 10^6-10^8 depending on the applied voltage [44]. The electric pulse at the anode of the PM tube can be directly counted without further amplification. Typical tubes have fast response times. When they are illuminated by a short light pulse, an electron pulse will be produced at the anode with a time width of a few nanoseconds after a delay time of 20–50 ns [44]. Scintillation detectors include solid and liquid scintillators as well as organic and inorganic scintillators. For all these different types, the basic principle used for the detection is fluorescence which is the prompt emission of visible radiation (light) [44].

3.4 Applied Measurement Techniques for this study

The phenomenon of radioactivity is based on the principle that every radionuclide emits a particle during its decay. So these particles need to be detected. Activity or concentration will be measured. To do this, electrical pulse generated by the decay of the corresponding radioisotope needs to be detected. Different strategies are used depending on the decay mode. A general overview of the detection of the different decay modes of the isotopes of interest is given. After that, the different devices and techniques used in this work for the measuring of radium and radon in different water sources are explained. The analytical techniques used during the experimental work include alpha spectroscopy and rad-7 radon monitor. Alpha spectrometry sample preparation is delicate enough to a possibility to lose the sample in preparation as explained in Subsection 3.2.2, therefore gamma spectroscopy is employed to check recovery of samples.

3.4.1 Alpha Spectrometry for analysis of Radium

Alpha spectrometry is a widely applied radiation analytical technique, primarily due to its high counting efficiency and low intrinsic background (resulting in a high sensitivity) [44], its versatility in terms of both the range of radionuclides which can be determined and sample types that can be analyzed, and the reliability of the technique due to the possibility to use an alpha emitting isotope of the element of interest as an internal tracer [44]. In Ref. [44], few advantages of this technique are highlighted as follows:

- The number of radionuclides that can be determined using alpha spectrometry is quite large. It includes almost all of the alpha-emitting radionuclides with half-lives long relative to the time required for source preparation.

- It is highly sensitive, with detection limits as low as 1 mBq per sample being easily achievable, thus making it possible to analyze relatively small sample sizes.

- A further advantage is that the capital cost for an alpha spectrometry system, including detector, counting chamber, and associated electronics,

is significantly lower than that for a number of other systems capable of isotope discrimination.

- Alpha spectrometry is element-based, in the sense that each spectrum consists of the alpha-emitting radionuclides of one element (plus those alpha-emitting progeny which grow on the source in the interval between preparation and counting). This implies that a separate source must be prepared and counted for each element of interest in the sample. Thus, it gives rise to the advantage that the spectrum is in a sense "predictable".

Alpha particles of different kinetic energies are "detected" using various types of nuclear detectors in alpha spectrometry, most common being the semiconductor and scintillation detectors as explained. The energy of the alpha particle is transformed into a measurable physical quantity, e.g. electric charge, current, or voltage. In the process of detection, the charge carriers are collected and converted to electric pulses. In spectrometry, pulses are processed in the 'pulse mode' where each interacting particle is detected independently [44]. Electric pulse processing units such as preamplifiers and amplifiers attached to the detector output, both amplify and form (shape) the pulse. Pulses are then digitized by an analog-to-digital converter (ADC). From a series of digitalized pulses of different heights at the ADC output, the multichannel analyzer (MCA) generates a pulse-height spectrum by sorting the pulses according to their heights and assigning them to a channel number proportional to the pulse height [44].

A schematic diagram of an alpha spectrometer as presented by Ref. [65] is illustrated in Fig. 3.9. Alpha spectrometers contain vacuum chambers surrounding the detector and the source. Vacuum supply units usually contain vacuum pumps such as oil rotation pumps, vacuum gauge, and occasionally a vacuum control system to adjust the desired pressure. In a spectrometric application, the basic information of the radiation (i.e. the type of radiation, the energy of the particles, and the activity of the source) is conserved in the form of the shape and height of the electric pulses, and the pulse frequency or count rate [44].

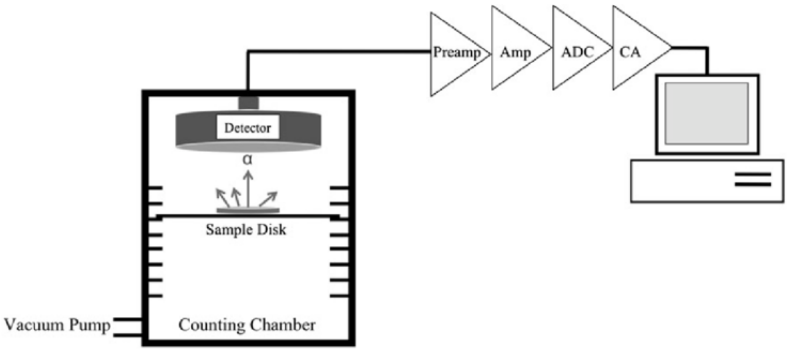


Figure 3.9: Schematic representation of alpha spectrometry system, including associated electronics and recording devices, (taken from Ref. [65])

3.4.2 Alpha Spectroscopy Experimental Set-up

Alpha ray spectroscopy is used to identify and quantify radionuclides based on the alpha particles emitted in the decay process. In this study, two Alpha spectrometry systems, were employed for analysis of radium isotopes, specifically ^{226}Ra within water samples. The instruments were used for analysis of prepared samples and encapsulated into discs (as shown in Fig. 3.8) to determine activity concentrations of ^{226}Ra for samples prepared. Both detector systems are Passivated Implanted Planar Silicon (PIPS) detectors situated at the NNR Laboratory, Pretoria. These detectors have Alpha Analyst interface manufactured by CANBERRA. Each system has 12 labelled chambers per measurement with shelves inside facing the detector.

The detector has an in-built multichannel analyser (MCA). Data acquisition, analysis of alpha-ray spectra and data display are achieved using Genie 2000 software. Vacuum pump with pressure range set at 12 mbar (Fig. 3.11) is connected to the detector to suck in air within each chamber. The measurement has to be made in vacuum conditions so that the alpha particles are not shielded by air. The sources that are measured have to be carefully prepared so as to have a layer as thin and uniform as possible so that alpha particles are not diffused and absorbed within the source itself.



Figure 3.10: Alpha spectroscopy chambers manufactured by CANBERRA



Figure 3.11: LHS: display with Genie 2000 software. RHS: Vacuum pump

.

3.4.3 Calibration of Alpha Spectrometry

Radium (^{226}Ra) measurements in water samples were carried out using an alpha spectrometer, which is an active instrument that gives information in energy and intensity of any emitted α-ray from a radionuclide. Before any energy measurement is performed, the detector was calibrated for energy and efficiency with a standard source certified by Eckert & Ziegler Analytics. This standard radionucide was prepared by electrode-deposition onto a stainless steel disk (Fig. 3.12). The standard is composed of ^{238}U, ^{234}U, ^{239}Pu and ^{241}Am

isotopes with know activities as shown in Table 3.2. Eckert & Ziegler Analytics explains that the total alpha activity was determined with ZnS scintillation detector. Radionuclide activities and impurities were calculated from the total activity and the fraction of activity for each radionuclide determined by alpha spectroscopy. However, only the procedure for one chamber in one of the detector is described in this study since the procedure and the calibration source used are similar in each chamber of both detectors.

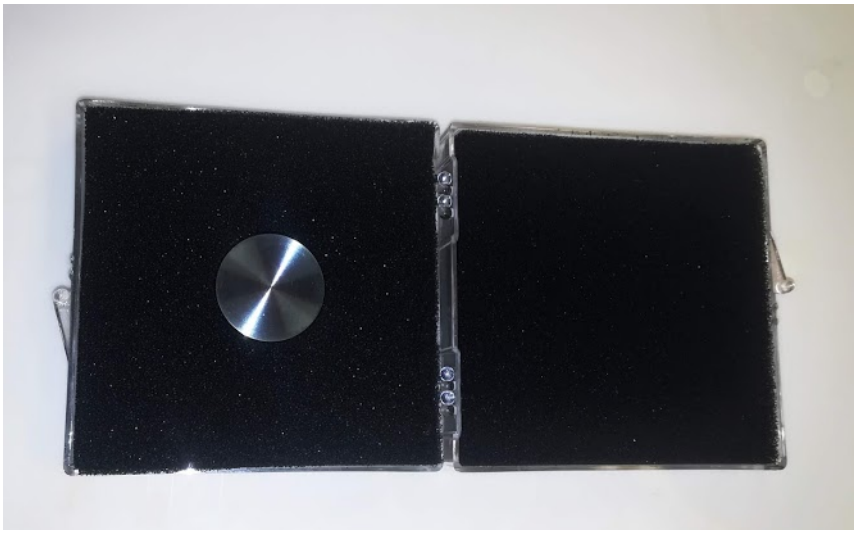


Figure 3.12: Calibration source prepared on a stainless steel disk.

3.4.3.1 Energy Calibration

The main objective of energy calibration is to derive a linear relationship between peak positions in the energy spectrum and the corresponding α-ray energy [1].

The energy calibration of the system was performed by counting a standard source with radionuclides such as uranium (^{238}U) with a known activity of 1.551 Bq, and well-defined energies. Within the energy range of interest from 4.184 MeV to 5.479 MeV, four distinct photo-peaks can be observed as illustrated in Fig. 3.13 and Table 3.2.

Table 3.2: Calibration source with corresponding activity and photo-peak energy

Isotope	Activity (Bq)	Energy Range (MeV)	Channels Number
^{238}U	1.551	4.184	244
^{234}U	1.497	4.761	328
^{239}Pu	1.463	5.148	384
^{249}Am	1.526	5.479	433

The calibration standard source was counted for a long enough time of about 6 hours (21600 Sec) to produce well defined photo peaks. Each channel number that corresponds to the peak position of full energy peaks on the MCA is shown in Fig 3.13.

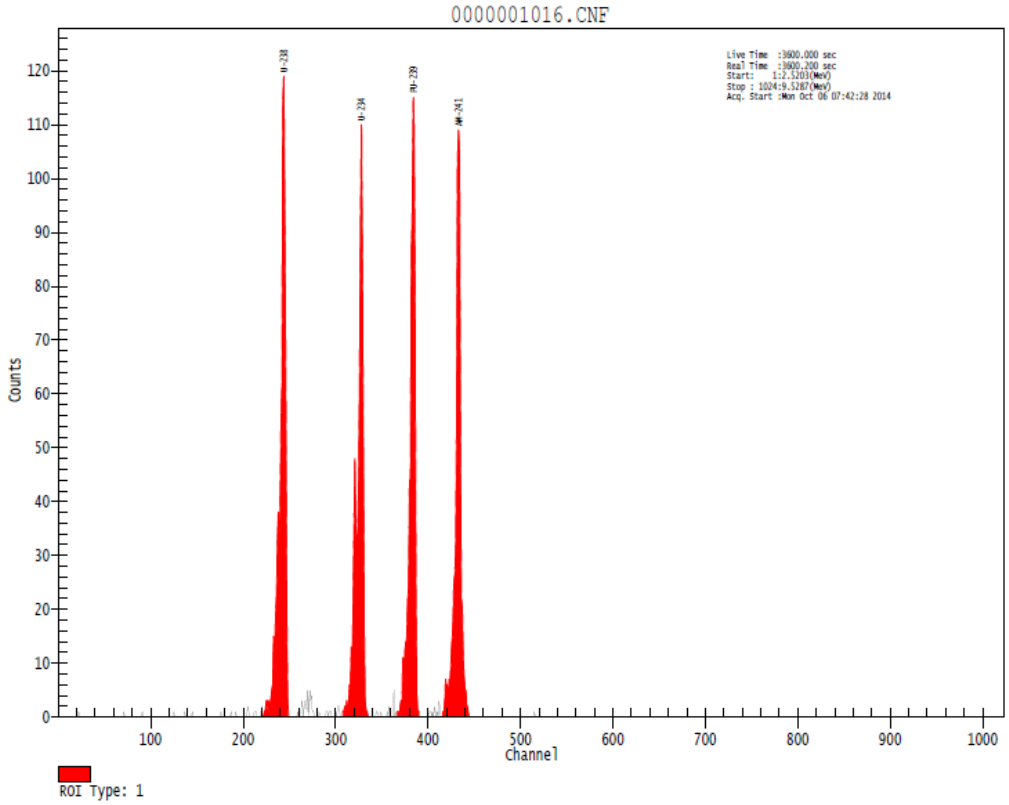


Figure 3.13: Energy Calibration of the detector

These were recorded and plotted to obtain a linear curve with a second order polynomial as shown in Fig 3.14. Second order polynomial was used to plot the curve because it provides the best approximation of the relationship between the energy and the channels. A broad range of function can be fit under it.

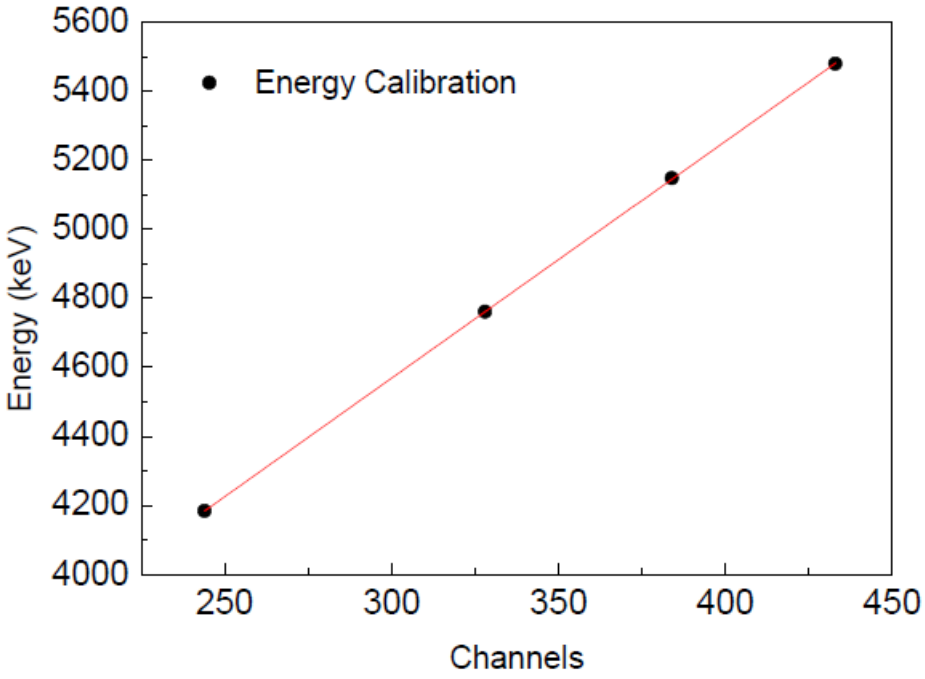


Figure 3.14: Plot of energy calibration curve for the standard source with photo-peak energies listed in Table 3.2

3.4.3.2 Efficiency Calibration

The efficiency of the detector refers to the ratio of the actual number of counts registered by the detector to the total number of events emitted by the source of radiation (expected counts). An accurate efficiency calibration of the system is necessary to quantify radionuclides present in the sample. The standard sources ^{238}U, ^{234}U, ^{239}Pu and ^{249}Am with activities listed in the second column of Table 3.2 were used to calibrate detector efficiency. Equation 3.1 was applied in the calculation of detector efficiency accordingly.

$$E = \frac{N_c}{ExpectedCounts}, \tag{3.1}$$

where N_c is the number of counts recorded per unit time in the photo-peak and $ExpectedCounts$ = Activity $\times$ counting time.

The produced results for Efficiency are given in Table 3.3.

Table 3.3: Detector efficiency using calibration source

Radionuclide	N_c (Measured counts)	Expected counts	Efficiency
U-238	763	5583.6	0.137
U-234	708	5389.2	0.131
Pu-239	699	5266.8	0.133
Am-249	654	5493.6	0.119

The obtained values are used to plot the efficiency curve as shown in Fig 3.15. The line of best fit of these values was obtained considering a straight line, that is in equilibrium. This serves to conclude that the detectors efficiency to count samples is most reliable.

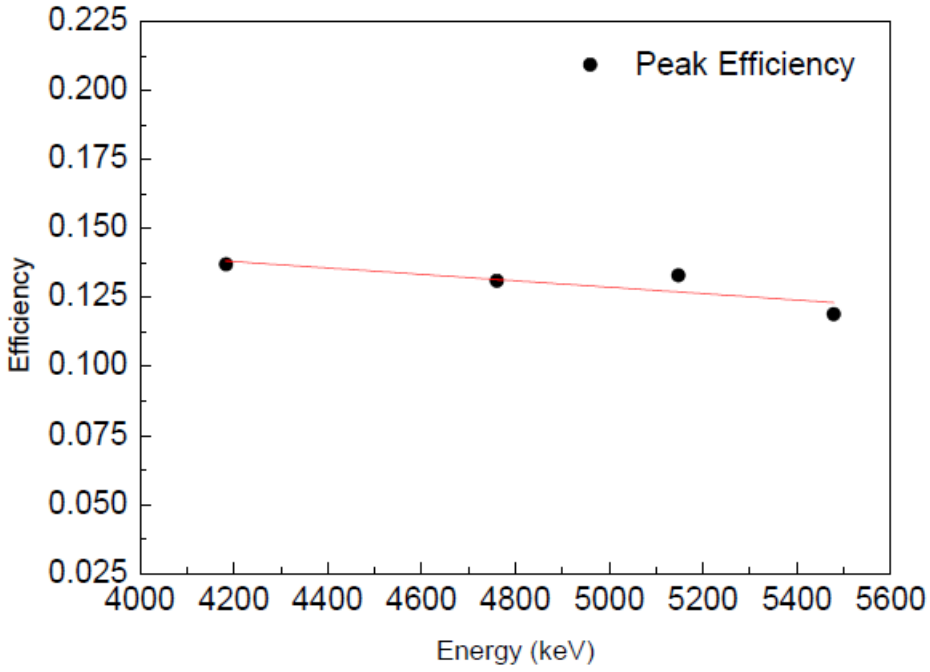


Figure 3.15: Energy peak efficiency as a function of energies for alpha spectroscopy detector

3.4.4 System background check

System background check refers to inspecting the number of counts registered within each detector when nothing is present in the sample chamber detector system. The Laboratory system background counts are performed periodically to identify any contamination that may be present within the sample chamber.

The spectra collected are also used for background subtraction during sample analysis.

The laboratory has set a threshold of 1 count per hour throughout the entire counting range channels. This is considered as the acceptable ratio, to indicate whether the detector is contaminated. The system background check was done for 24 hours (86400 seconds), similar to the samples counting time. This is crucial due to the fact that during counting procedure, the background number of counts in the region of the actual measurements for ^{226}Ra is mainly recognised in the detector. These background counts are finally subtracted from the actual sample measurement data.

3.5 Gamma Spectrometry

Gamma spectroscopy is the method where radionuclides through the analysis of the gamma-ray energy spectrum produced in a gamma-ray spectrometer are identified and quantified [1]. Further, it can also be defined as a branch of nuclear spectrometry that deals with the study of gamma radiation spectra and the various properties of the excited states of atomic nuclei that decay with associated gamma quantum emission. Gamma radiation is composed of photons which are uncharged particles but have a very high penetrating power. Following the general principle on radiation detection, the particle being subjected to detection generates a signal that can be processed later and converted into a digital signal. This study employs Gamma Spectrometry to check chemical recovery of prepared water samples analysed for ^{226}Ra.

3.5.1 Hyper-pure Germanium Detector

Intrinsic or Hyper-pure germanium (HPGe) detectors are Semi-conductor detectors made from ultra-pure germanium materials. They are typically made in various geometries, thus offering devices that can be tailored to the specific needs of the measurement [53]. Two different types of HPGe consist of Coaxial and Planar detector as shown in Fig. 3.16. Ref. [52] clearly explained that Planar type are usually small in size with a diameter of few centimeters and a maximum depletion region of 1-2 cm owing to their size, hence they are only suitable for low energy gamma radiation measurement. Coaxial type of detector is constructed to create a thicker depletion region required for more general gamma-ray measurement. The detector is a cylinder of germanium with an

n-type contact on the outer surface, and a p-type contact on the surface of an axial type. The n-type and p-type contacts are formed by diffusing lithium and implanting boron atoms respectively [52].

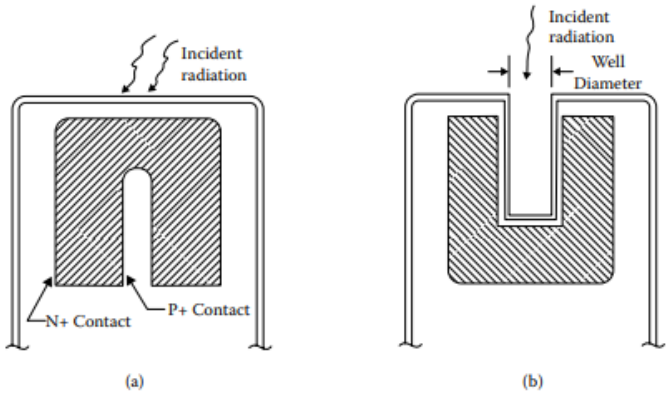


Figure 3.16: Two cross section examples of geometries used for Ge Detectors; (a) coaxial; (b) well or planar type. (taken from Ref. [53])

Gamma-ray spectroscopic technique is based on detecting gamma radiation emitted in the decay of the ^{238}U long-lived and short-lived daughters: ^{226}Ra and ^{222}Rn. The measurements are carried out in a laboratory under low-background conditions achieved by shielding the detector (e.g. by using lead) from ambient gamma radiation. Measurements are generally made over a period of 15 minutes for each counting cycle.

Standard nuclear electronics are used to process pulses from the detector, via a multi-channel analyzer (MCA) system, into a gamma-ray spectrum. One of the main advantages of this HPGe non-destructive method is that it allows the measurement of other gamma-ray emitting nuclides simultaneously [66]. The major advantage of Ge over Ge(Li) detectors is that the former can be stored at room temperature and cooled to liquid nitrogen temperature (77 K) only when in use. Cooling the detector, when in use, is necessary because germanium has a relatively narrow energy gap, and at room or higher temperatures, a leakage current due to thermally generated charge carriers induces such noise that the energy resolution of the device is destroyed [53]. In addition, there are benefits in reduced noise if certain components of the preamplifier are cooled. Because of this, it is routine to mount the preamplifier close to the detector [67]. The outer contact made out of diffusing lithium atoms will

increase in thickness if the detector is kept warm for extended periods (months or years). This will affect the efficiency of the detector, particularly at low energies [52]. Hence a typical germanium detector is often cooled by a reservoir of liquid nitrogen as depicted in Fig. 3.17.

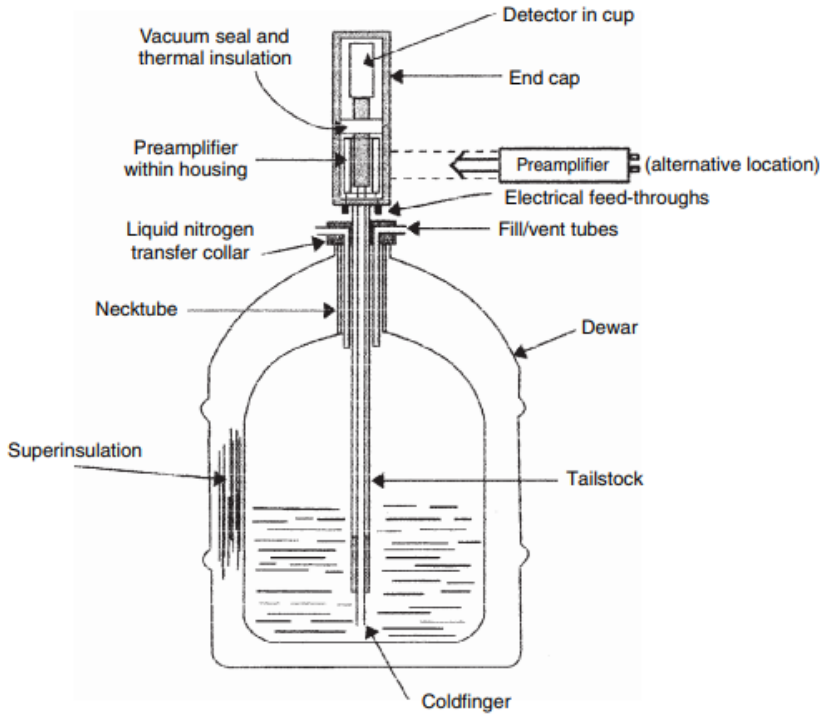


Figure 3.17: A typical schematic cross section of HPGE germanium detector set up cooled by a tank of nitrogen.(taken from Ref. [67])

3.5.2 Operational Principles of Gamma- ray Spectroscopy

The hyper-pure germanium (HPGe) detector, used for this study, is located at the National Nuclear Regulator (NNR) Environmental Laboratory, Pretoria. It is a Canberra p-i-n structure (model GC3018) with relative efficiency that is ≥ 30 % and has an energy resolution of ≤ 1.800 keV FWHM (full-width-at-half-maximum) at the 1.33 MeV and ≤ 0.877 keV at 122 keV. The recorded spectra by the detector were analyzed using Genie-2000 software. Figure 3.18 displays both side view and top view of this detector.

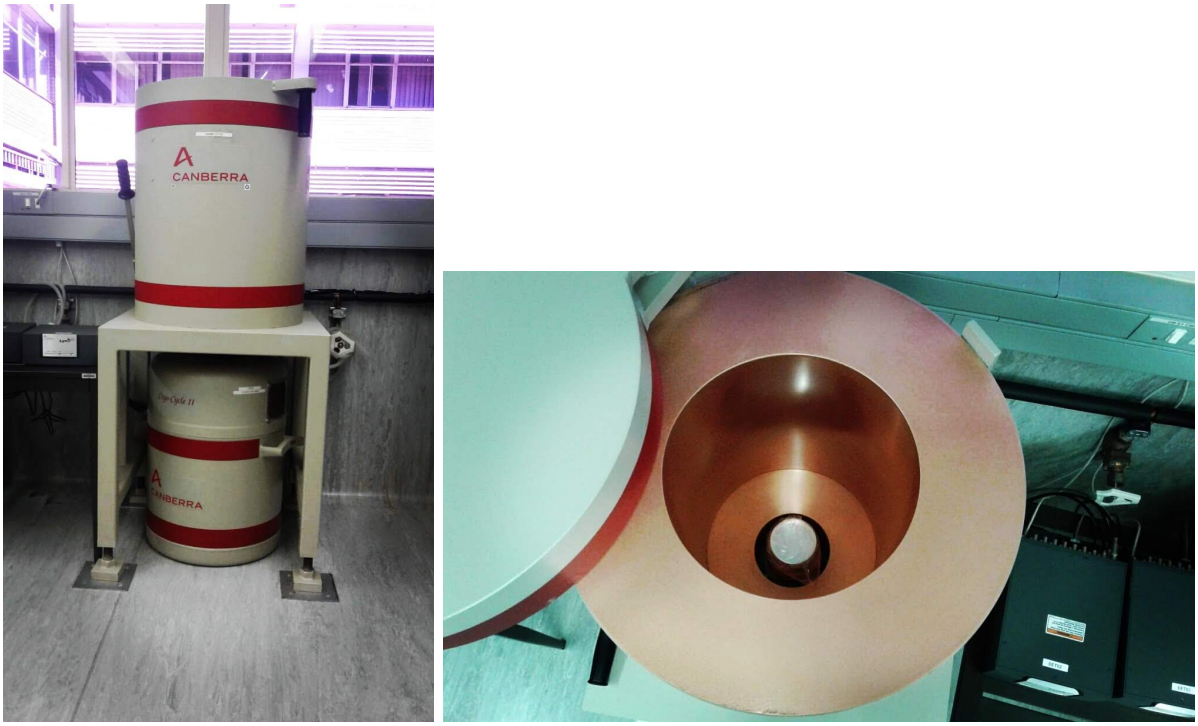


Figure 3.18: Pictures of HPGe detector situated at the NNR Environmental Laboratory

On the left hand side of Fig. 3.18 the cooling system and the entire detector is shown. On the right hand side, an internal part of the detector is shown. This detector was used for the determination of sample recovery in the water samples through out the preparation and analysis procedures.

The detector works based on gamma ray interaction with matter thereby produce a signal for every gamma photon entering into the system. During the interaction, the energy of gamma-ray is transferred to electrons hence creating ion-pairs within the active volume of the detector material [53]. Every interaction produces one ion pairs which in turn produce one pulse within the detector.

The bias voltage supply provides the electric field to sweep the electron–hole pairs out of the detector, which are then collected by the preamplifier[67]. The multichannel analyser (MCA) sorts the pulses by pulse height and counts the number of pulses within individual pulse height intervals.

3.6 Solid-state Alpha Detectors for Radon measurements

A RAD-7 detector [68] is a highly versatile instrument used to measure radon in real-time and it applies the α-spectrometry process. Figure 3.19 below represents an experimental set-up using grab sample and radon-in-air monitor, which uses well defined signals in a solid-state alpha detector as a continuous radon monitor.

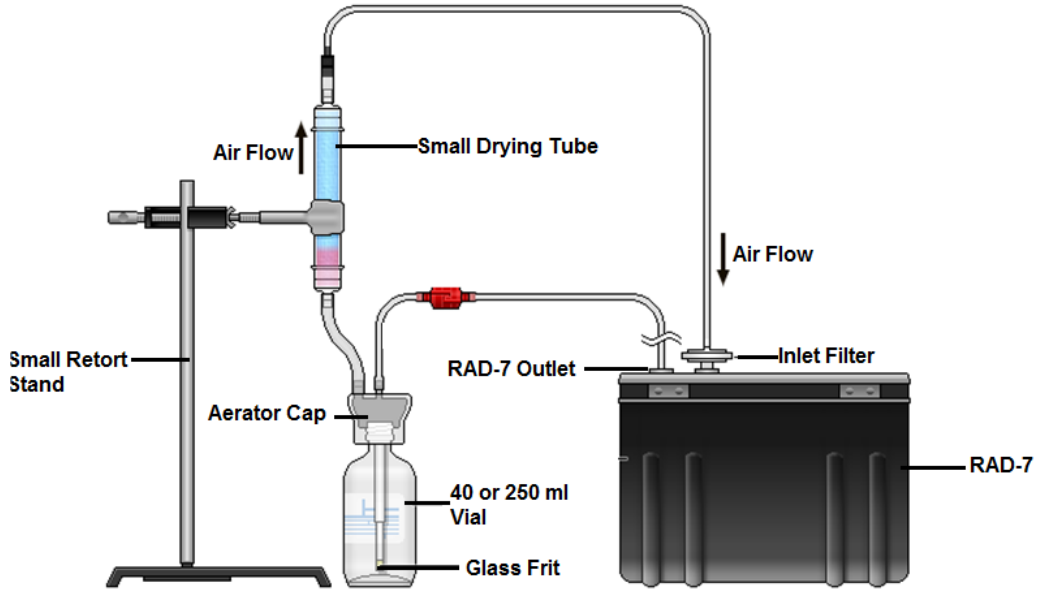


Figure 3.19: Schematic representation of the experimental setup of RAD7 using a grab sample and a radon-in-air monitor, an α-spectrometry method (taken from Ref. [23])

This was recommended in Ref.[1], for accurate and quick results, in the measurement of radon levels with active techniques, since radon concentration changes significantly and rapidly with time. A major advantage of the RAD-7 detector is its high sensitivity and capability to achieve detection limits as low as 1.0 mBq per sample. The RAD-7 detector uses the RAD-H2O accessory which enables it to measure radon in water over a concentration range from less than 10 $pCi.l^{-1}$ (3.7×10^{-1} $Bq.l^{-1}$) to greater than $4.0 \times 10^{5} pCi.l^{-1}$ (1.48×10^{4} $Bq.l^{-1}$) in a short time [68]. The Durridge RAD-7 radon monitor used in this work is version 2.5f 991128, model 711 and serial 01052. It is housed in the Nuclear Skills and Development Centre at Nuclear Energy Corporation of

South Africa (NECSA), Pretoria, South Africa. The system comprises of three main units as shown in Fig. 3.20 below that can be described as follows [1]:

1. The RAD-7 unit
2. (RAD-H2O) accessory
3. An Infrared (IR) printer through which the RAD-7 output results are captured.

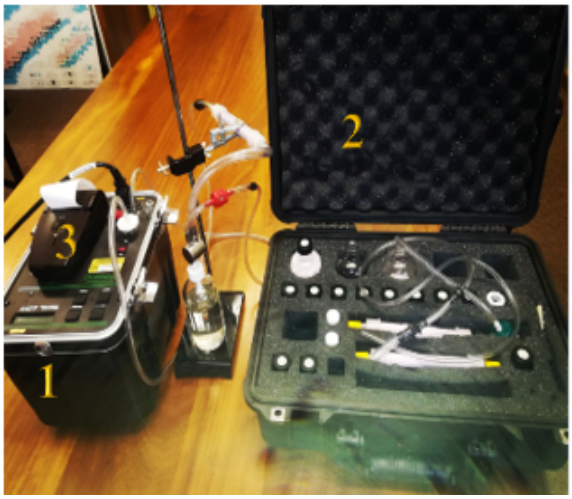


Figure 3.20: A RAD-7 system aerating 250 ml water sample at Necsa's Radio-Analysis Laboratory, Pretoria. With the RAD-7 unit, RAD-H2O accessory, and An Infrared (IR) printer numbered 1-3 respectively.

3.6.1 RAD-7 unit

The RAD-7 is an electronic radon detector manufactured by DURRIDGE COMPANNY Inc. The internal cell of RAD-7 instrument is a dome with volume of 0.7 litres, coated on the inside with an electrical conductor. The centre of the dome is composed of ion-implanted, planar and silicon solid-state α-detector, and an air pump. A representation of the measurement chamber with the detector is shown in Fig. 3.21 and Fig. 3.22.

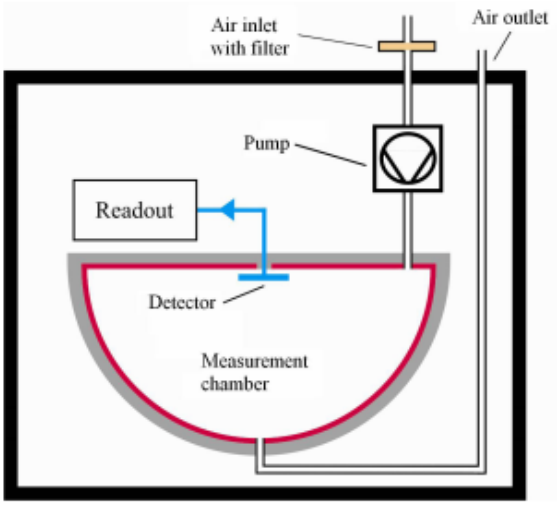


Figure 3.21: Measurement chamber of the RAD-7 (taken from Ref. [69])

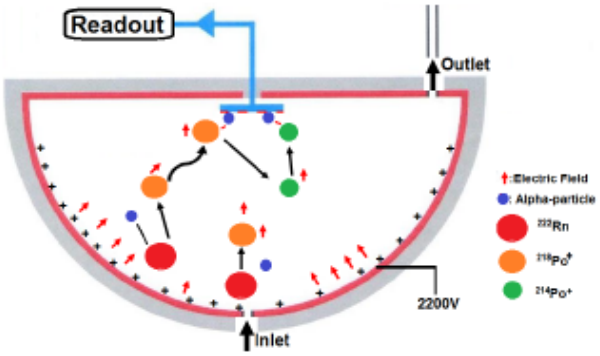


Figure 3.22: The internal process of the measuring chamber of the RAD-7 detector (taken from Ref. [68])

The inside of the conductor is charged by the high voltage power circuit to a potential of 2000 to 2500 Volts relative to the detector, creating an electric field throughout the volume of the cell [1]. The electric field pushes the positive charges onto the detector. In the detection of radon in air, the RAD-7 detects alpha-decaying radon progeny ^{218}Po and ^{214}Po. The radon monitor (RAD-7) uses a high electric field above a silicon semi-conductor detected at ground potential to attract the positively charged polonium daughters, $^{218+}$Po ($t_{1/2}$= 3.05 min; α-energy=6.00 MeV) and $^{214+}$Po ($t_{1/2}$= 164 μs; α-energy=7.67 MeV) which are counted as a measure of ^{222}Rn concentration in air [70]. The emitted alpha particles of characteristic energy produce an electrical pulse signal. The

signal is amplified electronically and transformed into a digital signal and the energy of the signal is histogrammed by the microprocessor to form a spectrum [23]. The energy of the alpha particle is linearly proportional to the electrical pulse voltage [23].

3.6.1.1 RAD-H20

The RAD-7 H2O is an accessory to RAD-7 that enables measurement of radon in water over a concentration range from 10 pCi/l to greater than 4 x 10^5 pCi/l [71]. This kit has a set of vials (bottles) 40 ml and 250 ml, pipes for connections, diffusing aerator; small desiccant tube. The equipment is portable and battery-operated, and the measurement is fast. Activity results of the measured sample are produced in about 30 minutes, and is connected to a desiccant and the RAD-7 as shown in Fig. 3.20. The system bubbles air through a 40 ml or 250 ml vial with water sample in minutes, so that the radon is aerated from the water sample [23]. ^{222}Rn air given out from the water sample circulates via a desiccant column then on to the RAD-7 detector, and then back to the water sample (vial) to accumulate equilibrium between the radon in the water and air. The system waits for another five minutes, making it 10 minutes after bubbling so that ^{218}Po and ^{222}Rn are in equilibrium. After that, the RAD-7 runs a further four five-minute counting cycles, thus making the total analysis time to be 30 minutes [1].

In some cases where in-situ measurements of water analysis are not possible, and the measurements are to be made after 24 h of the collection of samples, the measurements must be corrected for the decay time by multiplying the RAD-7 results with a decay correction factor (DCF) calculated using the equation [72]:

$$DCF = e^{0.00755T}, \tag{3.2}$$

where T is the decay time in hours and 0.00755 is the 1/(mean half-life of ^{222}Rn isotope) with mean half-life of 132.4 hours. Decay correction can be used for samples counted up to 10 days after sampling.

3.6.2 An Infrared (IR) printer

The HP printer labeled 3 in Fig. 3.20 is an infrared printer through which the analysis results of RAD-7 are printed out every five minutes in the case of

radon measurement using RAD-H2O.

3.6.3 RAD-7 Spectrum Analysis

Inside the detector, half of the α-particles emitted by the polonium hit the detector's active surface and produce a signal that is proportional to the α-particle energy. In this way, the RAD-7 measures some of the α-particles emitted by radon and/or thoron daughters and it distinguishes between the various radionuclides by their α-particle energy [66].

The RAD-7 then processes and stores these signals in the microprocessor. The signal that is stored is associated with the decay of a specific radionuclide and in the process of accumulating many of these signals, then a spectrum can be formed [1]. The RAD-7 accumulates their results (signals) in a spectrum with energy scale 0 to 10 MeV. This spectrum scale is divided into 200 channels of 0.05 MeV each.

The analysis of the spectrum is simplified because the electronics of RAD-7 are manufactured to group the 200 channels into 8 windows, of which four are the major windows namely A, B, C and D [66]. In Fig. 3.23, windows A and C are for radon and contain ^{218}Po (E_α = 6.00 MeV) and ^{214}Po (E_α = 7.69 MeV) peaks, respectively. Windows B and D are for thoron and contain ^{216}Po (E_α = 6.78 MeV) and ^{212}Po (E_α = 8.78 MeV) peaks, respectively[1]. However, in the cases where "old" thoron is present inside the detector, i.e., when window D contains counts, window A will contain 34% of the counts in window D as illustrated in Fig. 3.23 (b). This is applicable based on the fact that the RAD-7 cannot discriminate between the ^{212}Bi (E_α = 6.05 MeV) and the ^{218}Po (E_α = 6.00 MeV) [66].

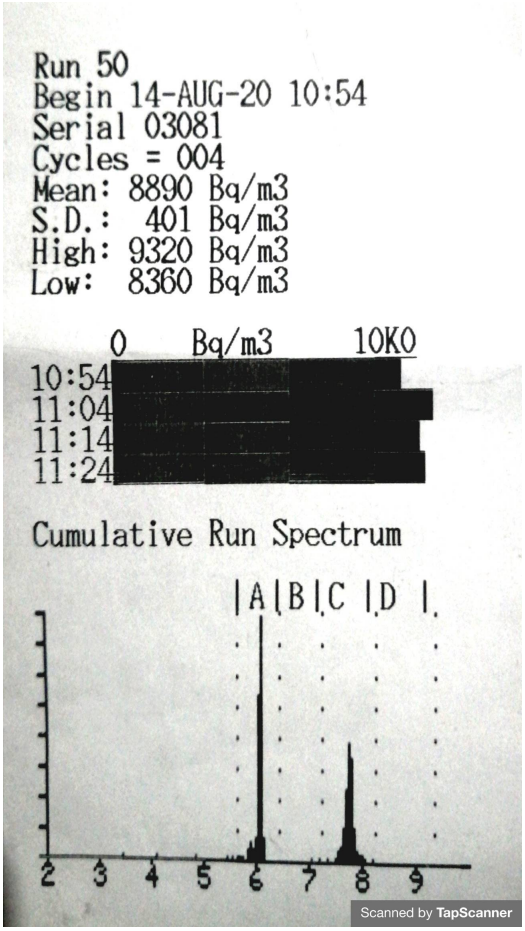


Figure 3.23: Produced results summary by the RAD-7 instrument for a trial run measurement exhibiting data information, that entails time, the mean radon concentration and its standard deviation, a bar chart for the complete set of readings and a cumulative spectrum. In the cumulative spectrum, the main four windows are shown separated by dots

The print-out is a test summary that shows the run number, date and time of the measurement, the serial number of the instrument, the number of cycles in the test, the radon in water average value and its standard deviation, highest and lowest readings, a bar chart and a cumulative alpha spectrum.

3.6.4 Measurement procedure for the study

The water samples were placed in 250 ml glass vials and capped for the RAD-7 system. Safety measures for water sample to be in contact with air were strictly considered. The RAD-7 was first purged with dried and radon-free air to dry and clean the system. The purging continued until the relative humidity

(RH) dropped to 10% or less, by using the desiccant before starting the sample test.

The microcomputer executes all the subsequent steps automatically: starting by pumping air in a closed loop for five minutes causing radon to be released from the water sample by bubbling; the radon-rich air is then dried by passing through a Drierite desiccants and eventually accumulates in the test chamber.

According to Ref. [73], the detection efficiency of the RAD-7 instrument decreases with increase in relative humidity, owing to the neutralization of Polonium ion by water particles. Also, Ref. [74] broadly explains that factors that affect the measurement accuracy and precision of RAD-7 radon detector are the sampling technique, sample concentration, sample size, counting time, temperature, relative humidity and background effects. Additionally, Ref. [73] suggests that RAD-H2O requires that the desiccant must be used to maintain relative humidity (RH) at level lower than 6%–10% in the radon chamber and also to dry the air stream before it enters the RAD-7 detector for the entire 30 min of the measurement.

3.7 Quality Control of RAD-7 alpha-Spectrometer

The performance of the RAD-7 instrument was monitored by counting a check source. A standard sample containing at least two α-emitting radioisotopes, which are ^{218}Po and ^{214}Po, are used to check their energies, the Full Width Half Maximum (FWHM) and the efficiency calibration of the detector or α-spectrometer" [20, 44]. The samples were counted under fixed conditions similar to those used for the check source which are discussed below. The parameters characterizing the stability of the system are the peak location, the FWHM, and the counting efficiency of a selected radionuclide present in the check source [44].

3.7.1 Preparation of standards

Aqueous standard solution was prepared and measured on the RAD-7 radon monitor. The standard solution was used to verify the results of the analysis from α-spectrometry using RAD-7. For quality assurance (QA) purposes, the aqueous standard solutions of different ^{226}Ra activity concentrations were prepared using a reference ^{226}Ra standard solution with code ACS/DC35/03, from the Analytical and Calibration Services (ACS) laboratories at Necsa. The

initial ^{226}Ra standard used to prepare the master solutions had activity 1.00± 0.03 Bq/l. A blank sample (no added ^{226}Ra standard solution) within these samples was prepared for conformation of the instruments quality assurance. Because one out of the two available protocols (Wat-40 and Wat-250) have to be selected depending on the size of vial (40 or 250 mL) that's being used for sample run, the prepared sample standards were transferred into 40 mL sample bottles.

Figure 3.24 below shows the standard samples prepared in the laboratory. Five known different radium activity concentrations which were placed in closed vials of 20 ml and kept for 30 days to allow the decay equilibrium between ^{226}Ra ($T_{1/2}$ = 1600 years), its immediate daughter ^{222}Rn and the four short-lived radon progeny. ^{222}Rn activity (mBq) entailed from the original reference sample is denoted by the values in Fig.3.24 (i.e 4.32-20.75 mBq). The presence of ^{210}Pb and its progeny was neglected due to the long half-life of ^{210}Pb ($T_{1/2}$ = 22.3 years).

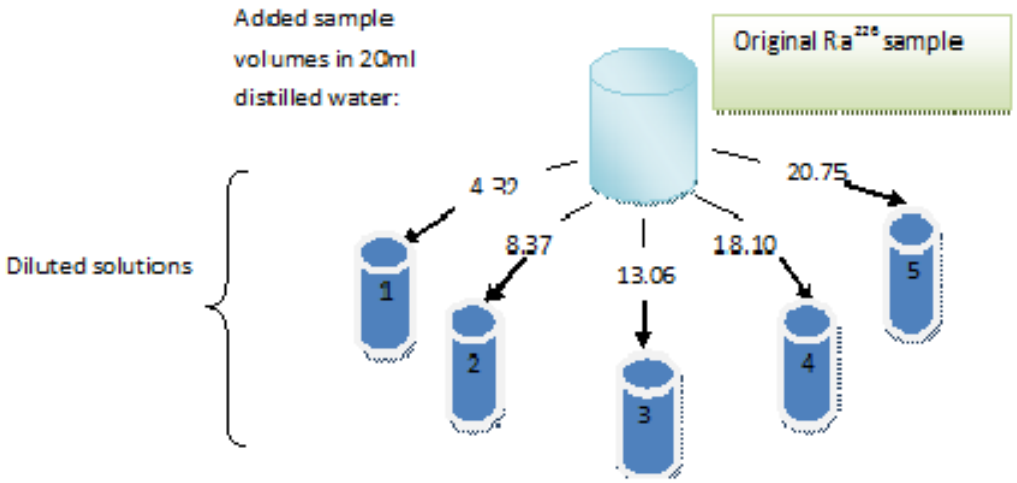


Figure 3.24: Laboratory prepared ^{226}Ra standard samples.

3.7.2 RAD-7 Calibration

To assess the functionality of the ^{222}Rn detector of choice in the current study, measurement using standard samples of radon concentration was carried out to

get an inter-comparison between theoretical concentration and measurements yield from RAD-7 instrument. The theoretically produced and measured values of radon concentration from the standard samples are presented in Table 3.4. The five ^{222}Rn standard sample solutions with known concentrations (Rn-CStd) ranging from 213.13 to 1022.15 mBq/l were measured by RAD-7 (Rn-CRAD-7) technique.

Table 3.4: Radon standard sample concentrations (Rn-CStd) measured by Rad-7 (Rn-C_{RAD-7})

Vials no:	Dissolved ^{226}Ra (g):	Final solution (ml)	Con. ^{226}Ra (mBq/g)	Dissolved ^{226}Ra (mBq/l)	Rn-CStd (mBq/l)	Rn-CRAD-7 (mBq/l)
1	0.4221	20.2713	0.213129918	213.13	213.13	276.72 ± 24.0
2	0.8173	20.5866	0.406356807	406.36	406.36	1158.84 ± 21.6
3	1.2757	20.1124	0.649225134	649.23	649.23	1718.28 ± 69.5
4	1.768	20.117	0.899559122	899.59	899.56	1188.81 ± 27.65
5	2.027	20.2979	1.022146879	1022.15	1022.15	2097.90 ± 71.7

The measured concentrations varied from 276.72 mBq/l to 2097.90 mBq/l for the $\alpha-$spectrometry technique applied. The results differences for measured results using RAD-7 and theoretical results might be caused by systematic uncertainties most likely associated with sampling. Figure 3.29 shows the results of this inter-comparison experiment performed in the current study. It was observed that the measured results closely matched with that of the standard sample by 0.81 factor. This figure also shows the correlation between the measured values of radon concentration by the Rad-7 $\alpha-$spectrometry technique.

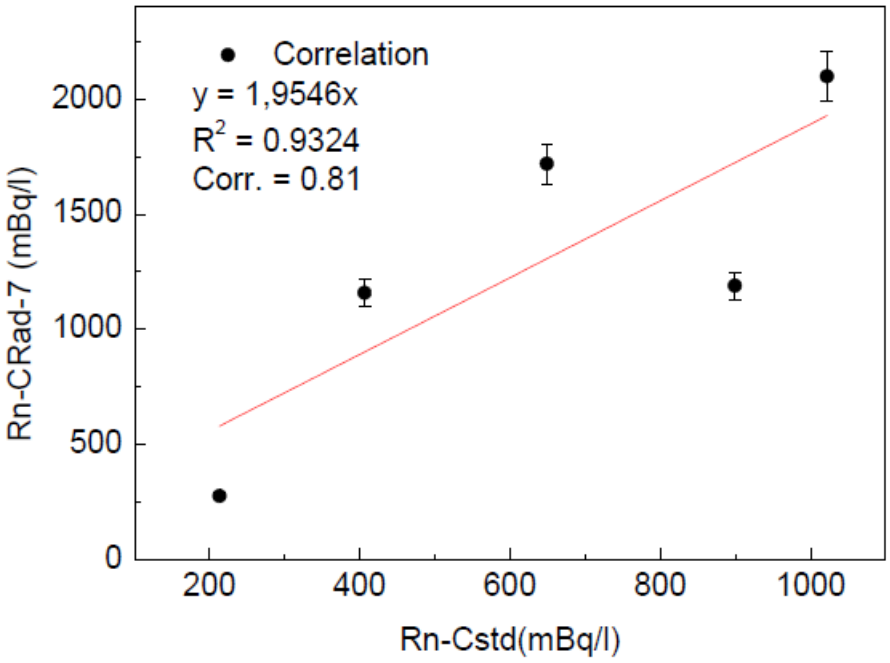


Figure 3.25: Correlation between measured ^{222}Rn and RAD-7 measured results

3.7.3 Effects of measuring time on Radon Concentration

The RAD-7 instrument is a counting system in a closed air-loop, it is assumed that only decay and leakage would lead to lower concentrations over time [75]. As shown in Table 3.5 and Fig. 3.26, it was observed that there was a slight drop in activity concentration during the counting periods.

Table 3.5: Measuring time with corresponding radon activity observed in ordinary tap water

Time (hours)	Time Stamp (Hours)	Rn-C (mBq/l)
0	23:21	325±11.85
0.30	23:51	300±11.55
1.00	00:21	300±11.55
1.30	00:51	250±10.8
2.0	01:21	250±10.8
2.30	01:51	247±10.65
3.0	02:21	200±10
3.30	02:51	175±9.6
4.0	03:21	150±9.6

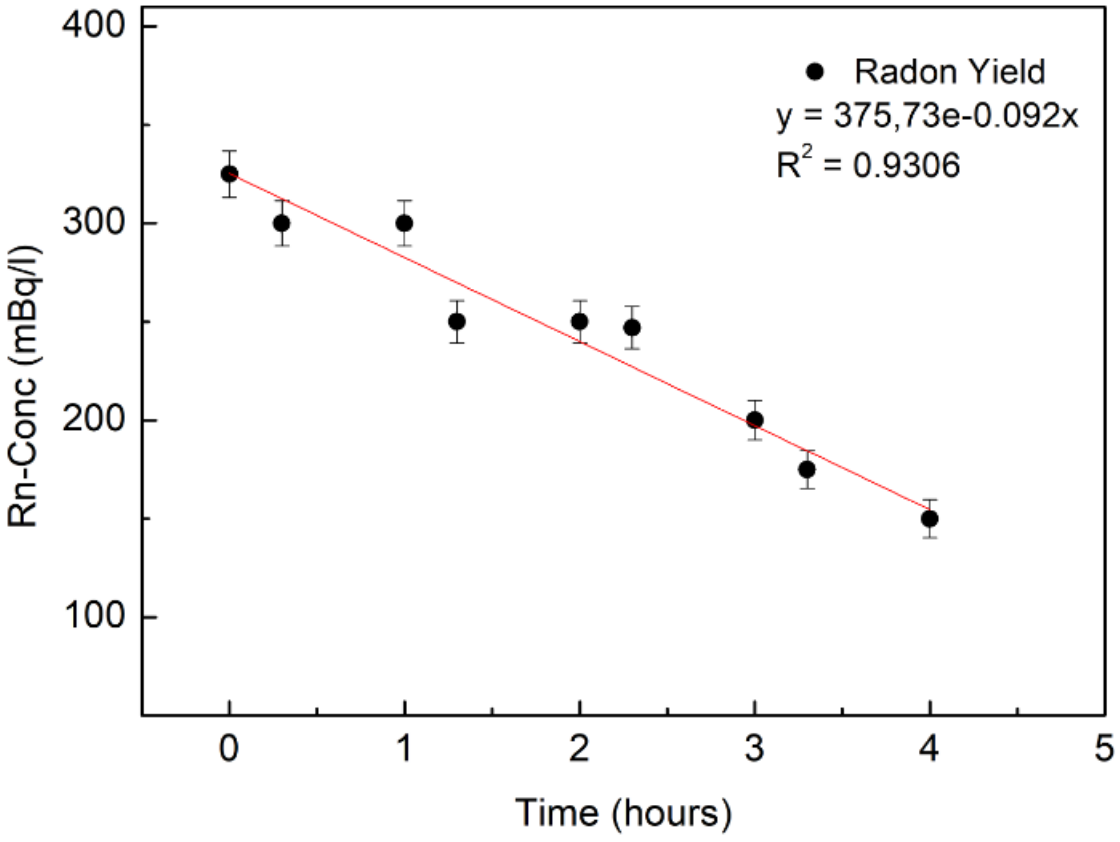


Figure 3.26: Effects of time in radon concentration yield inside the Rad-7 chamber

3.7.4 Decay correction

Mine water sampling was done to survey the level of radium and radon in different water sources in the West-Rand area of Johannesburg, Gauteng Province during the period from June 2019 to March 2020. Water samples were collected in 2 litre plastic bottles. As the samples were collected from the former uranium mines, the time between sampling and analysis in the laboratory had to be compensated for as some radon loss occurred due to decay [76]. The amount of radon loss was calculated using the decay formula

$$C_t = C_0 \times \exp^{-\lambda t} \tag{3.3}$$

where C_t (Bq/m^{-3}) is the radon concentration at time t (sec), C_0 is the radon concentration at time t = 0 and lambda is the radon decay constant (per second) [76]. Measuring C_t one may obtain the C_0 values while the addition of exhalation corrections would provide the initial radon concentrations.

3.8 Statistical Analysis of result

The difference in the mean values of two mutually independent groups can be evaluated by comparing them using T-test. However, to determine whether any of the differences between the mean values of three or more groups are statistically significant, the one way analysis of variance (ANOVA) method is applied. The method compare the p-value to the significance level to assess the null hypothesis. The p-value is the probability of obtaining results at least as extreme as the observed results of a statistical hypothesis test. The null hypothesis states that the population means are all equal. Usually, a significance level (denoted as α^* or alpha) of 0.05 works well. A significance level of 0.05 indicates a 5% risk of concluding that a difference exists when there is no actual difference.

When the p-value $< \alpha^*$, the differences between some of the mean values are statistically significant. If the p-value is less than or equal to the significance level, the null hypothesis is rejected and conclude that not all of population mean values are equal and vice versa when p-value $> \alpha^*$. If one-way ANOVA p-value is less than significance level (0.05), this indicates that some of the groups mean values are different, but not which pairs of groups hence evaluation of means comparisons within pair of groups. Confidence intervals that do not

contain zero indicate a mean values difference that is statistically significant. This type of statistical analysis has been applied in the case of rare earth element found in uranium soil samples in Ref.[77].

Chapter 4

Results, Analysis and Discussions

The present study was conducted to measure the concentration levels of radium and radon radionuclides in water samples around former uranium mines in the West Rand area of Johannesburg. The motivation was to appraise the health risks that these radionuclides may pose to nearby members of the public and environment. Water samples were collected at and nearby former uranium mines in the West Rand. These samples were collected for four consecutive seasonal terms, that is from June 2019 to March 2020. This was done as to establish seasonal variations in the presence of the nuclides under investigation. The West Rand extends from Randfontein in the west to Roodepoort in the east, in the Gauteng Province of South Africa. Additional drinking water samples were also collected from nearby communities, to serve as control samples. These samples were prepared and analysed at the National Nuclear Regulator laboratory and RadioAnalysis laboratory of the Nuclear Energy Corporation of South Africa (NECSA) both situated in Pretoria, South Africa. The physicochemical properties of the surveyed water samples namely pH and electrical conductivity (EC) were also studied. The measurements were conducted at the ARC-Institute for soil, climate and water using the pH-Meter (pH 700 Eutech) and EC Meter (Multi 9310 IDS) instruments. The ARC is situated in Pretoria, Arcadia.

4.1 Activity of Radium in water

Alpha spectroscopy was employed to determine the activity concentrations of ^{226}Ra radionuclide in water samples under investigation. Section 3.5 shows the gamma spectrometer, that was used together with alpha spec (subsection 3.4.1) to check and estimate chemical recovery of samples after the intense sample preparation required for Alpha Spectroscopy. This procedure include addition of ^{133}Ba tracer to each sample, then quantitatively determine recovery by comparing a ^{133}Ba standard disc with each sample. The ^{133}Ba standard disc had the same amount of tracers as per samples, and comparison was made by counting both standard and sample with a gamma detector. Table 4.1 presents the activity concentrations of ^{226}Ra obtained with their uncertainties in water samples collected at different sampling points per mining area, for four consecutive seasons.

4.1.1 Overview of the Ra-226 data collected over four seasons

The samples collected from different sampling points in selected former Uranium mines as listed in Table 3.1 were prepared and analyzed by Alpha Spec. Measurements were taken in winter (June 2019), Spring (September 2019), Summer (December 2019), and Autumn (March 2020). Raw measured data is presented in Table 4.1 below. The ^{226}Ra activity concentration values ranged from (1.58±2.74 to 164.42±18.47) mBq/l, (11.23±3.89 to 136.01±15.4) mBq/l, (-3.38±-2.39 to 156.15±18.14) mBq/l, and (4.25±1.23 to 108±8) for June 2019, September 2019, December 2019 and March 2020 water samples, respectively. The highest and lowest values were recorded at (Ezul in) Ezulwini inlet in winter (June 2019) and (Kloof down) Kloof downstream point in Summer (December 2019) and these were found to be (164.42±18.47) mBq/l, and (-3.38±-2.39) mBq/l, respectively.

Table 4.1: Activity concentration results of ^{226}Ra in the measured water samples including their uncertainties.

Sample ID	June_19	Sept_19	Dec_19	Mar_20
	^{226}Ra (mBq/l)	^{226}Ra (mBq/l)	^{226}Ra (mBq/l)	^{226}Ra (mBq/l)
Bly 4	122.93±13.92	134.13±12.51	156.15±18.14	108±8
Bly6	46.9±8.41	61.57±8.92	76.3±11.01	37.9±3.7
Bly comb	101.2±12.85	124.65±12.53	149.98±17.74	105±7
Drie down	56.87±8.74	11.23±3.89	55.47±10.28	4.25±1.23
Drie settl	35.67±6.31	42.76±7.23	60.76±13.58	41.5±4.1
Drie8	30.28±8.02	32.51±6.92	48.71±10.63	44.8±4.5
Kloof 10	147.19±15.1	136.01±15.4	60.67±10.06	138±8
Kloof down	3.4±4.16	73.17±10.14	-3.38±-2.39	10.8±2.0
Ezul	97.31±10.62	81.33±10.31	107.39±13	86.89±12.02
Ezul in	164.42±18.74	109.38±11.79	73.59±10.96	59.97±10.75
Drink	1.58±2.74	13.99±5.54	1.72±2.97	32.31±2.9

Measurement of nuclear decay processes is often associated with statistical fluctuations. The need of describing inaccuracies is valid, since optimization involves systematic uncertainties due to sampling, measurement and analysis. In the context of the current work, the appropriate concept for expressing inaccuracies is an uncertainty and that the value should be provided by an uncertainty analysis. An uncertainty is a possible value that the error might take on in a given measurement [78]. The employed Alpha spectrometry for radium analysis has produced the reported uncertainty results that are only statistical errors from counts.

4.1.2 Interpretation and discussion of radium results

The variations of ^{226}Ra in water samples from different selected former mining sites across West-Rand area of Johannesburg are illustrated in Fig. 4.1 - 4.4 and plotted together in Fig. 4.5. Figure 4.6 shows the percentage contribution of the total radium concentration in the water samples from the four surveyed seasons in the current study. The radium activity concentrations observed in all four surveyed seasons were almost evenly distributed (Fig.4.6), with a small exception of autumn samples. The autumn season, that is March 2020 have the least total radium activity concentration. Figure 4.7 shows the percentage contribution of the total radium concentration in each sample area during the surveyed seasons. The discharge from shaft-4 at Blyvooruitzicht (Bly4) former uranium mine have higher ^{226}Ra radioactivity as compared to the other samples, about 16.88% of the total contribution of radium. While the drinking water sample have low ^{226}Ra radioactivity. This could be because

its a sample that is prepared for domestic use and drinking.

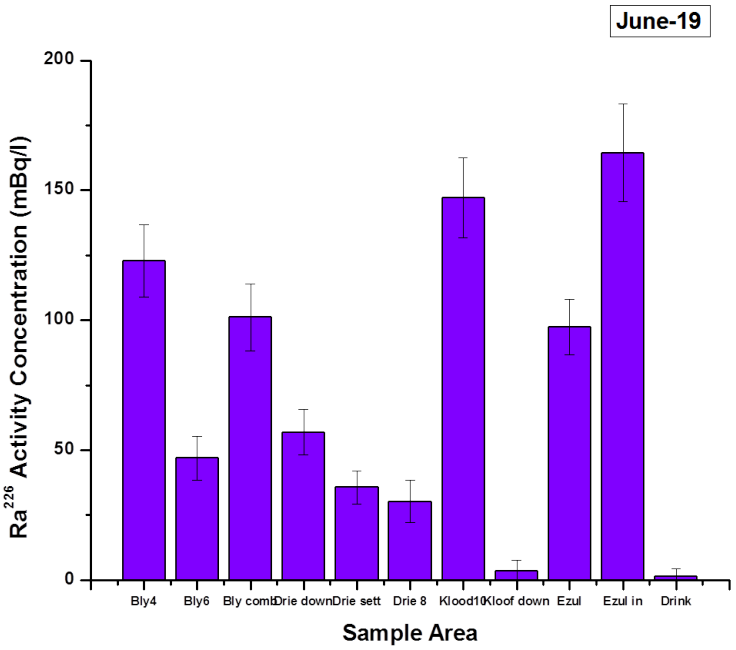


Figure 4.1: June 2019 ^{226}Ra concentration results

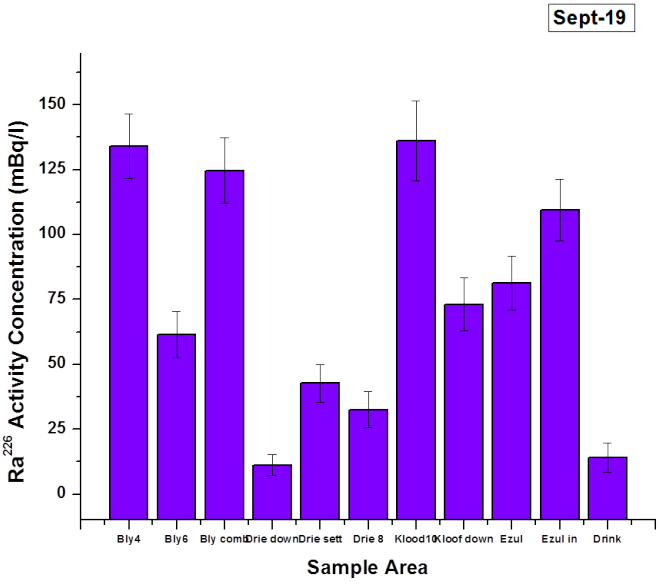


Figure 4.2: September 2019 ^{226}Ra concentration results

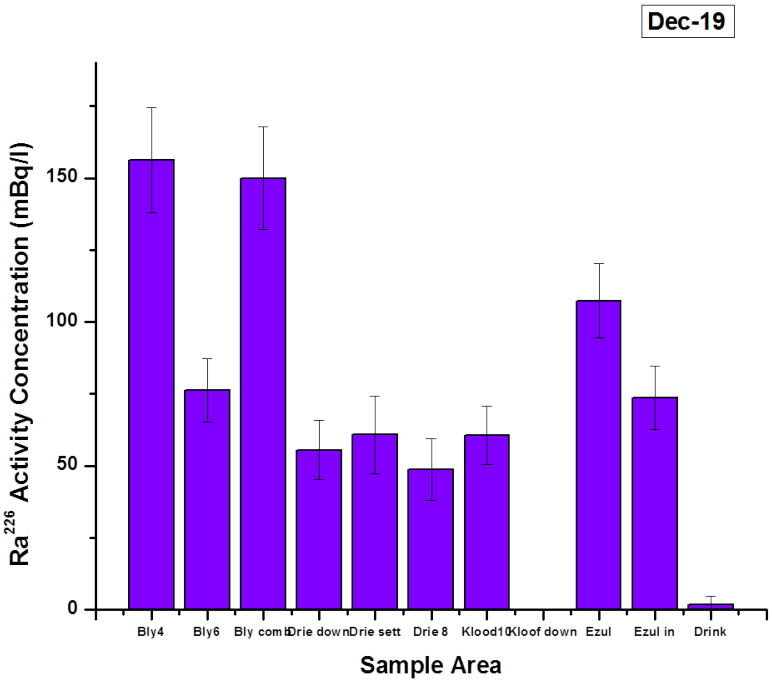


Figure 4.3: December 2019 ^{226}Ra concentration results

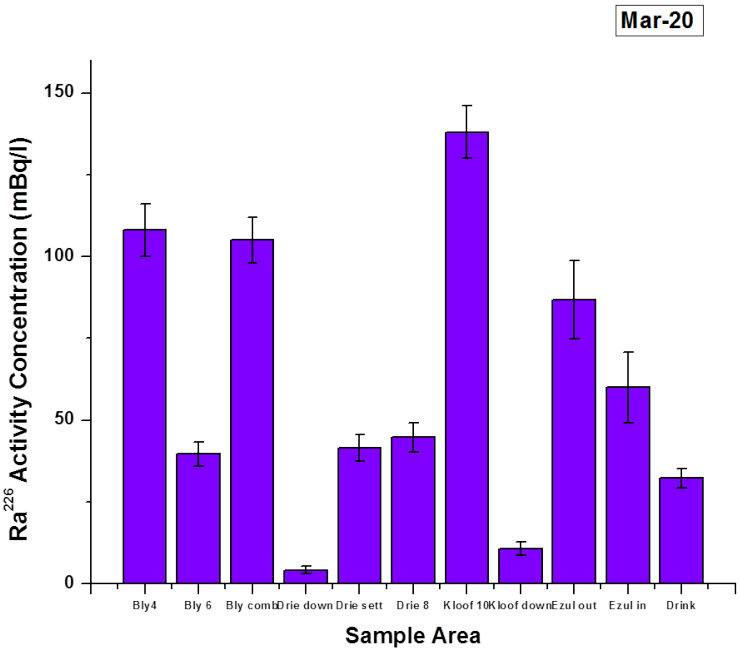


Figure 4.4: March 2020 ^{226}Ra concentration results

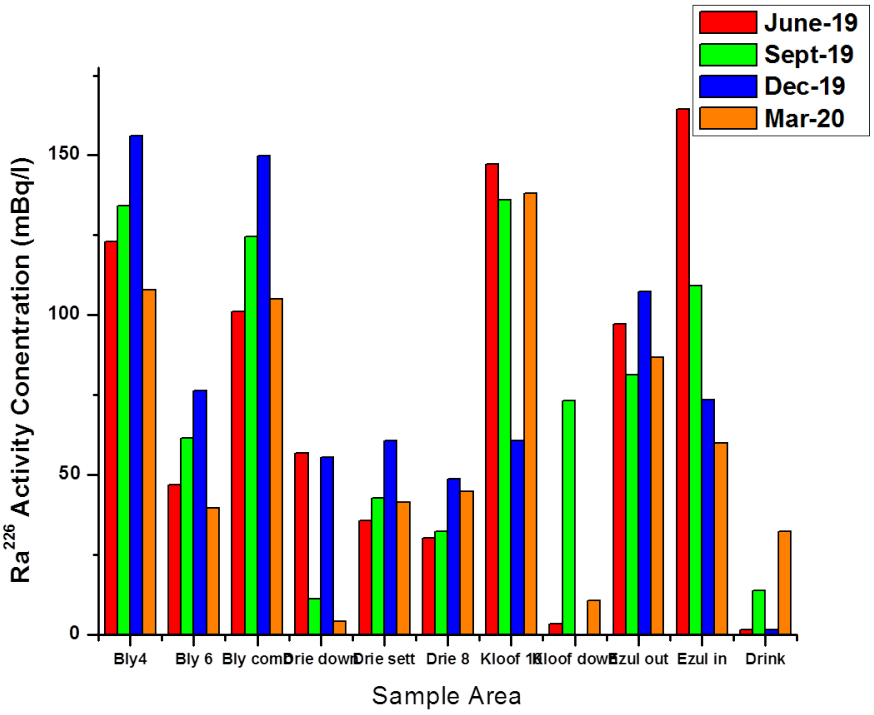


Figure 4.5: Bar graph showing the radium concentration from June 2019 to March 2020

Based on the Environmental Protection Agency (EPA) [1], a maximum contamination levels of 555 mBq/l has been suggested that, and the observed results showed radium concentration lower than (555) mBq/l. Observing Fig.4.5, samples from Blyvooruitzicht, namely Bly4, Bly 6 and Bly comb follow a pattern, the least activity concentration is in March 2020, followed by June 2019, September 2019 and the highest activity concentration is in December 2019 in all the surveyed seasons. Within the above mention samples, Bly4 sample always has the highest activity concentration, followed by Bly comb sample throughout the seasons. Taking into account that Bly comb sample is a combination of water from discharge 4 and 6, this implies that Bly 4 water activity concentration dominates making Bly comb to have higher activity than Bly 6. Samples from Driefontein, that is Drie down, Drie sett, Drie 8 had low ^{226}Ra activity concentrations throught the seasons. Samples from Drie sett and Drie 8 are following a similar pattern in which the December 2019 sample

has higher activity concentration, while June 19 has the highest activity in Drie down sample. Water sampled from Kloof has the lowest activity concentration such that there is a negative result in December 2019 from Kloof down sample. The negative concentration value indicates that the sample's concentration was below the determination limits of the analytical method, that is Alpha Spec Canberra PIPS detector applied for ^{226}Ra analysis. The Ezulwini samples, that is Ezul Out and Ezul in have high concentrations and there is no specific pattern followed in this particular mining area. It is observed that the Ezul in had the highest activity concentration of all surveyed samples in June 2019. Finally, the Drink water sample has low activity concentration. Seasonal climate and its differences may cause discrepancies and changes in activity concentrations for each sampling points throughout the years.

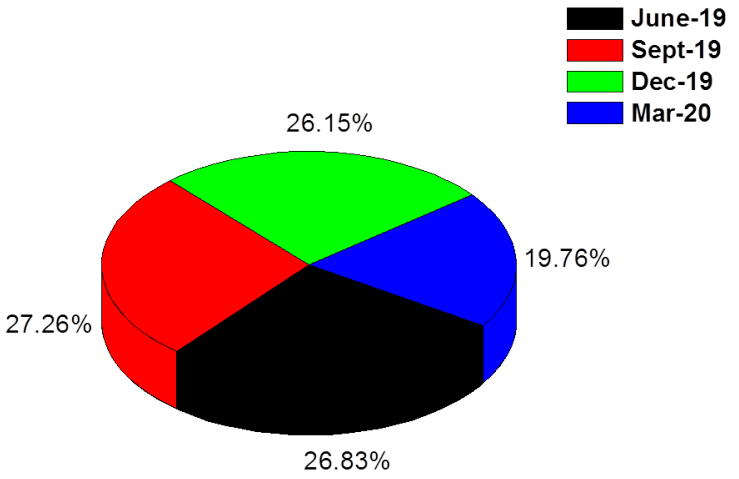


Figure 4.6: Percentage composition of the total radium concentration of water samples during the seasonal survey.

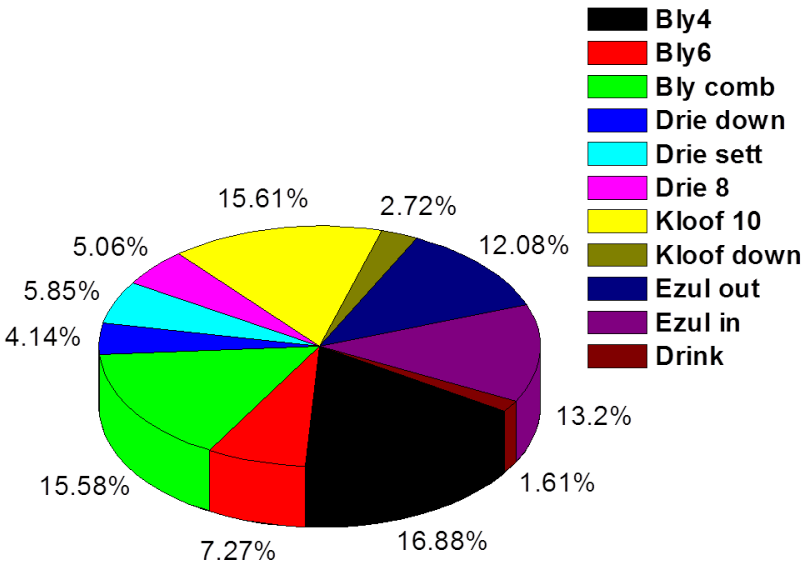


Figure 4.7: Percentage composition of the total radium concentration per sample area for all the seasonal survey.

4.2 Activity of Radon in water

General survey of the radon concentration level in water with the meteorological parameters of temperature (Tint) and relative humidity (RH) with the sample volumes of 250 ml used the RAD-7 instrument are listed in Table 4.2. Samples were measured using the α-spectrometry technique in the RAD-7 instrument as discussed in Section 3.6. Obtained radon activity concentration results for collected mine water samples as well as deionised water, Valpre (commercial drinking water) and commonly available tap water are presented in Table 4.2. The results from RAD-7 were obtained with standard protocols WAT250 of the RAD-7 instrument. Moreover, the main idea was to also verify the quality of the instrument employed by testing radon concentration in the water samples in subject. The World Health Organisation (WHO) has established a limit of 1000 mBq/l activity concentration for ^{222}Rn in water samples, and the reported radon results from this study are below the stipulated limit [79]. Meanwhile, the maximum concentration level (MCL) of ^{222}Rn in drinking water, has been also suggested as 11.1 Bq/l by the EPA (Environmental Protection Agency, May 2012)[80], and the results are below the MCL.

4.2.1 Overview of radon data collected over four seasons

The radon raw data results from former uranium mines samples are tabulated in Table 4.2 below. Meteorological parameters such as humidity (RH) and internal temperature (Tint) of the detector, which have an influence on radon release from water, were also measured as shown in Table 4.2. The ^{222}Rn activity concentration results ranged from (37.1±74.1 to 269±79.2) mBq/l, (57.2±73.9 to 190±94.9) mBq/l, (76.6±63.2 to 211±146) mBq/l, and (56.3±71.1 to 289±272) mBq/l for the Winter (June 2019), Spring (September 2019), Summer (December 2019) and Autumn (March 2020), respectively.

The highest ^{222}Rn activity value was recorded at (Bly 6) Blyvooruitzicht shaft 6 discharge in Autumn (March 2020), and was found to be (289±272) mBq/l. Whereas the lowest activity value was recorded at (Ezul) Ezulwini Outlet discharge in Winter (June 2019), and was found to be (37.1±74.1) mBq/l. This could be associated with the wet weather conditions during winter, that results in high humidity, which causes dissolution and corrosion of

the functional group of most of the ^{226}Ra mother radionuclide (^{228}U) bearing minerals [81]. The values of the activity for the radionuclide ^{222}Rn for different seasons are very low, and are noted to be well below the world average values. Similarly, with the reported ^{226}Ra uncertainy results, the Rad-7 has produced the reported uncertainty results that are mainly due to statistical error from counts.

Table 4.2: Activity concentration results of ^{222}Rn in the measured water samples including their uncertainties.

Sample ID	June_19			Sept_19			Dec_19			Mar_20		
	Rn (mBq/l)	RH (%)	Tint (°C)	Rn (mBq/l)	RH (%)	Tint (°C)	Rn (mBq/l)	RH (%)	Tint (°C)	Rn (mBq/l)	RH (%)	Tint (°C)
Bly 4	96±39.3	14.25	27.85	57.2±73.9	10.25	28.225	171±91.3	10.5	29.35	212±184	11.5	26.8
Bly6	171±91.3	15.75	27.85	96.8±74.1	9.5	28.3	211±146	10.5	29.5	289±272	11.25	26.8
Bly comb	172±131	12.5	28.15	190±94.9	9.5	28.3	77.5±89.5	11.25	29.275	58.0±74.1	11.25	26.7
Drie down	172±33.8	11.25	28.225	116±134	9.75	28.05	136±132	9.75	28.525	190±94.8	11.75	27.1
Kloof down	77.6±110	15	27.55	116±134	8.5	29	77.4±110	9.75	28	63.3± 25.7	11.5	27.025
Ezul	37.1±74.1	10.5	28.3	76.6±63.2	9.25	27.7	76.6±63.2	9	28.075	114±98.9	12	26.8
Drink	269±79.2	19.25	24.825	231±91.7	11.5	28.675	190±130	15.75	25.975	56.3±71.1	12.5	26.95
Deionized 2020	38.6±44.6	10.25	24.9									
Valpre 2020	58.0±74.1	14	25.875									
Tap water 2020	152±86.4	15.25	21.45									

4.2.2 Discussion of radon results

Figures 4.8 - 4.11 present activity concentration results recorded in Table 4.2, and later combined in Fig. 4.12 showing the variation of radon in water samples from different former mining sites across West-Rand area of Johannesburg. Figure 4.13, and 4.14 plotted together for comparison the percentage contribution of the total radon concentration in the water samples from the general survey conducted in the current study. Observed radon activity concentrations for all the seasons are evenly distributed. Figure 4.14 show the percentage contribution of the total radon concentration in each sample area during the surveyed seasons. The discharge from shaft six at Blyvooruitzicht (Bly6) former uranium mine has highest contribution of radon as compared to the other samples, contributing 20.2% percent of the total radon. Meanwhile, the point with low ^{222}Rn radioactivity considered from Ezulwini as illustrated in Fig. 4.14 with 8.01% of the total annual radon activity concentration.

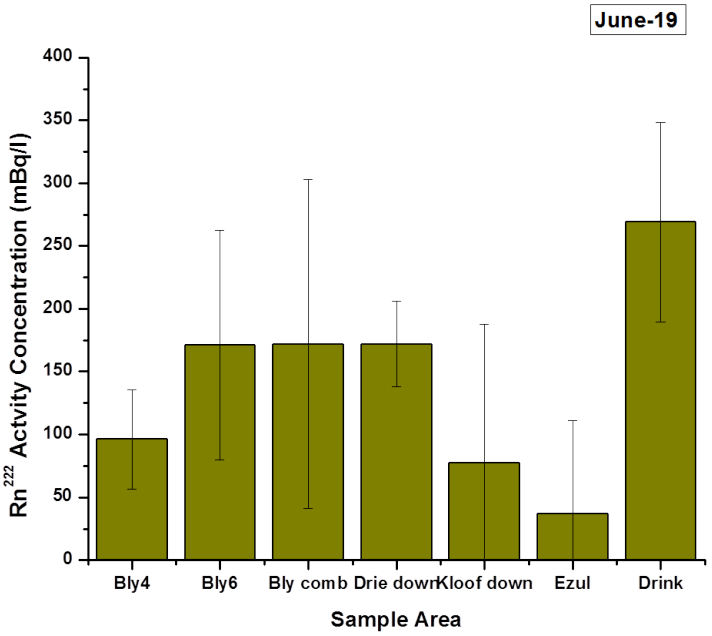


Figure 4.8: June 2019 ^{222}Rn concentration results

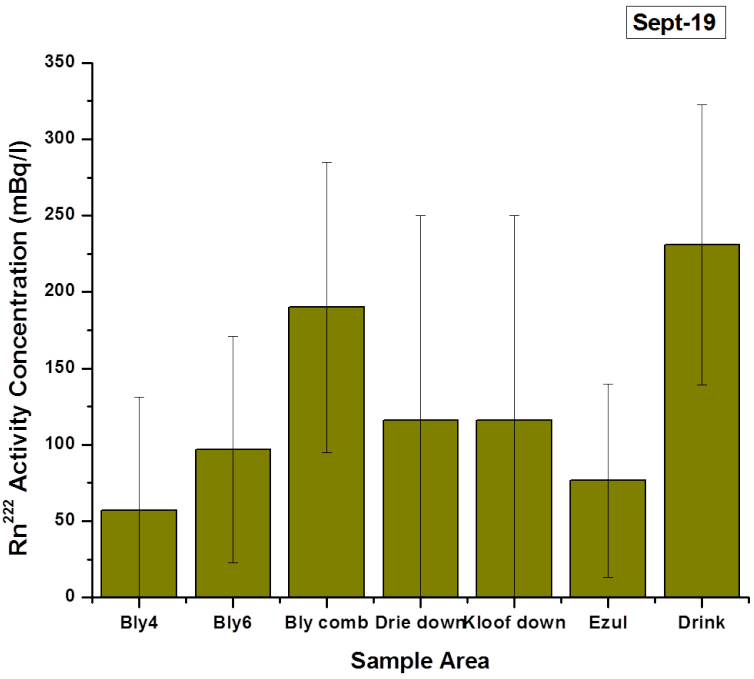


Figure 4.9: September 2019 ^{222}Rn concentration results

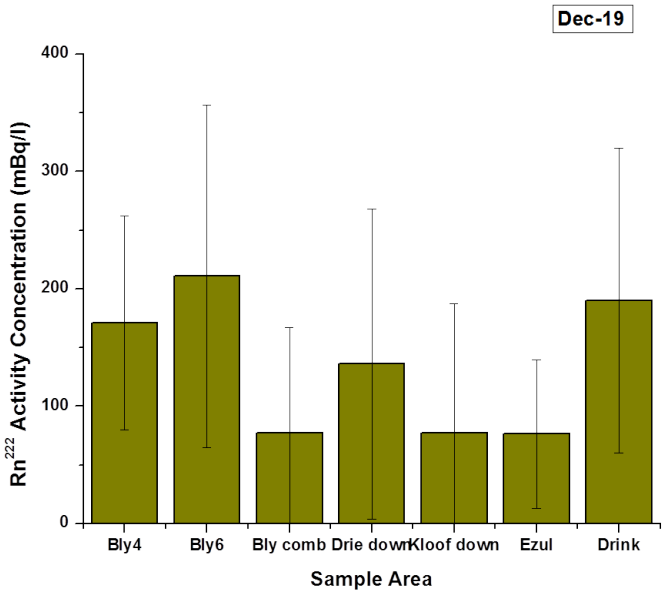


Figure 4.10: December 2019 ^{222}Rn concentration results

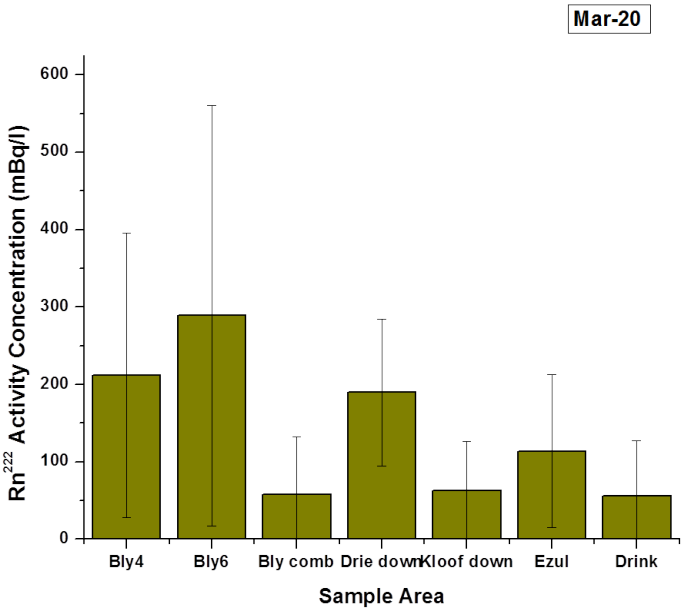


Figure 4.11: March 2020 ^{222}Rn concentration results

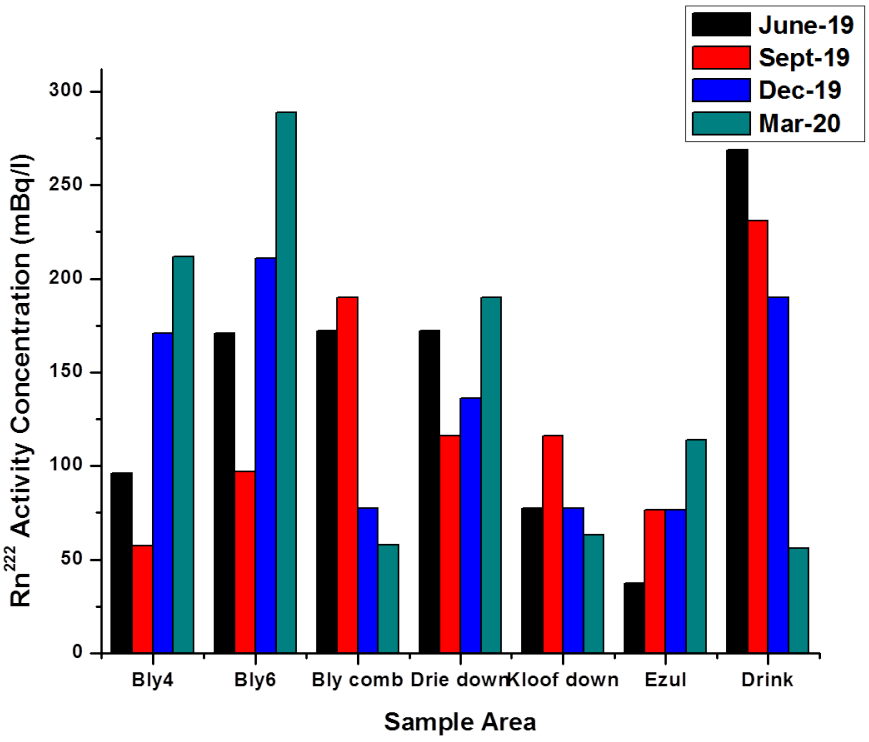


Figure 4.12: Bar graph showing the radon concentration from June 2019 to March 2020.

Overviewing Fig 4.12, samples from Blyvooruitzicht, namely Bly4, Bly6 follow a similar pattern, the lowest activity concentration is in September 2019, followed by June 2019, December 2019 and the highest activity concentration was found in March 2020 in all the surveyed seasons. On the contrary, the Bly comb sample has the lowest activity concentration in March 2020, followed by December 2019, June 2019 and the highest activity in found in June 2019. Moreover, Bly 6 sample has the highest ^{222}Rn activity concentration found in March 2020. The Drinking water sample has higher activity concentrations in June 2019, as compared to samples from Drie down, Kloof down and Ezul.

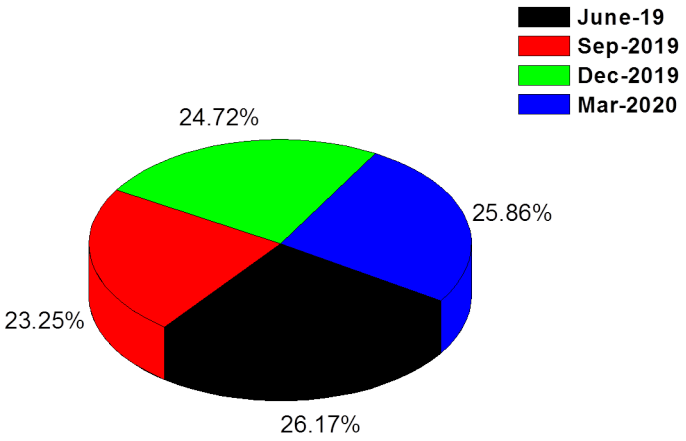


Figure 4.13: Percentage composition of the total radon concentration of water samples during the seasonal survey.

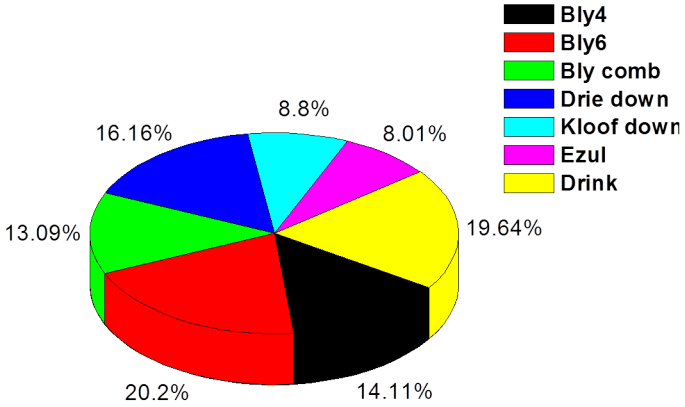


Figure 4.14: Percentage composition of the total radon concentration per sample area for all the seasonal survey.

The detection efficiency and accuracy of the RAD-7 is affected by relative humidity, and the internal temperature, therefore, it is important to keep both quantities as low and constant as possible. Figures 4.15 and 4.16 illustrate the meteorological data (humidity and temperature, respectively) observed during measurements of radon in the selected samples in this study. It is important to report that the humidity was controlled and the resulting internal temperature inside the RAD-7 detector chamber. With reference to Fig.4.13, June 2019 has the highest overall radon activity percentage composition and this is corroborated in Fig.4.15 where the highest humidity level was portrayed in a samples collected in June 2019. This clearly indicates that humidity levels have to be kept as low as possible, as to measure most accurate results. Fig. 4.14 shows that the drinking water sample is highly radioactive. The drinking water sample is collected from a waste water treatment facility near Driefontein mine. Treatment of water for drinking purposes has high potential to concentrate radioactive materials [82]. The high activity readings suggests local conditions of area, the treatment process and the subsequent generation of waste could be the reason the particular sample is highly radioactive.

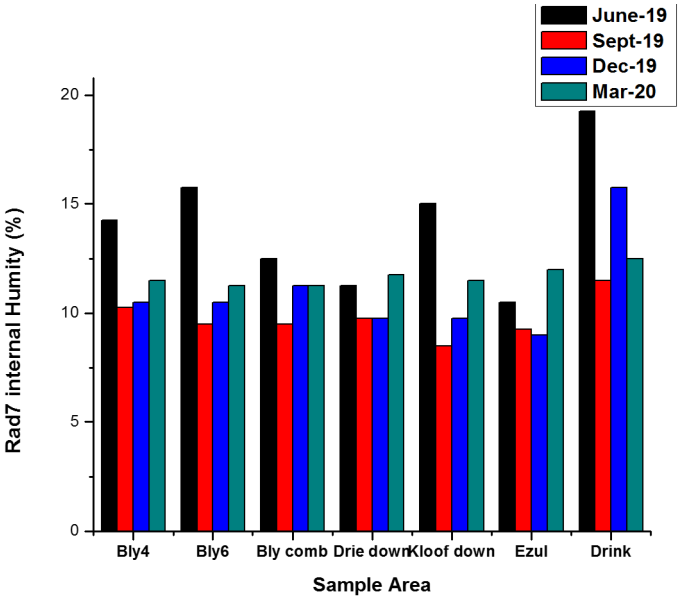


Figure 4.15: Humidity inside the the RAD-7 chamber as the samples were counting

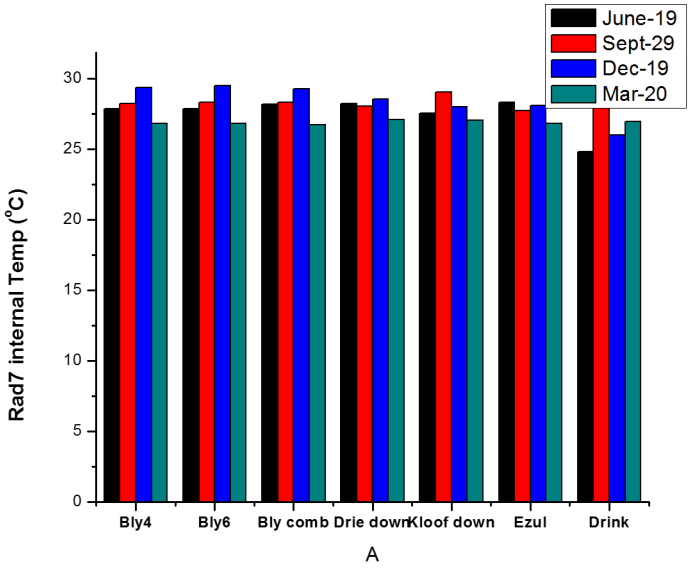


Figure 4.16: Temperature inside the the RAD-7 chamber as the samples were counting

4.3 Statistical analysis of results

ANOVA was applied to the activity concentration of ^{226}Ra and ^{222}Rn observed in all the surveyed seasons as well as the results of AED and ECLR, respectively. The statistical analysis method is detailed broadly is Section 3.8.

4.3.1 Overall Average Activity Concentrations

Determination of the differences between the mean values of groups are statistically significant, the one way ANOVA method is as explained in Section 3.8. Here, the significant levels of the group of observed data will be described. Figure 4.17 presents the activity concentration of ^{226}Ra and ^{222}Rn in water samples under investigation for all the surveyed seasons. Since radium (^{226}Ra) is a mother radionuclide of radon gas (^{222}Rn) with a long half-life of 1600 years, it has been clearly confirmed that the ^{222}Rn activity concentration yield is always higher that ^{226}Ra concentration for all the investigated seasons. Following this, the highest activity concentration in June 2019 samples was measured in drinking water sample and the lowest was found in Ezul downstream of operations sample (Fig.4.8). The highest activity concentration in September 2019 was in the drinking water sample, and also the sample from Blyvooruitzicht shaft comb is also observed to be high and the lowest is from Blyvooruitzicht shaft 4 (Fig.4.9). Highest activity concentration in December 2019 was sample from Blyvooruitzicht shaft 6 and lowest was in a sample from Kloof downstream of operations (Fig.4.10). The highest activity concentration in March 2019 was measured in Blyvooruitzicht shaft 6 and lowest was in a sample from drinking water sample (Fig.4.11).

With reference to Appendix A Table A1. the activity concentration of radium analysed samples mean values are not significantly different ($p>0.05$) from June 2019 to March 2020 consecutive seasons. The comparison of mean values within pair of groups shows no statistical significance. ^{222}Rn activity concentration (mBq/l) mean values are not significantly different ($p>0.05$) from June 2019 to March 2020 consecutive seasons, as presented in appendix A Table A.2. The mean comparisons within pair of groups of all confidence intervals indicates a mean differences that are not statistically significant.

Table A.8 and A.11 in appendix A clearly shows that ^{226}Ra and ^{222}Rn activity concentration in June 2019 and March 2020 water samples showed

a mean significant difference ($p< 0.05$). However, the activity concentration mean values of ^{226}Ra and ^{222}Rn in water samples in September 2019 and December showed no significant difference ($p>0.05$), as tabulated in Table A.9 and A.10 in Appendix A. The ^{226}Ra annual effective dose in Table A.3 in appendix showed significant different mean values within the set ($p<0.05$), the pairs of groups that are posing the mean difference in mean values are Mar 20-June 19, Mar 20-Sept 19 and Mar 20-Dec 19 (Sig=1). While, the annual effective dose of ^{222}Rn in Table A.6 showed no significant difference ($p> 0.05$) and the means differences between the grouped classes are not significant (sig = 0). The ^{226}Ra and ^{222}Rn excess life time cancer risk mean values showed no significant difference in the water samples from June 19 to March 2020 ($p>0.05$) and the mean values differences between the grouped classes are not significant (sig = 0).

The concentration of radium and radon vary and this could be caused by geological environment variation and the mining history in different regions in the West-Rand. The general survey of different water samples from different sources within the former uranium mines show that radon concentration is always higher than radium in all seasons investigated. This may be observed because, ^{238}U decays through a series of shorter-lived radionuclides eventually produces ^{226}Ra, which has a half-life of 1600 years and ^{226}Ra then decays by alpha-particle emission directly to ^{222}Rn, which is short-lived (half-life = 3.82 days).

The physical-chemical properties of the water samples such as pH and electrical conductivity (EC) are presented in Table 4.3 for collected samples in June 2019, September 2019, December 2019 and March 2020. The pH values ranged from (1.14 to 1.23), (0.73 to 0.94), (0.73 to 1.31), and (1.18 to 1.21), while the EC values ranged from (3050 to 3220), (1930 to 11 700), (2540 to 3210), and (2990 to 3390) mS/m, respectively. The pH mean averages were (1.18), (0.94), (1.13) and (1.20), while the EC averages were (3134), (5566), (2872), and (3086) mS/m, respectively. Measurements of the physicochemical properties were carried out for overall assessment of quality of water, to quantify the level of dissolved substances in the studied areas. WHO (1971) recommended a safe limit for pH of 6.5-8.5 [83], and the pH of the studied samples ranged between (0.73 to 1.31), therefore the surveyed water samples have pH values below the safe limits. Thus the studied water samples are cat-

Table 4.3: Activity concentration results of ^{226}Ra and ^{222}Rn in the measured water samples including the corresponding pH and Conductivity.

Sample ID	June-19				Sept-19				Dec-19				Mar-20			
	Ra226 (mBq/l)	^{222}Rn (mBq/l)	PH	EC (mS/m)	Ra226 (mBq/l)	^{222}Rn (mBq/l)	PH	EC (mS/m)	Ra226 (mBq/l)	^{222}Rn (mBq/l)	PH	EC (mS/m)	Ra226 (mBq/l)	^{222}Rn (mBq/l)	PH	EC (mS/m)
Bly4	122.93	96	1.16	3180	134.13	57.2	1.31	1930	156.15	171	1.15	2690	108	212	1.21	3000
Bly6	46.9	171	1.15	3060	61.57	96.8	0.73	11700	76.3	211	1.14	3210	39.7	289	1.20	3070
Bly comb	101.2	172	1.18	3050	124.65	190	0.86	4680	101.2	77.5	1.18	2840	105	58	1.18	2990
Drie down	56.87	172	1.18	3130	11.23	116	0.93	3500	55.47	136	1.03	2920	4.25	190	1.20	3090
Kloof down	3.4	77.6	1.14	3140	73.17	116	0.94	4610	-3.38	77.4	1.07	2880	10.8	63.3	1.19	3390
Ezul	30.28	37.1	1.19	3160	81.33	76.6	0.90	6860	107.39	76.6	1.13	2540	86.89	114	1.21	3050
Drink	1.58	269	1.23	3220	13.99	231	0.93	5680	8.72	190	1.18	3021	31.31	56.3	1.2	3011

egorised as acidic, since the measured pH levels are lower than 7. Meanwhile, the electrical conductivity values of the analysed water samples are varying in a range of 1930 to 11 700 microsiemens/m, which indicate that there is significant presence of heavy metals that can lead to serious health effects, especially for September 2019 samples. Distilled water has a standard conductivity in the range of 0.5 to 3 μsiemens/cm. The total dissolved solids concentration in milligrams per liter (mg/L) can also be calculated by multiplying the conductivity result by a factor between 0.55 and 0.9, which is empirically determined (Standard Methods #2510, APHA 1992).

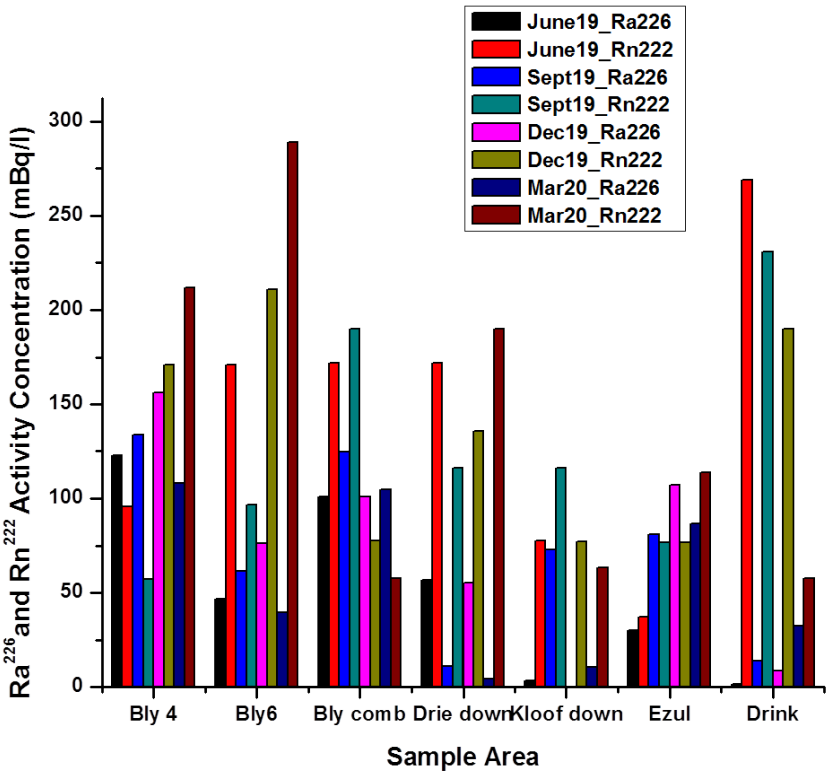


Figure 4.17: ^{226}Ra and ^{222}Rn activity concentration in June 2019

4.4 Estimations of Radiation Protection quantities due to Radium and Radon in water sources

In the present study, ingestion of water from different sources which may be contaminated is one of the concerns. Section 2.8 describes how radiation can have harmful effects on human tissues depending on various factors explained

in the section. Absorbed dose rate is considered for environmental samples in terms of annual effective dose by taking into account conversion factors from absorbed dose in air and the occupancy factors [52]. Moreover, adsorbed dose is primarily explained in subsection 2.8.2 as it is one of the fundamental physical quantity in dosimetry. Therefore estimation of average annual effective dose and excess lifetime cancer risk from ingestion of radium and radon in water is determined using the documentation of United Nations Scientific Committee Effects of Atomic Radiation (UNSCEAR) and Eq. 4.1 and 4.2, respectively [84, 85]. Effective doses quantities are well defined in subsection 2.8.4 and recommended tissue weighting factors for different organs of the body are enlisted in Table 2.7 as well as organ conversion factor for different body organs. Annual Effective Dose (AED) can be described in Eq. 4.1 as:

$$AED_{Rn}(mSv/y) = C_{Rn}W \times I_a \times Df \tag{4.1}$$

where
AED_{Rn} is the committed annual effective dose from drinking water containing ^{222}Rn (mSv/y),
$C_{Rn}W$ (mBq/l) is the radon concentration in water,
I_a is the water consumption rate per year taken to be 60 litres for ^{222}Rn.
Df is the ingestion dose conversion factor for ^{222}Rn (nSv/Bq), equal to 1×10^{-8} Sv/Bq as recommended by UNSCEAR [56]. Similarly represented for radium in Eq. 4.2 as:

$$AED_{Ra}(mSv/y) = C_{Ra}W \times DWI \times Y \times Df \tag{4.2}$$

where
AED_{Ra} is the committed annual effective dose from drinking water containing ^{226}Ra (mSv/y),
$C_{Ra}W$ (mBq/l) is the radium concentration in water,
D_{WI} is the daily consumed of water (taken to be 2 litres per day) [86],
Df is the ingestion dose conversion factor for ^{226}Ra (nSv/Bq), equal to 2.8×10^{-7} Sv/Bq [85],
and Y is year (365 days) [86].

Exposure to ionizing radiation can cause cancer over a period of time [52]. Some studies strongly advises that there is a need for precise determination of cancer risk from low doses [87]. Probability of developing cancer over a

lifetime with the mean intake of ^{226}Ra and ^{222}Rn radionuclides in collected water samples can be estimated by determination of excess lifetime cancer risk (ELCR) in Eq. 4.3 [88].

$$ECLR = AED \times DL \times RF \tag{4.3}$$

where
$ELCR$ is the excess life time cancer risk (mSv/y),
AED is the annual effective dose in (mSv/y),
DL is Average lifespan (year) 70/1 years, RF is the fatal cancer risk per Sievert, risk factor (Sv^{-1}) taken to be 0.057 Sv^{-1}[89].

Table 4.4 show the calculated values of annual effective doses due to ingestion of radium and radon in collected water samples for adults using Eq. 4.1 and 4.2, respectively. The obtained values for radium annual effective dose (AED_{Ra}) ranged from (3.23E-04 to 2.51E-02), (2.30E-03 to 2.74E-02), (-6.91E-04 to 3.19E-02), and (8.69E-04 to 2.21E-02) mSv/y from June 19 to March 20, respectively. While, radon annual effective dose (AED_{Rn}) ranged from (2.23E-05 to 1.61E-04), (3.43E-05 to 1.35E-04), (4.60E-05 to 2.78E-04), and (3.49E-05 to 3.38E-04) mSv/y from June 19 to March 20, respectively. The maximum AED_{Ra} value was found at Bly4 in December 19 (Summer) to be 3.19E-02 mSv/y. Meanwhile, maximum AED_{Rn} effective dose value was found from the drinking water sample (Drink) in March 20 (Autumn) to be 3.38E-04 mSv/y. The estimated annual effective dose poses increased vulnerability due to an exposure from ^{226}Ra radionuclide, this could be the result of higher activity concentrations measured from the radioelement. Also, the parameters considered when estimating the AED such the consumption and dose conversion factor may have influence since these radionuclides have their different specific values, as recommended.

Table 4.4: Annual effective dose for ingestion of radium and radon results.

Sample ID	June 19		Sep_19		Dec_19		Mar_20	
	AED_Ra (mSv/y)	AED_Rn (mSv/y)	AED_Ra (mSv/y)	AED_Rn (mSv/y)	AED_Ra (mSv/y)	AED_Rn (mSv/y)	AED_Ra (mSv/y)	AED_Rn (mSv/y)
Bly 4	2,51E-02	5.76E-05	2,74E-02	3.43E-05	3,19E-02	1.03E-04	2,21E-02	1.27E-04
Bly 6	9,59E-03	1.03E-04	1,26E-02	5.81E-05	1,56E-02	1.27E-04	8.11E-03	1.73E-04
Bly comb	2,07E-02	1.03E-04	2,55E-02	1.14E-04	2,07E-02	4.65E-05	2,15E-02	3.48E-05
Drie down	1,16E-02	1.03E-04	2,30E-03	6.96E-05	1,13E-02	2.78E-04	8.69E-04	1.14E-04
Kloof down	6,95E-04	4.66E-05	1,50E-02	6.96E-05	-6,91E-04	4.64E-05	2.21E-03	3.80E-05
Ezul	6,19E-03	2.23E-05	1,66E-02	4.60E-05	2,20E-02	4.60E-05	1.78E-02	6.84E-05
Drink	3,23E-04	1.61E-04	2,86E-03	1.39E-04	1,78E-03	1.14E-04	6.60E-03	3.38E-04

Table 4.5: Excess Lifetime Cancer Risk (ELCR) for ingestion of radium and radon results.

Sample ID	June 19		Sept_19		Dec_19		Mar_20	
	ECLR_Ra (uSv/y)	ECLR_Rn (mSv/y)	ECLR_Ra (uSv/y)	ECLR_Rn (mSv/y)	ECLR_Ra (uSv/y)	ECLR_Rn (mSv/y)	ECLR_Ra (uSv/y)	ECLR_Rn (mSv/y)
Bly 4	1,00E-01	2,30E-01	1,09E-01	1,37E-01	1,27E-01	4,09E-01	8,81E-02	5,08E-01
Bly6	3,82E-02	4,09E-01	5,02E-02	2,32E-01	6,22E-02	5,05E-01	0.0323589	6,92E-01
Bly comb	8,25E-02	4,12E-01	1,02E-01	4,55E-01	8,25E-02	1,86E-01	8,56E-02	1,39E-01
Drie down	4,64E-02	4,12E-01	9,16E-03	2,78E-01	4,52E-02	3,26E-01	3.47E-03	4,55E-01
Kloof down	2,77E-03	1,86E-01	5,97E-02	2,78E-01	-2,76E-03	1,85E-01	8.82E-03	1,52E-01
Ezul	2,47E-02	8,88E-02	6,63E-02	1,83E-01	8,76E-02	1,83E-01	7.09E-02	2,73E-01
Drink	1,29E-03	6,44E-01	1,14E-02	5,53E-01	7,11E-03	6,50E-03	0.026334	1,39E-01

The radon annual ingestion dose from the current study were lower than the European Commission and the World Health Organization proposed concentration of ^{222}Rn in drinking water of 100 Bq/l [2]. The results of this study indicate that the total annual effective doses from the intake of ^{226}Ra and ^{222}Rn radionuclides in sampled water in West-Rand area were below the World Health Organisation (WHO) recommended limit of 0.1 mSv/y as well as the average radiation dose of 0.29 mSv/y received per head worldwide due to ingestion of natural radionuclides assessed by UNSCEAR (2000) [3].

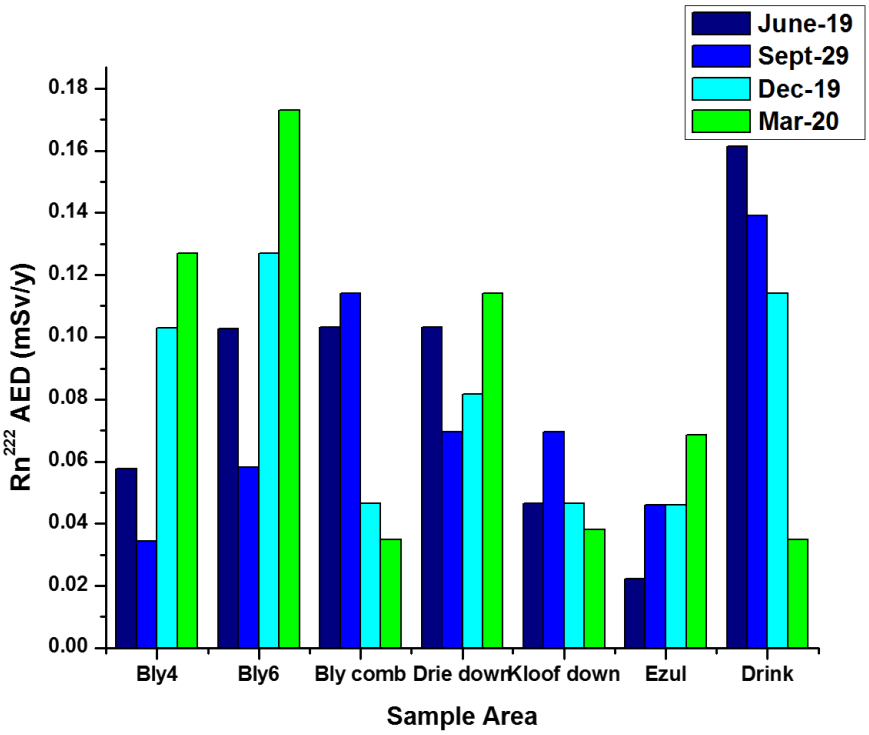


Figure 4.18: Estimated annual effective dose due to ^{222}Rn from June 2019 to March 2020

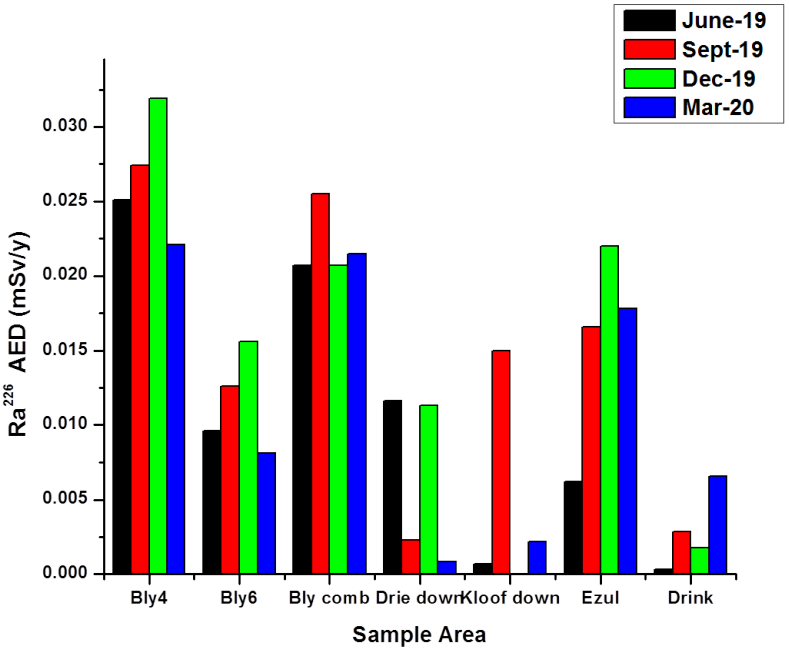


Figure 4.19: Estimated annual effective dose due to ^{226}Ra exposure from June 2019 to March 2020

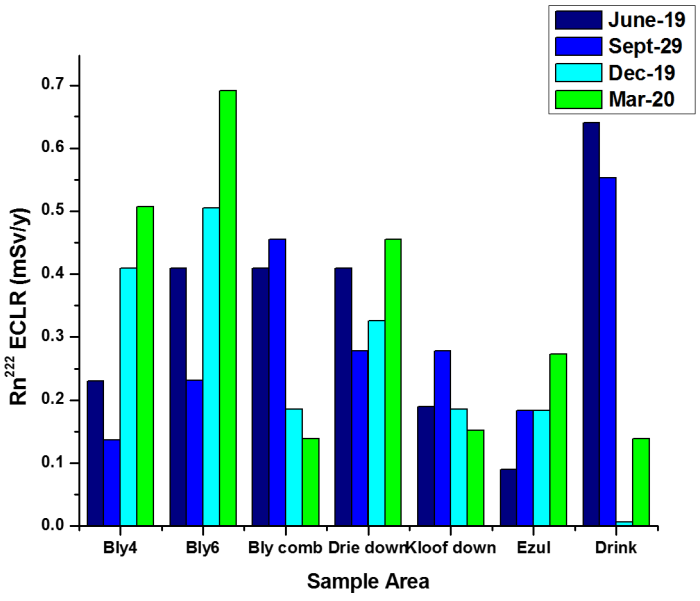


Figure 4.20: Estimated Excess lifetime Cancer risk due to ^{222}Rn from June 2019 to March 2020

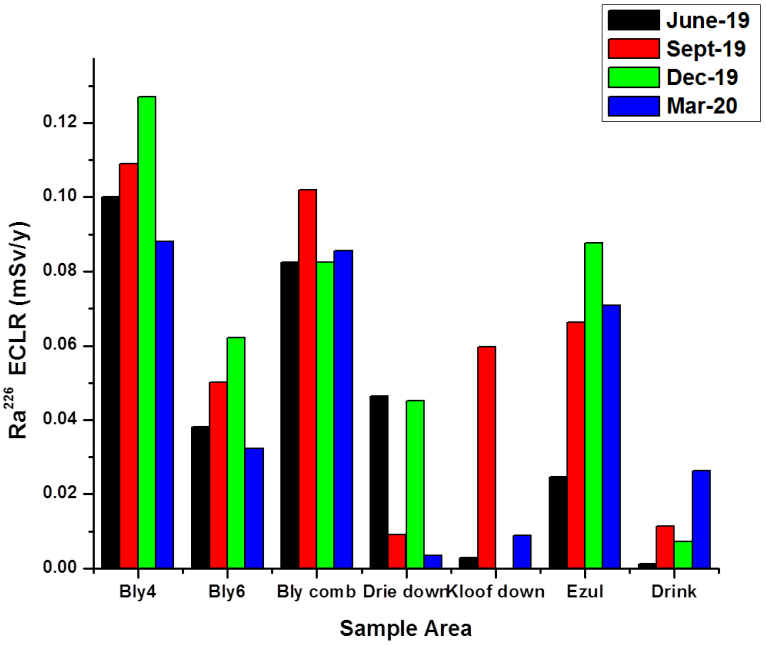


Figure 4.21: Estimated Excess lifetime Cancer risk due to ^{226}Ra from June 2019 to March 2020

Table 4.6 presents the radioactivity classification of drinking water quality according to Department of Water Affairs and Forestry (DWAF 2002) document [90]. A study using these standards as a benchmark was carried out in the Klip River Catchment, Gauteng [91]. Surface water and groundwater were monitored for radioactivity. It was recommended that discharges from mines should be kept at a minimum in order to maintain the water quality at the time. Then it was also concluded that if water quality should deteriorate then it would be unfit for human consumption.

The radiation doses from different former mining sites in the West-Rand area for radium and radon analyses are classified by colour-codes in Table 4.7 according to DWAF (2002) document [91] presented in Table 4.6 which clearly indicates that there is no need for any intervention because there were no health effects observed.

Table 4.6: Classification of radiation dose for drinking water [68].

Dose class	**Color**	**Dose range (mSv/y)**	**Health Effects**	**Intervention indicators time frame**
Class 0, (ideal quality)		0.01–0.1	No observable health effects	No intervention required
Class 1, (good quality)		>0.1–1	No observable health effects	No intervention required, but ALARA principle applies
Class 2, (marginal quality)		>1–10	Small increase in cancer mortality risk	Consider intervention within 2 years
Class 3, (poor quality)		>10–100	Cancer risk statistically detectable in very large population groups	Intervention required within 1 year
Class 4, (unacceptable quality)		>100	Health effects clinically detectable	Immediate intervention required.

Table 4.7: ^{222}Rn average annual effective dose due to the ingestion (AED) of radon in river water samples and color code classification.

Sample ID	June-19				Sept-19				Dec-19				Mar-20			
	AED_Ra (mSv/y)	Color code	AED_Rn (mSv/y)	Color code	AED_Ra (mSv/y)	Color code	AED_Rn (mSv/y)	Color code	AED_Ra (mSv/y)	Color code	AED_Rn (mSv/y)	Color code	AED_Ra (mSv/y)	Color code	AED_Rn (mSv/y)	Color code
Bly4	2.51E-02		5.76E-05		2.74E-02		3.43E-05		3.19E-02		1.03E-04		2.21E-02		1.27E-04	
Bly6	9.59E-03		1.03E-04		1.26E-02		5.81E-05		1.56E-02		1.27E-04		8.11E-03		1.73E-04	
Bly comb	2.07E-02		1.03E-04		2.55E-02		1.14E-04		2.07E-02		4.65E-05		2.15E-02		3.48E-05	
Drie down	1.16E-02		1.03E-04		2.30E-03		6.96E-05		1.13E-02		8.16E-05		8.69E-04		1.14E-04	
Kloof down	6.95E-04		4.66E-05		1.50E-02		6.96E-05		-6.91E-04		4.64E-05		2.21E-03		3.80E-05	
Ezul	6.19E-03		2.23E-05		1.66E-02		4.60E-05		2.20E-02		4.60E-05		9.83E-03		6.84E-05	
Drink	3.23E-04		1.61E-04		2.86E-03		1.39E-04		1.78E-03		1.14E-04		6.60E-03		3.48E-05	

Chapter 5

Conclusion and Recommendations

This study investigated the radioactivity level of naturally occurring radionuclides, specifically the radioelements ^{226}Ra and ^{222}Rn in water samples around former Uranium mines in the West-Rand area of Johannesburg, in Gauteng Province of South Africa. Following the assessment of the influence of former Uranium mining activities on the activity concentrations of the radionuclides in water samples in relation with national and international standards, in conjunction with the associated health risk, the current study was conducted. Ample water samples from different sources were collected and analysed to quantify the risks of exposure to the population in the surrounding area. A total of 32 water samples were collected, and analysed for ^{226}Ra and ^{222}Rn using Alpha spectroscopy and Rad-7 instruments, respectively. The following conclusions were reached:

- The values of ^{226}Ra and ^{222}Rn activity concentration in the public water samples in general are less than the maximum recommended contamination level (MCL) by USEPA that is 11.1 Bq/L [72].
- The results of radium concentration measurement in water samples were below the suggested level of radium in drinking water recommended by EUC and WHO (0.555 Bq/l).
- The reported ^{222}Rn results are below the established limit of 1 Bq/l activity concentration for ^{222}Rn in water samples by WHO (2011) [79].
- The ^{222}Rn activity concentration in the three water samples used to verify the quality of the Rad-7 instrument namely Deionised 2020, Valpre

2020 and Tap water was below the minimum detectable limit (MDL) of the RAD-7 instrument (0.4 Bq/l), and that may be the case because the above samples are purified and processed water. Thus, the $\alpha-$spectrometry technique as applied by the RAD-7 instrument was shown to be appropriate for determination of radon concentrations.

- It has been observed that the radon annual ingestion dose from the current study was lower than the European Commission and the World Health Organization proposed concentration of 100 Bq/l [2] ^{222}Rn in drinking water. Also, both results of this study indicate that the total annual effective doses from the intake of ^{226}Ra and ^{222}Rn radionuclides in sampled water in West-Rand area were below the World Health Organisation (WHO) recommended limit of 0.1 mSv/y as well as the average radiation dose of 0.29 mSv/y received per head worldwide due to ingestion of natural radionuclides assessed by UNSCEAR (2000) [3].

- The annual effective radiation doses from different former mining sites in the West-rand for radium and radon (AED_{Ra} and AED_{Rn}) analyses are classified by colour-codes in Table 4.5 according to reference Table 4.6 which clearly indicates that there is no need for any intervention because there were no health effects observed

- The variation in radium and radon activity concentrations in water samples might be due to the differences in the geological formation, geographical nature of these regions and the period of operation in each mining area.

- The obtained measured results show that the selected water sources in the West-Rand area are safe for domestic use or drinking when purification and treatment has been applied.

- The probability of developing cancer over a lifetime with the mean intake of ^{226}Ra and ^{222}Rn radioelements in the surveyed water samples is estimated by determination of excess lifetime cancer risk (ELCR) which was found to be very low in both cases.

- The levels of ^{226}Ra and ^{222}Rn concentration measured in the current study do not pose a health problem to the public.

- The physical-chemical properties of the water samples such as pH and electrical conductivity (EC) were measured in this study, and the pH of

the studied samples ranged between (0.73 to 1.31) which is below the WHO (1971) recommended safe limit for pH (6.5-8.5) [83]. Thus the studied water samples can be categorised as acidic, since the measured pH levels are lower than 7. The samples analyzed had conductivity values ranging from 1930 to 11 700µS/cm, which had no health significance.

5.1 Recommendations for future studies

There is a need for assessment of similar studies, some may be conducted on soil samples or sediment samples around the former areas of operation in the West-Rand area. As the decades go by, leaching, weathering and erosion are taking place in the area and the radionuclides concentration in the soil builds up in the studied area and accumulates in sediment along the bank of the mining water sources. This will further validate the conclusion drawn from this study. It will be recalled that these natural radionuclides also have inhalation pathways into members of the public, which constitute internal exposure to radiation. Thus the amount of radionuclides inhaled should be studied by sampling the dust in the air, within the precinct of former uranium mined rubble and wastes. Furthermore, urine samples from selected members of the public that live close in the area may be examined. This should be over a certain period of time on a periodic bases to understand the rate of accumulation of these radionuclides in humans over time.

Studies may also be conducted on water sources from a different location in West-Rand to compare the results with areas where there is no influence from the mining activities. Reference detectors should be employed in order to compare and get results more precisely for determination of ^{226}Ra and ^{222}Rn activity concentration in water samples, such as Inductively Coupled Plasma Mass Spectrometry (ICP-MS) and Liquid Scintillator instrument. Lastly, frequent awareness is needed about the dangers that can be caused by exposure to excessive radiation, particularly to South African citizens who stay near the mines.

Bibliography

[1] Saman Ezzulddin. Radon-222 and radium-226 activity concentration measurement in erbil governorate drinking water resources using active and passive detection methods. Master's thesis, Salahaddin University, 2016.

[2] Sanitation Water, World Health Organization, et al. Guidelines for drinking-water quality [electronic resource]: incorporating first addendum. vol. 1, recommendations. 2006.

[3] I Fatima, JH Zaidi, M Arif, and SNA Tahir. Measurement of natural radioactivity in bottled drinking water in pakistan and consequent dose estimates. *Radiation Protection Dosimetry*, 123(2):234–240, 2007.

[4] Canadian Nuclear Safety Commission et al. Radon in canada's uranium industry. 2014.

[5] Organisation for Economic Co-operation and Development. *Environmental activities in uranium mining and milling*. OECD Publishing, 1999.

[6] A Faanu, OK Adukpo, L Tettey-Larbi, H Lawluvi, DO Kpeglo, EO Darko, G Emi-Reynolds, RA Awudu, C Kansaana, PA Amoah, et al. Natural radioactivity levels in soils, rocks and water at a mining concession of perseus gold mine and surrounding towns in central region of ghana. *SpringerPlus*, 5(1):98, 2016.

[7] JF Durand. The impact of gold mining on the witwatersrand on the rivers and karst system of gauteng and north west province, south africa. *Journal of African Earth Sciences*, 68:24–43, 2012.

[8] Frank Winde and EJ Stoch. Threats and opportunities for post-closure development in dolomitic gold mining areas of the west rand and far west rand (south africa)-a hydraulic view part 1: mining legacy and future threats. *Water SA*, 36(1):69–74, 2010.

[9] National Research Council. *Comparative dosimetry of radon in mines and homes*. National Academies Press, 1991.

[10] Robert J Budnitz. Radon-222 and its daughters u a review of instrumentation for occupational and environmental monitoring. *U. S. Atomic Energy Commission under Contract W -7405-ENG-48*, 1973.

[11] Caspah Kamunda, Manny Mathuthu, and Morgan Madhuku. An assessment of radiological hazards from gold mine tailings in the province of gauteng in south africa. *International Journal of environmental research and public health*, 13(1):138, 2016.

[12] Saphina Biira, Akisophel W Kisolo, and Florence Mutonyi D'ujanga. Concentration levels of radon in mines, industries and dwellings in selected areas of tororo and busia districts, eastern uganda.". *Adv Appl Sci Res*, 5(6):31–44, 2014.

[13] Irina Guseva Canu, Olivier Laurent, Nathalie Pires, Dominique Laurier, and Isabelle Dublineau. Health effects of naturally radioactive water ingestion: the need for enhanced studies. *Environmental health perspectives*, 119(12):1676–1680, 2011.

[14] Ava Nourian Dehkordi. Assessment of radiation doses to the west rand public due to inhalation of 222rn and its daughter products. Master's thesis, University of the Witwatersrand, 2012.

[15] Patitapaban Sahu, Durga Charan Panigrahi, and Devi Prasad Mishra. Sources of radon and its measurement techniques in underground uranium mines–an overview. *Journal of Sustainable Mining*, 13(3):11–18, 2014.

[16] Patitapaban Sahu, Durga Charan Panigrahi, and Devi Prasad Mishra. A comprehensive review on sources of radon and factors affecting radon concentration in underground uranium mines. *Environmental Earth Sciences*, 75(7):617, 2016.

[17] Henri Becquerel. La radioactivité. *Paris, Payot*, 1924.

[18] Gopal B Saha. Radioactive decay. In *Fundamentals of Nuclear Pharmacy*, pages 11–32. Springer, 2018.

[19] Frank Herbert Attix. *Introduction to radiological physics and radiation dosimetry*. John Wiley & Sons, 2008.

[20] Michael F L'Annunziata. *Radioactivity: introduction and history, from the quantum to quarks*. Elsevier, 2016.

[21] Nabil Hamed. *Measurement of radon concentration in soil at north gaza*. PhD thesis, Islamic University of Gaza, 2005.

[22] James E Turner. *Atoms, radiation, and radiation protection*. John Wiley & Sons, 2008.

[23] Livhuwani Masevhe. *An analytical study of radon concentration in water from some rivers in Gauteng using a solid-state α- detector*. PhD thesis, University of Johannesburg, 2017.

[24] Edward L Alpen. *Radiation biophysics*. Academic press, 1997.

[25] William R Hendee and E Russell Ritenour. *Medical imaging physics*. John Wiley & Sons, 2003.

[26] John L Humm, Oliver Sartor, Chris Parker, Oyvind S Bruland, and Roger Macklis. Radium-223 in the treatment of osteoblastic metastases: a critical clinical review. *International Journal of Radiation Oncology* Biology* Physics*, 91(5):898–906, 2015.

[27] Gavin K Gillmore, FE Perrier, and Robin GM Crockett. Radon, health and natural hazards. Geological Society of London, 2018.

[28] Jacqueline Michel. Relationship of radium and radon with geological formations. *Radon, radium and uranium in drinking water*, 7:83–95, 1990.

[29] Gordon T Cook and Angus B MacKenzie. Radioactive isotope analyses of skeletal materials in forensic science: a review of uses and potential uses. *International journal of legal medicine*, 128(4):685–698, 2014.

[30] J Mc Laughlin. An historical overview of radon and its progeny: applications and health effects. *Radiation protection dosimetry*, 152(1-3):2–8, 2012.

[31] Frédéric Girault, Frédéric Perrier, and Tadeusz A Przylibski. Radon-222 and radium-226 occurrence in water: a review. *Geological Society, London, Special Publications*, 451(1):131–154, 2018.

[32] Gregory Choppin, Jan-Olov Liljenzin, and Jan Rydberg. *Radiochemistry and nuclear chemistry*. Butterworth-Heinemann, 2002.

[33] James Edward Turner, Darryl J Downing, and James S Bogard. *Statistical methods in radiation physics*. Wiley-VCH, 2012.

[34] Richard C Ropp. *Encyclopedia of the alkaline earth compounds*. Newnes, 2012.

[35] Deutsch English Français Español. Historical uses. *Scientific American (Macklis RM, The great radium scandal. Sci. Am. 1993 Aug: 269 (2)*, 94: 99.

[36] Harold W Kirby and Murrell Leon Salutsky. *The radiochemistry of radium*, volume 3057. National Academies, 1964.

[37] F Kulalı and İ Akkurt. Investigation of radon concentrations in pamukkale-turkey. *Acta Phys Pol A*, 128:445–446, 2015.

[38] Robert E Krebs. *The history and use of our earth's chemical elements: a reference guide*. Greenwood Publishing Group, 2006.

[39] F Ward Whicker and Vincent Schultz. *Radioecology: nuclear energy and the environment*, volume 2. CRC press Boca Raton, FL, 1982.

[40] C Richard Cothern and James E Smith Jr. *Environmental radon*, volume 35. Springer Science & Business Media, 2013.

[41] James BR Battat, J Brack, E Daw, A Dorofeev, AC Ezeribe, JR Fox, J-L Gauvreau, M Gold, LJ Harmon, JL Harton, et al. Radon in the drift-ii directional dark matter tpc: emanation, detection and mitigation. *Journal of Instrumentation*, 9(11):P11004, 2014.

[42] Jeffrey L Schwartz. Radiation injury and radiation carcinogenesis with special reference to combination effects with chemical agents. In *Chemical Induction of Cancer*, pages 473–508. Springer, 1995.

[43] GF Knoll. Radiation detection and measurement3rd edition john wiley and sons. *New York*, 2000.

[44] Michael F L'Annunziata. *Handbook of radioactivity analysis*. Academic press, 2012.

[45] Kenneth S Krane, David Halliday, et al. *Introductory nuclear physics*. 1987.

[46] Jeanne Mager Stellman. *Encyclopaedia of occupational health and safety*, volume 1. International Labour Organization, 1998.

[47] Nureddin Ahmed S Musa. Effects of long term low x-ray radiation dose on blood compounds of radiology staff of health centers in libya. Master's thesis, The National Ribat University, 2017.

[48] Tuukka Turtiainen. Radon and radium in well water: Measurements and mitigation of exposure. 2013.

[49] Omar Desouky, Nan Ding, and Guangming Zhou. Targeted and non-targeted effects of ionizing radiation. *Journal of Radiation Research and Applied Sciences*, 8(2):247–254, 2015.

[50] Mohammad Saeed Mohammad Hassan and Adnan Lahham. Assessment of radiation protection awareness, policies and practices among palestinian radiographers in governmental hospitals-palestine. Master's thesis, AL-Quds University, 2018.

[51] CC Lushbaugh. Guidance on radiation received in space activities. *Radiation Research*, 121:344, 1990.

[52] Masok Felix Bitrus. *Anthropogenic Radioactivity Measurement and Water Sampling: A case study of rock phosphate storage facility at Richards Bay, South Africa*. PhD thesis, University of Johannesburg, 2017.

[53] Nicholas Tsoulfanidis. *Measurement and detection of radiation*. CRC press, 2010.

[54] Gopal B Saha. *Physics and radiobiology of nuclear medicine*. Springer Science & Business Media, 2012.

[55] Radiological Protection. Icrp publication 103. *Ann ICRP*, 37(2.4):2, 2007.

[56] Henryk Bem, Urszula Plota, Marta Staniszewska, Ewa Maria Bem, and Daria Mazurek. Radon (222 rn) in underground drinking water supplies of the southern greater poland region. *Journal of Radioanalytical and Nuclear Chemistry*, 299(3):1307–1312, 2014.

[57] volume i:Sources Unscear. effects of ionizing radiation. *United Nations, New York*, pages 453–487, 2000.

[58] volume ii:Effects Unscear. effects of ionizing radiation. *United Nations, New York*, pages 453–487, 2000.

[59] DAE Darwish, KTM Abul-Nasr, and AM El-Khayatt. The assessment of natural radioactivity and its associated radiological hazards and dose parameters in granite samples from south sinai, egypt. *Journal of Radiation Research and Applied Sciences*, 8(1):17–25, 2015.

[60] Alan Martin. *An Introduction to Radiation Protection 6E*. CRC Press, 2012.

[61] Frank Winde and Ewald Erasmus. Peatlands as filters for polluted mine water?—a case study from an uranium-contaminated karst system in south africa—part i: Hydrogeological setting and u fluxes. *Water*, 3(1): 291–322, 2011.

[62] SA Stats. Census 2011 municipal report–gauteng. *Statistics South Africa. Available from: http://www. statssa. gov. za/Census2011/Products/GP_Municipal_Report. pdf*, 2012.

[63] William R Leo. *Techniques for nuclear and particle physics experiments: a how-to approach*. Springer Science & Business Media, 2012.

[64] Syed Naeem Ahmed. *Physics and engineering of radiation detection*. Academic Press, 2007.

[65] Floyd Stanley, Apryll Stalcup, and H. Spitz. A brief introduction to analytical methods in nuclear forensics. *Journal of Radioanalytical and Nuclear Chemistry*, 295, 07 2012. doi: 10.1007/s10967-012-1927-3.

[66] Siddig Abdalla Talha Abdalla. *Measurements and applications of radon in South African aquifer and river waters*. PhD thesis, University of the Western Cape, 2009.

[67] Gordon Gilmore. *Practical gamma-ray spectroscopy*. John Wiley & Sons, 2011.

[68] L Masevhe, LM Mavunda, and SH Connell. A general survey of radon concentration in water from rivers in gauteng, south africa using a solid-state -detector. 2017.

[69] Mohammed D Alenezy. Radon concentrations measurement in aljouf, saudi arabia using active detecting method. *Natural Science*, 6(11):886, 2014.

[70] A El-Taher. Measurement of radon concentrations and their annual effective dose exposure in groundwater from qassim area, saudi arabia. *Journal of Environmental Science and Technology*, 5(6):475–481, 2012.

[71] V Duggal, R Asha, and M Rohit. In situ measurements of radon level in groundwater in northern rajasthan, india. *Advances in Applied science research*, 3(6):3825–3830, 2012.

[72] N Khattak, M Khan, M Shah, and M Javed. Radon concentration in drinking water sources of the main campus of the university of peshawar and surrounding areas, khyber pakhtunkhwa, pakistan. *Journal of Radioanalytical and Nuclear Chemistry*, 290(2):493–505, 2011.

[73] Irene Opoku-Ntim, Aba Bentil Andam, Tetteh T Akiti, JJ Flectcher, and Vicenzo Roca. Annual effective dose of radon in groundwater samples for different age groups in obuasi and offinso in the ashanti region, ghana. *Environmental Research Communications*, 1(10):105002, 2019.

[74] Ivana Stojković, Branislava Tenjović, Jovana Nikolov, Miroslav Vesković, Dušan Mrđa, and Nataša Todorović. Improvement of measuring methods and instrumentation concerning 222rn determination in drinking waters–rad7 and lsc technique comparison. *Applied Radiation and Isotopes*, 98: 117–124, 2015.

[75] Bo-chao Xu, W Burnett, Derek Lane-Smith, and Zhi-gang Yu. A simple laboratory-based radon calibration system. *Journal of radioanalytical and nuclear chemistry*, 283(2):457–463, 2010.

[76] A Jalili-Majareshin, A Behtash, and D Rezaei-Ochbelagh. Radon concentration in hot springs of the touristic city of sarein and methods to reduce radon in water. *Radiation Physics and Chemistry*, 81(7):749–757, 2012.

[77] Liteboho Ntsohi. Characterization of uranium mined ore for nuclear forensic applications. Master's thesis, University of the Witwatersrand, 2019.

[78] SJ Kline. The purposes of uncertainty analysis. 1985.

[79] Jaqueline Kappke, Sergei A Paschuk, Janine N Correa, Marilson Reque, Camila Garcia Tabuchi, Flavia Del Claro, Allan Felipe Perna, and Valeriy Deniak. Measurements of radon and radium activity in bottled mineral water. 2013.

[80] Yadolah Fakhri, Morteza Kargosha, Ghazaleh Langarizadeh, Yahya Zandsalimi, Leila Rasouli Amirhajeloo, Mahboobeh Moradi, Bigard Moradi, and Maryam Mirzaei. Effective dose radon 222 of the tap water in children and adults people; minab city, iran. *Global journal of health science*, 8(4):234, 2016.

[81] I Inigo Valan, S Maniyarasan, R Mathiyarasu, SGD Sridhar, V Narayanan, and A Stephen. Seasonal observation on radionuclide concentration in krusadai island mangroves, gulf of mannar, india. *Journal of Radioanalytical and Nuclear Chemistry*, 310(3):1277–1288, 2016.

[82] Ross Ivan Kleinschmidt. *Radioactive residues associated with water treatment, use and disposal in Australia*. PhD thesis, Queensland University of Technology, 2011.

[83] Kumar Ajay, Kumar Arvind, Singh Surinder, et al. Analysis of radium and radon in the environmental samples and some physico-chemical properties of drinking water samples belonging to some areas of rajasthan and delhi, india. *Advances in Applied Science Research*, 3(5):2900–2905, 2012.

[84] M Malakootian and Y Soltani Nejhad. Determination of radon concentration in drinking water of bam villages and evaluation of the annual effective dose. *International Journal of Radiation Research*, 15(1):81, 2017.

[85] Boonsom Porntepkasemsan and Kanitha Srisuksawad. Assessment of 226ra age-dependent dose from water intake. *Applied Radiation and Isotopes*, 66(11):1654–1656, 2008.

[86] A Abbasi and V Bashiry. Measurement of radium-226 concentration and dose calculation of drinking water samples in guilan province of iran. *International Journal of Radiation Research*, 14(4):361–366, 2016.

[87] Ljubica Župunski, Vesna Spasić-Jokić, Mirjana Trobok, and Vojin Gordanić. Cancer risk assessment after exposure from natural radionuclides in soil using monte carlo techniques. *Environmental Science and Pollution Research*, 17(9):1574–1580, 2010.

[88] unscear 1996 report to the general assembly with scientific annex Unscear. United nations scientific committee on effects of atomic radiation, effects of ionising radiation. *United Nations, New York*, pages ISBN 7–5022–2135–2, 1996.

[89] Mohammad Mirdoraghi, Safdar Masoumi, and Daniel Einor. Data on assessment excess lifetime cancer risk and risk of lung cancer from inhalation of radon 222 in radiotherapy centers in tehran, iran. *Data in brief*, 20:1367–1370, 2018.

[90] DWAF. Institute of water quality studies. radioactivity dose calculation and water quality evaluation guideline for domestic water use. *DWAF (Department of Water Affairs and Forestry)*, 2002.

[91] NRMP DWAF. Report on the radioactivity monitoring programme in the klip river catchment. *National Monitoring Programme. Report No., N000000REQ0403, Resource Quality Services, Department of Water Affairs and Forestry, Pretoria, South Africa*, 2003.

Appendix A

Anova Analysis

Table A.1: ^{226}Ra Activity Concentration (mBq/l) from June 2019 – March 2020 in water samples

Data Summary				
Groups	N	Mean	Std Dev.	Std. Error
June19	11	73.43182	56.43034	17.01439
Sept19	11	74.61182	46.60629	14.05232
Dec19	11	71.57818	51.11302	15.41116
Mar20	11	61.02	42.90157	12.93531

ANOVA Summary					
Source	DF	Sum of Squares SS	Mean Square MS	F-Stat	Prob>F
Between Groups	3	1276.8175	425.60583	0.17355	0.91366
Within groups	40	98096.15009	2452.40375		
Total	43	99372.96759			

Mean comparisons within pair of groups

	MeanDiff	SEM	q Value	Prob	Alpha	Sig	LCL	UCL
Sept19 June19	1.18	21.11615	0.07903	0.99994	0.05	0	-55.42014	57.78014
Dec19 June19	-1.85364	21.11615	0.12414	0.99975	0.05	0	-58.45378	54.7465
Dec19 Sept19	-3.03364	21.11615	0.20317	0.99892	0.05	0	-59.63378	53.5665
Mar20 June19	-12.41182	21.11615	0.83126	0.93519	0.05	0	-69.01196	44.18832
Mar20 Sept19	-13.59182	21.11615	0.91029	0.91713	0.05	0	-70.19196	43.00832
Mar20 Dec19	-10.55818	21.11615	0.70711	0.95859	0.05	0	-67.15832	46.04196

Table A.2: ^{226}Ra Activity Concentration (mBq/l) from June 2019 – March 2020 of radon identical water samples

Data Summary				
Groups	N	Mean	Std Dev.	Std. Error
June19	7	51.88	46.32714	17.51001
Sept19	7	71.43857	48.10632	18.18248
Dec19	7	71.69286	56.51532	21.36078
Mar20	7	55.27857	43.97643	16.62153

ANOVA Summary					
Source	DF	Sum of Squares SS	Mean Square MS	F-Stat	Prob>F
Between Groups	3	2305.23361	768.4112	0.32056	0.81041
Within groups	24	57529.97991	2397.0825		
Total	27	59835.21352			

Mean comparisons within pair of groups

	MeanDiff	SEM	q Value	Prob	Alpha	Sig	LCL	UCL
Sept19 June19	19.55857	26.17023	1.05693	0.87688	0.05	0	-52.63484	91.75199
Dec19 June19	19.81286	26.17023	1.07067	0.87274	0.05	0	-52.38056	92.00627
Dec19 Sept19	0.25429	26.17023	0.01374	1	0.05	0	-71.93913	72.4477
Mar20 June19	3.39857	26.17023	0.18366	0.99919	0.05	0	-68.79484	75.59199
Mar20 Sept19	-16.16	26.17023	0.87327	0.92549	0.05	0	-88.35342	56.03342
Mar20 Dec19	-16.41429	26.17023	0.88701	0.92229	0.05	0	-88.6077	55.77913

Table A.3: ^{226}Ra AED estimation (mSv/y) in water samples

Data Summary				
Groups	N	Mean	Std Dev.	Std. Error
June19	7	0.0106	0.00946	0.00358
Sept19	7	0.01461	0.00983	0.00372
Dec19	7	0.01466	0.01156	0.00437
Mar20	7	55.27857	43.97643	16.62153

ANOVA Summary					
Source	DF	Sum of Squares SS	Mean Square MS	F-Stat	Prob>F
Between Groups	3	16034.82075	5344.94025	11.0551	9.45387E-5
Within groups	24	11603.5594	483.48164		
Total	27	27638.38016			

	Mean Diff	SEM	q Value	Prob	Alpha	Sig	LCL	UCL
Sept19 June19	0.00401	11.7532	4.82369E-4	1	0.05	0	-32.41846	32.42648
Dec19 June19	0.00406	11.7532	4.88025E-4	1	0.05	0	-32.41841	32.42653
Dec19 Sept19	4.7E-5	11.7532	5.65532E-6	1	0.05	0	-32.42242	32.42252
Mar20 June19	55.26797	11.7532	6.65017	4.82662E-4	0.05	1	22.8455	87.69044
Mar20 Sept19	55.26396	11.7532	6.64968	4.83075E-4	0.05	1	22.84149	87.68643
Mar20 Dec19	55.26392	11.7532	6.64968	4.83079E-4	0.05	1	22.84145	87.68639

Mean comparisons within pair of groups

Table A.4: ^{226}Ra ECLR estimation (mSv/y) in water samples

Data Summary				
Groups	N	Mean	Std Dev.	Std. Error
June19	7	0.04227	0.03771	0.01425
Sept19	7	0.05825	0.03921	0.01482
Dec19	7	0.05841	0.04601	0.01739
Mar20	7	0.04508	0.03587	0.01356

ANOVA Summary					
Source	DF	Sum of Squares SS	Mean Square MS	F-Stat	Prob>F
Between Groups	3	0.00153	5.10557E-4	0.32095	0.81013
Within groups	24	0.03818	0.00159		
Total	27	0.03971			

Mean comparisons within pair of groups

	MeanDiff	SEM	q Value	Prob	Alpha	Sig	LCL	UCL
Sept19 June19	0.01599	0.02132	1.06041	0.87583	0.05	0	-0.04283	0.0748
Dec19 June19	0.01614	0.02132	1.07074	0.87272	0.05	0	-0.04267	0.07495
Dec19 Sept19	1.55714E-4	0.02132	0.01033	1	0.05	0	-0.05866	0.05897
Mar20 June19	0.00281	0.02132	0.18654	0.99916	0.05	0	-0.056	0.06162
Mar20 Sept19	-0.01317	0.02132	0.87388	0.92535	0.05	0	-0.07199	0.04564
Mar20 Dec19	-0.01333	0.02132	0.88421	0.92295	0.05	0	-0.07214	0.04548

Table A.5: ^{222}Rn Activity Concentration (mBq/l) from June 2019 – March 2020 in water samples

Data Summary				
Groups	N	Mean	Std Dev.	Std. Error
June19	7	142.1	77.4998	29.2922
Sept19	7	126.2286	62.3793	23.5772
Dec19	7	134.2143	57.9198	21.8916
Mar20	7	140.6143	91.1859	34.465

ANOVA Summary					
Source	DF	Sum of Squares SS	Mean Square MS	F-Stat	P-value
Between Groups	3	1098.9522	366.3174	0.0679	0.9764
Within groups	24	129401.806	5391.7419		
Total	27	130500.7581			

Mean comparisons within pair of groups

	Mean Diff	SEM	q Value	Prob	Alpha	Sig	LCL	UCL
Sept19 June19	-15.87143	39.24918	0.57187	0.97713	0.05	0	-124.14457	92.40172
Dec19 June19	-7.88571	39.24918	0.28414	0.99705	0.05	0	-116.15886	100.38743
Dec19 Sept19	7.98571	39.24918	0.28774	0.99694	0.05	0	-100.28743	116.25886
Mar20 June19	-1.48571	39.24918	0.05353	0.99998	0.05	0	-109.75886	106.78743
Mar20 Sept19	14.38571	39.24918	0.51834	0.98276	0.05	0	-93.88743	122.65886
Mar20 Dec19	6.4	39.24918	0.2306	0.99841	0.05	0	-101.87315	114.67315

Table A.6: ^{222}Rn AED estimation (mSv/y) in water samples

Data Summary				
Groups	N	Mean	Std Dev.	Std. Error
June19	7	0.0853	0.0465	0.0176
Sept19	7	0.0757	0.0374	0.0141
Dec19	7	0.0805	0.0348	0.0131
Mar20	7	0.0844	0.0547	0.0207

ANOVA Summary					
Source	DF	Sum of Squares SS	Mean Square MS	F-Stat	Prob>F
Between Groups	3	0.0004	0.0001	0.0691	0.9759
Within groups	24	0.0466	0.0019		
Total	27	0.047			

Mean comparisons within pair of groups

	Mean Diff	SEM	q Value	Prob	Alpha	Sig	LCL	UCL
Sept19 June19	-0.00946	0.02355	0.56802	0.97757	0.05	0	-0.07443	0.05551
Dec19 June19	-0.00462	0.02355	0.27723	0.99726	0.05	0	-0.06959	0.06036
Dec19 Sept19	0.00484	0.02355	0.29078	0.99684	0.05	0	-0.06013	0.06982
Mar20 June19	-9.74286E-4	0.02355	0.0585	0.99997	0.05	0	-0.06595	0.064
Mar20 Sept19	0.00849	0.02355	0.50952	0.9836	0.05	0	-0.05649	0.07346
Mar20 Dec19	0.00364	0.02355	0.21873	0.99864	0.05	0	-0.06133	0.06862

Table A.7: ^{222}Rn ECLR estimation (mSv/y) in water samples

Data Summary				
Groups	N	Mean	Std Dev.	Std. Error
June19	7	0.3402	0.1855	0.0701
Sept19	7	0.3022	0.1493	0.0564
Dec19	7	0.2573	0.1673	0.0632
Mar20	7	0.3366	0.2183	0.0825

ANOVA Summary					
Source	DF	Sum of Squares SS	Mean Square MS	F-Stat	Prob>F
Between Groups	3	0.0312	0.0104	0.3141	0.815
Within groups	24	0.7941	0.0331		
Total	27	0.8252			

Mean comparisons within pair of groups

	MeanDiff	SEM	q Value	Prob	Alpha	Sig	LCL	UCL
Sept19 June19	-0.03781	0.09694	0.55155	0.97939	0.05	0	-0.30524	0.22962
Dec19 June19	-0.08274	0.09694	1.20704	0.82833	0.05	0	-0.35017	0.18469
Dec19 Sept19	-0.04493	0.09694	0.65549	0.96628	0.05	0	-0.31236	0.2225
Mar20 June19	-0.00337	0.09694	0.04915	0.99998	0.05	0	-0.2708	0.26406
Mar20 Sept19	0.03444	0.09694	0.5024	0.98425	0.05	0	-0.23299	0.30187
Mar20 Dec19	0.07937	0.09694	1.15789	0.84502	0.05	0	-0.18806	0.3468

Table A.8: ^{226}Ra and ^{222}Rn Activity concentration (mBq/l) in June 2019 water samples

Data Summary				
Groups	N	Mean	Std Dev.	Std. Error
Radium	7	51.88	46.3271	17.51
Radon	7	142.1	77.4998	29.2922

ANOVA Summary					
Source	DF	Sum of Squares SS	Mean Square MS	F-Stat	P-Value
Between Groups	1	28488.7694	28488.7694	6.989	0.0214
Within groups	12	48914.5152	4076.2096		
Total	13	77403.2846			

Table A.9: ^{226}Ra and ^{222}Rn Activity concentration (mBq/l) in September 2019 water samples

Data Summary				
Groups	N	Mean	Std Dev.	Std. Error
Radium	7	71.4386	48.1063	18.1825
Radon	7	126.2286	62.3793	23.5772

ANOVA Summary					
Source	DF	Sum of Squares SS	Mean Square MS	F-Stat	P-Value
Between Groups	1	10506.8044	10506.8044	3.3863	0.0906
Within groups	12	37232.359	3102.6966		
Total	13	47739.1634			

Table A.10: ^{226}Ra and ^{222}Rn Activity concentration (mBq/l) in December 2019 water samples

Data Summary				
Groups	N	Mean	Std Dev.	Std. Error
Radium	7	71.6929	56.5153	21.3608
Radon	7	134.2143	57.9198	21.8916

ANOVA Summary					
Source	DF	Sum of Squares SS	Mean Square MS	F-Stat	P-Value
Between Groups	1	13681.2391	13681.2391	4.1783	0.0635
Within groups	12	39292.0942	3274.3412		
Total	13	52973.3333			

Table A.11: ^{226}Ra and ^{222}Rn Activity concentration (mBq/l) in Mar 2019 water samples

Data Summary				
Groups	N	Mean	Std Dev.	Std. Error
Radium	7	55.27857	43.97643	16.62153
Radon	7	140.61429	91.18594	34.46504

ANOVA Summary					
Source	DF	Sum of Squares SS	Mean Square MS	F-Stat	P-Value
Between Groups	1	25487.64446	25487.64446	4.97378	0.04559
Within groups	12	61492.80606	5124.4005		
Total	13	86980.45052			